



Fall 12-22-2009

EFFECT OF HYDRATION AND MACROMOLECULAR CROWDING ON PEPTIDE CONFORMATION, AGGREGATION AND FOLDING KINETICS

SMITA MUKHERJEE

University of Pennsylvania, smita3@sas.upenn.edu

Follow this and additional works at: <http://repository.upenn.edu/edissertations>



Part of the [Biochemistry Commons](#), and the [Biophysics Commons](#)

Recommended Citation

MUKHERJEE, SMITA, "EFFECT OF HYDRATION AND MACROMOLECULAR CROWDING ON PEPTIDE CONFORMATION, AGGREGATION AND FOLDING KINETICS" (2009). *Publicly Accessible Penn Dissertations*. 90.
<http://repository.upenn.edu/edissertations/90>

EFFECT OF HYDRATION AND MACROMOLECULAR CROWDING ON PEPTIDE CONFORMATION, AGGREGATION AND FOLDING KINETICS

Abstract

Protein folding/misfolding in vivo takes place in a highly crowded and confined environment. Such crowded environment can possibly lead to fewer water molecules surrounding a protein of interest than that seen under in vitro conditions wherein typically dilute aqueous solutions are used. When considering the aforesaid cellular characteristics, such as water depletion and macromolecular crowding; it is reasonable to assume that proteins may experience different energy landscapes when folding in vivo than in vitro. Therefore, we have investigated how degrees of hydration and macromolecular crowding affect the conformation, aggregation and folding kinetics of short peptides.

In order to modulate the number of water molecules accessible to the peptide molecules of interest, we encapsulated the peptides in the aqueous core of reverse micelles formed by sodium bis(2-ethylhexyl)sulfosuccinate (AOT) and isooctane (IO) at different water loadings. Using this reverse micellar platform, we systematically studied the conformation and aggregation properties of alanine-based peptides and amyloid forming segments derived from amyloid beta peptides and yeast prion protein Sup35 at different hydration levels. Our studies demonstrated that limited hydration facilitates aggregate formation in these peptides and that removal of water imposes a free energy barrier to peptide association and aggregation. These studies have implications for understanding aggregate/amyloid formation in vivo where macromolecular crowding can change the solvation status of the peptides. Furthermore, we examined how the folding dynamics of secondary/supersecondary structural elements are modulated by a crowded environment in comparison to that of dilute aqueous solutions. To this effect we studied the thermal stability and folding-unfolding kinetics of three small folding motifs, i.e., a 34-residue alpha-helix, a 34-residue cross-linked helix-turn-helix, and a 16-residue beta-hairpin, in the presence of crowding agents (i.e. inert high mass polymers). Our results indicate that the folding-unfolding transition of alpha-helical peptides is insensitive to macromolecular crowding. However, we find that crowding leads to an appreciable decrease in the folding rate of the shortest beta-hairpin peptide. We propose a model considering both the static and dynamic effects arising from the presence of the crowding agent to rationalize these results.

Degree Type

Dissertation

Degree Name

Doctor of Philosophy (PhD)

Graduate Group

Chemistry

First Advisor

DR. FENG GAI

Keywords

HYDRATION, MACROMOLECULAR CROWDING, PEPTIDE AGGREGATION, FOLDING
KINETICS, PEPTIDE CONFORMATION, REVERSE MICELLES

Subject Categories

Biochemistry | Biophysics

**EFFECT OF HYDRATION AND MACROMOLECULAR
CROWDING ON PEPTIDE CONFORMATION, AGGREGATION
AND FOLDING KINETICS**

Smita Mukherjee

A Dissertation

In

Chemistry

Presented to the Faculties of the University of Pennsylvania

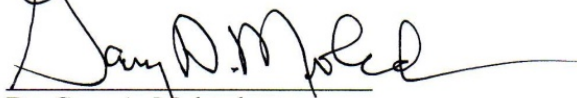
in Partial Fulfillment of the Requirements for the Degree of Doctor of Philosophy

2009



Dr. Feng Gai
Supervisor of Dissertation

Dr. Jeffery G. Saven
Committee Chair



Dr. Gary A. Molander
Graduate Group Chairperson

Dr. Ivan J. Dmochowski
Committee Member

Dr. Tobias Baumgart
Committee Member

DEDICATION

To My Family.

Acknowledgements

It has been a wonderful experience to be a graduate student at Penn. During my time here, I have been able to pursue my research interests because of the support, guidance, encouragement, and help that I have received from many people and I would like to thank each one of them.

I would like to express my deepest appreciation for my Ph.D. thesis advisor and mentor, Dr. Feng Gai. From the day I came to Penn as a prospective student to this very day, he has provided unwavering guidance and support to me. He has not only taught me to be a good scientist and ask pertinent questions but also the essence of knowing what one wants, paying attention to details, thinking practically and facing the world with confidence. I will forever appreciate him for providing a nurturing environment for me to grow as a scientist and more importantly as a strong individual.

I am also thankful to Drs. Jeffrey G. Saven, Ivan J. Dmochowski and Tobias Baumgart for serving as my committee members. I am fortunate to have had the opportunity to interact with them and benefit from their suggestions and insightful discussions. I also greatly appreciate my collaborators, Dr. William F. DeGrado, Dr. Daniel P. Raleigh and Humeyra Taskent for providing peptide samples and scientific inputs.

I would also like to thank the former and current members of the Gai Laboratory: Dr. Rolando Oyola, Dr. Pradipta Purkayastha, Dr. Pramit Chowdhury, Dr. Ting Wang, Dr. Yongjin Zhu, Dr. Deguo Du, Dr. Matthew Tucker, Dr. Yao Xu, Dr. Jia Tang, Dr. Michelle Bunagan, Jason Klemke, Lin Guo, Julie Rogers, Matthias Waegele, Arnaldo

Serrano, Kathryn Smith and Rob Culik for being such wonderful lab mates and friends. I would like to particularly thank Pramit for many scientific discussions, collaborations, guidance, and mentorship. In addition, I want to thank Michelle and Matthias for fruitful collaborations and all the current Gai group members and Michelle for critically reading the thesis.

I would also like to thank all my friends from Kolkata, Maryland and Philadelphia who have made my days as a graduate student a little less stressful and a little bit more fun. You guys are the best and I hope to continue our friendship for many more years to come!

Finally, I would like to thank my family: my wonderful and strong parents Tapan Kumar Mukherjee and Supriti Mukherjee, my thoughtful sisters Jayeeta and Sutapa, my fun and supportive brother-in-laws Jim and Rahul, my adorable niece and nephew Margo and Adi and finally my American mom Pat for providing unconditional love, encouragement, emotional support, happiness and care. I love you all with all my heart and I thank you so very much for being there for me for all these years.

ABSTRACT

EFFECT OF HYDRATION AND MACROMOLECULAR CROWDING ON PEPTIDE CONFORMATION, AGGREGATION AND FOLDING KINETICS

Smita Mukherjee

Prof. Feng Gai

Protein folding/misfolding *in vivo* takes place in a highly crowded and confined environment. Such crowded environment can possibly lead to fewer water molecules surrounding a protein of interest than that seen under *in vitro* conditions wherein typically dilute aqueous solutions are used. When considering the aforesaid cellular characteristics, such as water depletion and macromolecular crowding; it is reasonable to assume that proteins may experience different energy landscapes when folding *in vivo* than *in vitro*. Therefore, we have investigated how degrees of hydration and macromolecular crowding affect the conformation, aggregation and folding kinetics of short peptides.

In order to modulate the number of water molecules accessible to the peptide molecules of interest, we encapsulated the peptides in the aqueous core of reverse micelles formed by sodium bis(2-ethylhexyl)sulfosuccinate (AOT) and isooctane (IO) at different water loadings. Using this reverse micellar platform, we systematically studied the conformation and aggregation properties of alanine-based peptides and amyloid forming segments derived from amyloid beta peptides and yeast prion protein Sup35 at

different hydration levels. Our studies demonstrated that limited hydration facilitates aggregate formation in these peptides and that removal of water imposes a free energy barrier to peptide association and aggregation. These studies have implications for understanding aggregate/amyloid formation *in vivo* where macromolecular crowding can change the solvation status of the peptides. Furthermore, we examined how the folding dynamics of secondary/supersecondary structural elements are modulated by a crowded environment in comparison to that of dilute aqueous solutions. To this effect we studied the thermal stability and folding-unfolding kinetics of three small folding motifs, i.e., a 34-residue α -helix, a 34-residue cross-linked helix-turn-helix, and a 16-residue β -hairpin, in the presence of crowding agents (i.e. inert high mass polymers). Our results indicate that the folding-unfolding transition of alpha-helical peptides is insensitive to macromolecular crowding. However, we find that crowding leads to an appreciable decrease in the folding rate of the shortest β -hairpin peptide. We propose a model considering both the static and dynamic effects arising from the presence of the crowding agent to rationalize these results.

Table of Contents

DEDICATION.....	.ii
Acknowledgements	iii
ABSTRACT.....	v
Table of Contents	vii
List of Tables	xi
List of Figures.....	xii
Chapter 1: Introduction	1
1.1 Role of Water in Protein Folding.....	2
1.2 The Effect of Crowding on Protein Folding	4
1.3 The Effect of Confinement on Protein Folding	6
1.4 Model System: Reverse Micelles.....	7
1.5 Outline of the Thesis	11
Chapter 2: Experimental Methods and Materials.....	17
2.1 Static Spectroscopic Methods	17
2.1.1 Circular Dichroism.....	17
2.1.2 Infrared Spectroscopy.....	19
2.1.3 Transmission Electron Microscopy	23

2.1.4	<i>Dynamic Light Scattering</i>	24
2.2	Time Resolved Spectroscopic Methods	25
2.2.1	<i>Laser-Induced Temperature-jump Infrared Spectroscopy</i>	25
2.3	Materials and Methods	26
2.3.1	<i>Peptide Synthesis and Purification</i>	26
2.3.2	<i>Sample Preparation</i>	27
2.3.3	<i>Circular Dichroism Spectroscopy</i>	28
2.3.4	<i>Fourier Transform Infrared Spectroscopy</i>	29
2.3.5	<i>Transmission Electron Microscopy</i>	30
2.3.6	<i>Dynamic Light Scattering</i>	30
2.3.7	<i>T-Jump Infrared Spectroscopy</i>	30
Chapter 3: Effect of Hydration on the Amide I band of Helical Peptides		34
3.1	Introduction	35
3.2	Experimental Methods	37
3.3	Results	38
3.4	Discussion	40
3.5	Conclusions	44

Chapter 4: Probing the Site-Specific Hydration Status of a Peptide Inside a Membrane-Mimetic Environment	48
4.1 Introduction.....	50
4.2 Experimental Methods	52
4.3 Results and Discussion	54
4.4 Conclusions.....	62
Chapter 5: Effect of Hydration on the Helicity and Aggregation Properties of Five Alanine-Based Peptides	69
5.1 Introduction.....	71
5.2 Experimental Methods	74
5.3 Results and Discussion	75
5.4 Conclusions.....	86
Chapter 6: Effect of Limited Hydration on the Aggregation Kinetics of Two Amyloidogenic Peptides.....	93
6.1 Introduction.....	94
6.2 Experimental Methods	95
6.3 Results and Discussion	98
6.4 Conclusions.....	105

Chapter 7: Folding Kinetics of Naturally Occuring Helical Peptides.....	111
7.1 Introduction.....	113
7.2 Experimental Methods	115
7.3 Results.....	116
7.4 Discussion	119
7.5 Conclusions.....	123
Chapter 8: Effects of Crowding on the Folding Dynamics of Protein Secondary and Supersecondary Structures	129
8.1 Introduction.....	131
8.2 Experimental Methods	134
8.3 Results.....	136
8.4 Discussion	139
8.5 Conclusions.....	149
Chapter 9: Summary and Future Directions	163
REFERENCES.....	170

List of Tables

Table 4.1 Band position (ν) and full width at half-maximum ($\Delta\nu$) of the stretching vibration of $C\equiv N$ in MPx-CNy peptides.....	63
Table 8.1 Summary of the thermodynamic and kinetic data for Z34C-m1 and trpzip4-m1 obtained under different conditions.....	151
Table 8.2 Translational diffusion times determined by FCS at room temperature for R6G, the pHLIP peptide, and the HSA-NR complex.....	152

List of Figures

Figure 1.1 Crowded cellular environment.....	13
Figure 1.2 Excluded and available volume.....	14
Figure 1.3 Contrast between confinement and crowding.....	15
Figure 1.4 Structure of a reverse micelle and AOT molecule.....	16
Figure 2.1 Time-resolved laser-induced temperature-jump infrared set-up.....	32
Figure 2.2 Time-resolved absorption profile of D ₂ O after a temperature-jump.....	33
Figure 3.1 FTIR spectra of AKA ₂ and AKA ₆ at $w_0 = 6$	45
Figure 3.2 FTIR spectra of SPEAA in D ₂ O and at $w_0 = 6$	46
Figure 3.3 FTIR spectra of AKA ₂ and AKA ₆ at $w_0 = 10$ and 20.....	47
Figure 4.1 CD data of MPx-CN5 in water and at $w_0 = 6$ and 20.....	64
Figure 4.2 FTIR spectra of Phe _{CN} at $w_0 = 6, 20$, and 30.....	65
Figure 4.3 FTIR spectra of MPx-CNy peptides at $w_0 = 6$	66
Figure 4.4 FTIR spectra of MPx-CN5 at $w_0 = 6$ and 20.....	67
Figure 4.5 Orientation and location of the MPx peptide inside AOT reverse micelle....	68
Figure 5.1 CD data of AKA ₁ peptide in buffer and at $w_0 = 6$	87
Figure 5.2 Size distribution of reverse micelles	88
Figure 5.3 CD data for AKA ₃ peptide in buffer and at $w_0 = 4, 6, 10$, and 20.....	89
Figure 5.4 CD data for AKA _n peptides at $w_0 = 6$	90
Figure 5.5 FTIR spectra of AKA ₂ and AKA ₆ at $w_0 = 6$ and D ₂ O.....	91
Figure 5.6 FTIR spectra of AKA ₂ and AKA ₆ at $w_0 = 10$ and 20.....	92
Figure 6.1 Amide I' bands and CD spectra of A β ₁₆₋₂₂ and Sup35 ₇₋₁₃ peptides in D ₂ O...	106

Figure 6.2 Amide I' bands of A β ₁₆₋₂₂ and Sup35 ₇₋₁₃ peptides at $w_0 = 6$	107
Figure 6.3 Amide I' bands of Sup35 ₇₋₁₃ and A β ₁₆₋₂₂ peptides at $w_0 = 10$	108
Figure 6.4 Amide I' bands of Sup35 ₇₋₁₃ and A β ₁₆₋₂₂ at $w_0 = 20$	109
Figure 6.5 TEM images of A β ₁₆₋₂₂ -AOT reverse micelles and AOT reverse micelles at $w_0 = 6$	110
Figure 7.1 Ribbon representation of the structure of ribosomal protein L9.....	124
Figure 7.2 CD data for L9:41-74 and L9:48-64.....	125
Figure 7.3 FTIR data for L9:41-74.....	126
Figure 7.4 A representative <i>T</i> -jump relaxation trace of L9:41-74.....	127
Figure 7.5 Arrhenius plot of the <i>T</i> -jump induced conformational relaxation rates of L9:41-74.....	128
Figure 8.1 CD data for L9:41-74 in different media.....	153
Figure 8.2 CD data and Arrhenius plot of the <i>T</i> -jump induced conformational relaxation rates of L9:41-74 in different media.....	154
Figure 8.3 Representative <i>T</i> -jump relaxation traces of L9:41-74 in different media....	155
Figure 8.4 CD data for Z34C-m1 in different media.....	156
Figure 8.5 CD data and Arrhenius plot of the <i>T</i> -jump induced conformational relaxation rates of Z34C-m1 in different media.....	157
Figure 8.6 Far-UV CD data for trpzip4-m1 in different media.....	158
Figure 8.7 CD thermal melting curves of trpzip4-m1 in different media.....	159
Figure 8.8 Representative <i>T</i> -jump relaxation traces of trpzip4-m1 in Dextran 70.....	160
Figure 8.9 Arrhenius plot of the <i>T</i> -jump induced conformational relaxation rates of trpzip4-m1 in different media.....	161
Figure 8.10 Relative diffusion time of R6G versus Ficoll 70 concentration.....	162

Chapter 1: Introduction

The dilute aqueous solution used in most *in vitro* studies of protein folding is markedly different from the aqueous environment inside cells in which proteins have evolved to fold and function (Luby-Phelps, 2000). In a cellular environment, proteins often co-exist with a high concentration of soluble macromolecules and/or structural arrays (Figure 1.1), which collectively occupy between 10 to 40% of the total fluid volume of the cell (Fulton, 1982; Zimmerman and Trach, 1991). Such biological fluid media are often regarded as “crowded” rather than concentrated because no single macromolecule is present as the dominant species. Such a crowded environment could lead to a decrease in the number of water molecules surrounding a particular protein, in comparison to that observed under conditions where complete hydration of the peptide can occur. Moreover, the aqueous medium and its solutes are often found to be confined within nanometer sized compartments inside the cell. In light of these intrinsic features of the cellular environment, such as water depletion, crowding, and confinement, it is reasonable to assume that proteins may experience a different folding energy landscape *in vivo* than in the dilute aqueous solutions that are usually employed for *in vitro* studies (Ellis, 2001a; Minton, 2006). Motivated by the above considerations, in this thesis we investigate how degrees of hydration and macromolecular crowding affect the conformation, aggregation and folding dynamics of small peptides. Results from these studies provide new insights into our understanding of factors that control the free energy landscape of peptide folding and aggregation. Below we provide the necessary

background information relevant to the studies presented in this thesis as well as an outline of the thesis.

1.1 Role of Water in Protein Folding

A survey of the current literature on protein-water interactions provides a large body of evidence supporting the distinct role played by water molecules in protein folding at both the thermodynamic and kinetic levels (Levy and Onuchic, 2006; Mattos and Clark, 2008). In the process of protein folding, water is known to mediate the collapse of the extended polypeptide chain. The hydrophobic effect, as proposed by Kauzmann (Kauzmann, 1959), is driven by the unfavorable entropy decrease caused by the formation of ordered water structures near the surface of nonpolar groups. This unfavorable interaction, among other factors, guides the polypeptide chain to collapse, forming a tightly packed core containing mostly nonpolar side chains of the protein (Lesser and Rose, 1990), so as to minimize the solvent exposed hydrophobic surface. Furthermore, the hydrogen bond donors and acceptors present in the extended polypeptide backbone also to some extent restrict the motions of the water molecules in the unfolded state. These water molecules are released upon folding and this gain in translational entropy of water compensates considerably for the loss of conformational entropy of the protein (Harano and Kinoshita, 2004).

The process of protein folding is accompanied by a series of desolvation steps. However, exactly when the majority of water molecules are removed during folding is still a matter of debate. For example, one model suggests that the initiation of folding is accompanied by a reduction in water density at key nucleation sites which is followed by

the spontaneous collapse of the polypeptide chain to reduce the solvent-accessible hydrophobic area. In fact, such a dewetting transition has been shown to provide a large driving force towards the collapse of the melittin tetramer (Liu et al., 2005). Several other proteins have also been shown to undergo a dewetting transition at a late stage in folding (Hua et al., 2007). Another model suggests that the initial collapse of the extended yet hydrated polypeptide chain is followed by water expulsion from the hydrophobic core (Cheung et al., 2002; Guo et al., 2003). For example, it has been shown for the SH3 domain that after the fully solvated polypeptide undergoes an initial collapse to a native-like topology, there is a final obligatory dehydration step in which “water molecules are cooperatively squeezed out from the partially hydrated protein core” resulting in a dry, packed protein (Cheung et al., 2002). It has been proposed that the presence of a hydrated core may assist in the search for the protein native topology. Water molecules in the hydrated protein core may form bridging hydrogen bonds with polar backbone amides and charged side chains which confer flexibility to the protein for conformational rearrangements. This lubrication provided by the water molecules facilitates the formation of an optimally packed hydrophobic core (Sheinerman and Brooks, 1998; Cheung et al., 2002; Shea et al., 2002). Furthermore, it has been shown that incorporation of desolvation barriers in folding simulations can result in increased protein stability and rate of protein folding in comparison to simulations carried out in the absence of desolvation barriers. This happens because water molecules decrease energetic frustrations during the process of folding by favoring folding pathways that are well-defined and productive (Sessions et al., 2004). Although the role of water in protein

aggregation is yet to be fully ascertained, it is quite likely that desolvation is an important step along the course of protein association and subsequent aggregation/fibrillization. Recent computer simulation studies have alluded to the fact that expulsion of interfacial water molecules to be a key event in the dimerization/oligomerization of amyloid β (A β) peptides (Klimov and Thirumalai, 2003; Tarus et al., 2005). In an attempt to provide further insight into this feature, we have systematically investigated the aggregation properties of several peptides, including alanine-based peptides and amyloid forming segments derived from amyloid β peptides and yeast protein Sup35, under different degrees of hydration. Results from these studies will be discussed in Chapters 4 and 5.

1.2 The Effect of Macromolecular Crowding on Protein Folding

Most *in vitro* studies of protein folding are conducted under conditions wherein only dilute aqueous solutions are used. However, these idealized *in vitro* conditions are vastly different from those encountered within the cell. The cellular environment is crowded (Figure 1.1) due to the presence of high concentration of soluble and insoluble macromolecules which occupy 10-40% of the total fluid volume of the cell (Fulton, 1982; Zimmerman and Trach, 1991). One nonspecific interaction that is always present in a crowded environment is steric repulsion, arising from the excluded volume effect as illustrated in Figure 1.2. Depending on the size and shape of a test protein and the volume density, size and shape of the macromolecules present in the vicinity of a test protein, the thermodynamic activity of a test protein can increase by several orders of magnitude in a crowded biological medium (Minton, 1983; Zimmerman and Minton, 1993). Therefore, the equilibrium and rate constants observed for protein folding reactions in a crowded

environment can be quite different from those measured under dilute conditions. Due to excluded volume effects, the configurational entropy of macromolecules decreases in a crowded environment. This affects the extended unfolded state more than the compact native state. Theoretical studies have shown that macromolecular crowding therefore enhances the stability of the native state by destabilization of the unfolded state through an entropic mechanism. As a result, macromolecular crowding leads to an increase in the folding rates as it effectively decreases the free energy barrier to folding (Cheung et al., 2005; Minton, 2005). Although, the extent to which macromolecular crowding stabilizes the native state is still under debate (Zhou, 2004; Minton, 2005), the theoretical predictions stated above have been confirmed by several experimental studies (Van den Berg et al., 1999; Qu and Bolen, 2002; Sasahara et al., 2003; Ai et al., 2006; McPhie et al., 2006; Perham et al., 2007; Stagg et al., 2007). To simulate macromolecular crowding conditions for *in vitro* experiments, inert high mass polymers, referred to as crowding agents, are added as cosolutes in the aqueous medium along with the protein of interest. For example, using such crowding agents it has been shown that the presence of crowders can increase the stability of proteins such as lysozyme, ribonuclease A, apoflavodoxin and apomyoglobin against thermal and chemical denaturation (Sasahara et al., 2003; Tokuriki et al., 2004; Stagg et al., 2007) and increase the fast phase of the refolding kinetics of the hen lysozyme by 2-5 fold (Van den Berg et al., 2000). While these experimental studies have provided invaluable insight into the effect of crowding on the stability and folding rates of protein tertiary structures, almost none of the experimental studies have considered how macromolecular crowding will affect protein folding dynamics at the secondary structure level. This topic will be explored in detail in Chapter

8 where we consider both static (excluded volume) effects and dynamic (viscosity) effects arising from the presence of crowding agents to explain our observed results.

1.3 The Effect of Confinement on Protein Folding

Understanding the effects of confinement on the thermodynamics and folding kinetics of proteins is important because proteins *in vivo* are often found in confined spaces such as the chaperonin cavity, the proteosome, the ribosome exit tunnel, the translocon, etc. Such spatial confinement restricts the conformational space available to a protein, an effect akin to volume exclusion as described in section 1.2. However, geometrical confinement is related to but also distinct from macromolecular crowding. Under confinement, a particular protein can strictly sample volumes accessible within the confining “cage,” whereas in a crowded environment the available volume for that protein is found dispersed in space and therefore the protein can explore many different interstitial void spaces, especially given the possibility of density fluctuations of the crowding particles (Figure 1.3). This implies that the extent of destabilization of the denatured state ensemble via entropic mechanism is greater for proteins placed in a confined environment than in a crowded environment (Zhou, 2004).

Effects of confinement on protein folding have been studied both analytically and via simulation methods (Zhou and Dill, 2001; Klimov et al., 2002; Baumketner et al., 2003; Takagi et al., 2003; Zhou, 2004; Ziv et al., 2005; Hayer-Hartl and Minton, 2006; Rathore et al., 2006; Mittal and Best, 2008). The results from these studies predict that spatial confinement reduces the conformational entropy of the denatured state ensemble which leads to relative stabilization of the folded state and an increased rate of folding.

These theoretical predictions have been confirmed by experimental studies. Eggers and Valentine demonstrated that encapsulation of proteins in silica matrix results in dramatic enhancement of stability for folded proteins such as α -lactalbumin (Eggers and Valentine, 2001b; Eggers and Valentine, 2001a). Similar conclusions were also reached in experimental studies conducted by Ravindra et al. in which they confined ribonuclease A in silica glass and observed that the melting temperature of the protein increased by ~ 30 °C. In Chapters 3-6, we examine in detail the effects of encapsulating small peptides in the aqueous core of reverse micelles where we consider factors beyond confinement effects, such as hydration effects, in order to rationalize our results.

1.4 Model System: Reverse Micelles

In light of the important role played by water molecules in protein folding (see section 1.1), a systematic examination is warranted regarding the effect of degrees of hydration on the conformational properties of small peptides. In order to achieve this, we have used reverse micelles as a platform to modulate the number of water molecules accessible to the peptide molecule of interest. Below we give a brief overview on reverse micelles in order to facilitate further discussion in the remaining Chapters.

Reverse micelles are aggregates formed by the self-assembly of various surfactant molecules in nonpolar organic solvents. As shown in Figure 1.4, structurally reverse micelles have an external shell made by the hydrocarbon chains of the surfactant molecules extending into the apolar organic medium while the polar or charged head groups aggregate to form a polar core. The latter is known to solubilize water and therefore has been widely used as a means of providing a confined aqueous environment.

The amount of water solubilized in the polar core can be systematically varied. In practice it is done by changing the w_0 value, which is the ratio of the molar concentration of water to that of surfactant ($w_0 = [\text{H}_2\text{O}]/[\text{Surfactant}]$) (Maitra, 1984; Luisi et al., 1988). At a constant surfactant concentration, increasing the water content will result in a larger polar core. On the other hand, increasing surfactant concentration at a constant water concentration will result in smaller reverse micelles. If the water and surfactant concentration is increased at a constant ratio, then the number of individual reverse micelles will increase.

Many different surfactants, nonpolar phases, and polar phases have been utilized to form reverse micelles. One of the most well-characterized reverse micelles system is formed by sodium bis(2-ethylhexyl) sulfosuccinate (AOT) (Figure 1.4B), isooctane (IO) and water (Pileni, 1993; De and Maitra, 1995). This reverse micellar system has been used to conduct the experiments described in Chapters 3-6. The structure of individual AOT reverse micelle has been characterized using many different techniques such as NMR, dynamic light scattering, small angle X-ray and neutron scattering techniques (Zulauf and Eicke, 1979; Gulari et al., 1980; Kotlarchyk et al., 1984; Maitra, 1984; Luisi et al., 1988; De and Maitra, 1995; Bohidar and Behboudnia, 2001). The radius of the polar core of the AOT reverse micelles depends on the w_0 value (Luisi et al., 1988) and can be approximated to:

$$\text{Radius of water core (in nm)} = (0.175) * w_0$$

The polydispersity of the droplet radius (as indicated by the polydispersity parameter ($\gamma = 0.035$) in dynamic light scattering measurements) of AOT reverse micelles is very low

(Christ and Schurtenberger, 1994). Previous studies have shown that temperature does have an effect on the size of the micelles. However, such an effect has been shown to be minimal for reverse micelles of low w_0 values (Zulauf and Eicke, 1979) as has been used to conduct the experiments presented in this thesis.

The water distribution inside reverse micelles is heterogeneous in nature. It has been widely suggested that three types of water populations exist in reverse micelles and are often referred to as (a) bound water (i.e., bound to AOT head groups), (b) trapped water (i.e., trapped between polar head groups of surfactant molecules at the interface), and (c) free water (i.e., located in the center region of the cavity) (Maitra, 1984; Jain et al., 1989; Onori and Santucci, 1993; Faeder and Ladanyi, 2000; Venables et al., 2001; Cringus et al., 2005; Nucci and Vanderkooi, 2005; Dokter et al., 2006; Piletic et al., 2006; Cringus et al., 2007; Levinger and Swafford, 2009). There are very few “free” water molecules in reverse micelles of $w_0 \leq 10$. For example, at $w_0 = 6$, there are approximately 300 water molecules in the reverse micellar core, of which about 32% is considered ‘free’ and is capable of interacting with any guest molecules solubilized in the aqueous core of the reverse micelles (Chowdhury et al., 2000). As the w_0 value increases, the amount of free water molecules also increases (Maitra, 1984).

Various proteins have been solubilized in the AOT/IO/H₂O reverse micellar system (Luisi, 1985; Nicot et al., 1985; Luisi et al., 1988; Matzke et al., 1992; Shastry and Eftink, 1996; Wand et al., 1998; Raghuraman and Chattopadhyay, 2003; Mukherjee et al., 2007a; Mukherjee et al., 2009). Solubilization of proteins is achieved by three different methods as follows (Luisi et al., 1988):

- 1) Direct injection of a concentrated aqueous solution of protein into the organic solution containing surfactant molecules. The amount of water injected is determined by the intended w_0 value.
- 2) Addition of dry lyophilized protein to the reverse micelle solution at a particular w_0 value. This method is suitable for dissolving proteins that cannot be solubilized at very high concentrations in water.

If the correct conditions are chosen (i.e. temperature, concentration of protein and water content), the above two methods can be used to obtain a clear solution simply by gentle shaking or stirring. These two methods have been used in Chapters 3-6 to solubilize the peptides in reverse micelle solutions.

- 3) Phase-transfer between the bulk aqueous protein solution phase and the supernatant phase containing the surfactant and organic medium. This method is often used to quantitatively extract proteins into the organic micellar phase (Leser and Luisi, 1990).

The AOT/IO reverse micelles are dynamic in nature; colliding with each other in solution and occasionally allowing entrapped solute molecules to move from one polar core to another. It is proposed that the exchange process between the discrete reverse micelles happens through the transient fusion of two reverse micelles to form a short-lived “dimer droplet” (Fletcher, 1987). During the lifetime of this dimer species, the solubilized materials can randomly redistribute, followed by subsequent fission of the dimer (Luisi et al., 1988).

Experimentally a systematic variation of the degree of hydration of peptides is not easily achievable. However, as described above, one can control the water content present in the nanometer sized polar core of the AOT reverse micelles by changing the w_0 values. Therefore, we have used AOT reverse micelles at different water loadings as a unique platform for investigating how degrees of hydration affect the conformation of small peptides confined in the aqueous core of the reverse micelles.

1.5 Outline of the Thesis

In this thesis we have used spectroscopic tools to elucidate how degrees of hydration and macromolecular crowding affect the conformation, aggregation and folding kinetics of small peptides. The following Chapter will explain the techniques and the materials used to conduct the experiments that are described in the remainder of the thesis. Chapter 3 examines how degrees of hydration affect the underlying spectral features of the amide I' band of two alanine-based helical peptides at low temperatures. Chapter 4 shows how local and global infrared reporters can be used to probe the conformation and hydration status of an antimicrobial peptide in a membrane-mimetic environment. The procedure described in this Chapter is useful for determining the location of the peptide inside reverse micelles. Chapter 5 explores how hydration levels modulate the helicity and aggregation properties of five alanine-based peptides. Chapter 6 describes the effect of dehydration on the aggregation properties of two small amyloidogenic peptides. Chapter 7 discusses the study of a naturally occurring helical peptides stabilized by side chain-side chain interactions, the folding of which has important implications for the sequence dependence of secondary structure formation.

Chapter 8 details the effect of macromolecular crowding on the folding dynamics of protein secondary and supersecondary structural elements like naturally occurring monomeric α -helix, cross-linked helix-turn-helix motif and β -hairpin structure. Chapter 9 provides a summary of the work presented in this thesis as well as suggestions for future work that may be pursued.

Figure 1.1 Crowded and confined cellular interiors. (A) Using the technique of cryoelectron tomography, direct evidence for the crowded state of eukaryotic cell interiors is provided. The three-dimensional reconstruction of a part of the cytoplasm of a *Dictyostelium discoideum* cell is shown here. Actin filaments are depicted in orange, ribosomes and other macromolecular assemblies in grey, and membrane structures in blue. This figure is adapted from ref. (Medalia et al., 2002). (B) Cartoon of eukaryotic cytoplasm at a magnification of 10^6 X. The test protein molecule (*red*) is in a fluid medium that is crowded by soluble proteins (*green*), RNA species (*yellow*), and ribosomes (*pink*) and confined by cytoskeletal fibers (*blue*). This figure is adapted from ref. (Minton, 2001) and is a modified version of an illustration by Goodsell (Goodsell, 1994).

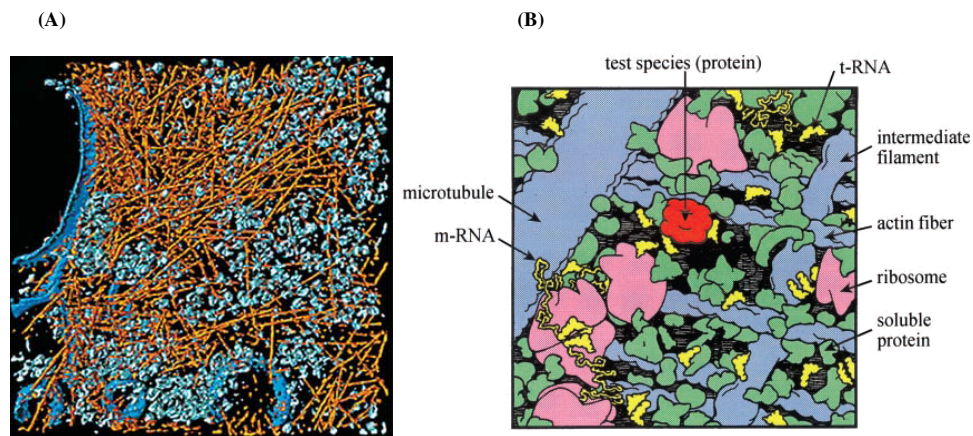


Figure 1.2 Excluded (pink and black) and available (blue) volume in a solution of spherical background macromolecules. (A) Volume available to a test molecule of infinitesimal size. (B) Volume available to a test molecule of size comparable with background molecules. This figure has been adapted from ref. (Minton, 2001).

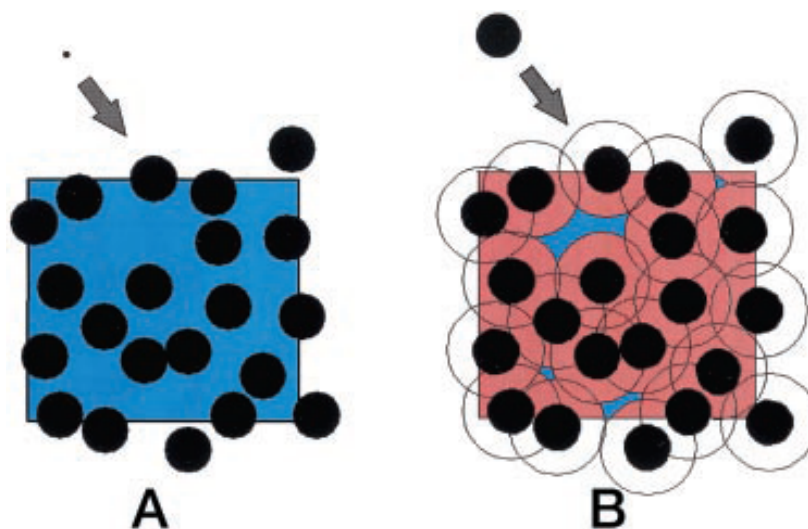


Figure 1.3 The contrast between (A) confinement and (B) crowding. In confinement a protein chain is restricted to a single cage, but in crowding the protein's accessible volumes are dispersed throughout space. This figure is adapted from ref (Zhou, 2004).

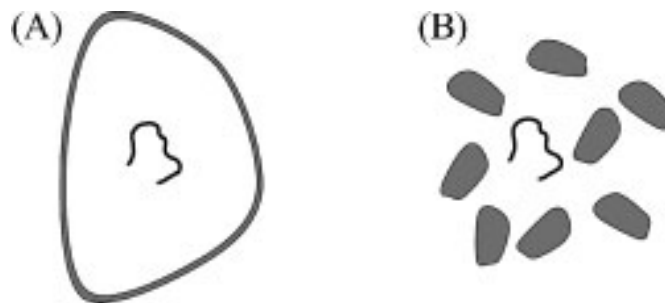
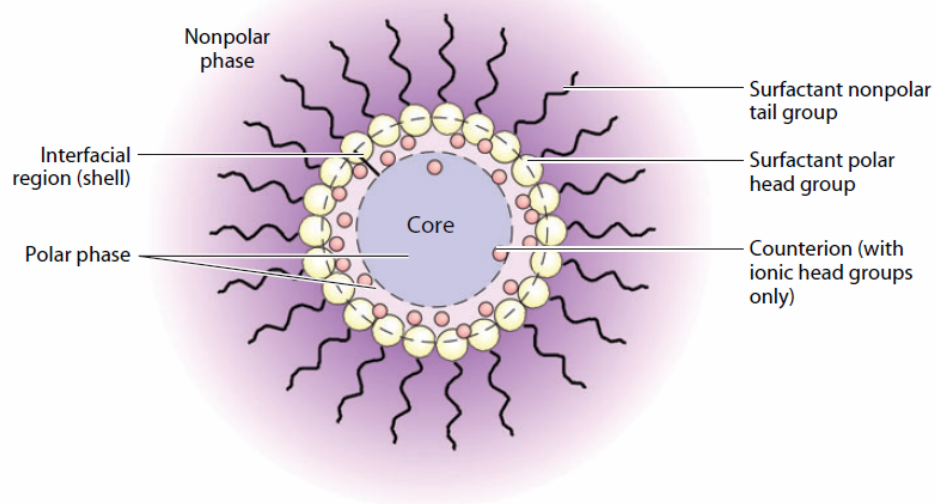
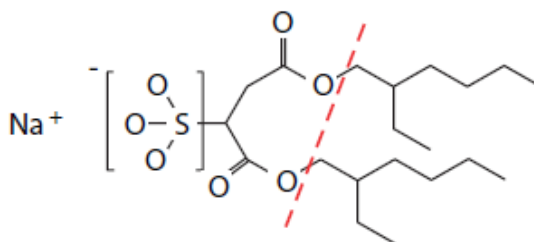


Figure 1.4 (A) Structure of a reverse micelle. (B) Structure of sodium bis(2-ethylhexyl) sulfosuccinate (AOT). The surfactant head group is on the left of the red line and the tail is on the right of the red line. This figure has been adapted from ref. (Levinger and Swafford, 2009).

(A)



(B)



Chapter 2: Experimental Techniques and Methods

The methods and techniques and the materials that were either synthesized or purchased in order to conduct the studies presented in the following Chapters are briefly discussed here.

2.1 Static Spectroscopic Methods

2.1.1 Circular Dichroism

Circular dichroism (CD) is a measure of the optical activity of molecules and reflects the difference in the absorption of the left and right circularly polarized components of plane polarized light. The CD signal of a particular chromophore is observed in the same spectral window as its absorption bands. CD spectroscopy is a useful technique for the study of protein secondary structure because in the far-UV region the amide protein backbone serves as the chromophore and has two electronic transitions, a weak but broad $n \rightarrow \pi^*$ and relatively intense $\pi \rightarrow \pi^*$. The $n \rightarrow \pi^*$ transition gives rise to a CD absorbance around 210 -230 nm and involves the non-bonding electrons of the carbonyl. The $\pi \rightarrow \pi^*$ transition yields absorbance in the region from 180 -200 nm and involves the π -electrons of the amide bond with a transition dipole in the plane of the amide oriented approximately in the N-O direction (ed.Berova et al., 2000). Different secondary structural elements corresponding to different chiral environments of the amide chromophores give rise to distinct characteristic bands in the far-UV CD spectra. The three-dimensional arrangement of all the amide chromophores present in a protein affects the collective electronic structure and hence the far-UV CD spectrum of a protein. Below

we briefly outline the expected CD spectral features that will be helpful in understanding some of the results presented in the following Chapters.

α -Helix: The α -helix is a dominant secondary structure in many proteins and exhibits characteristic CD spectrum with a negative band at 222 nm and 208 nm and a positive band at 192 nm. The band at 222 nm is due to the $n \rightarrow \pi^*$ transition while the 208 nm and 192 nm band results from the exciton splitting of the $\pi \rightarrow \pi^*$ transition (ed.Havel, 1996; Chin et al., 2002; Woody, 2005).

β -sheet: The shape of the β protein show weaker and more dissimilar spectra than the helical proteins. The shape of the CD spectrum the β protein depends among other factors on the length and orientation of the strands and the twist of the sheets. Most CD spectra of β structures have a negative band near 216 nm due to the peptide $n \rightarrow \pi^*$ transition and the positive band near 195 nm which is attributed to the $\pi \rightarrow \pi^*$ transition (ed. Havel, 1996; ed. Berova et al., 2000).

Unfolded conformations: Unfolded peptides generally show weak CD signals with a positive band at 212 nm and a negative band at 195 nm (ed. Havel, 1996; ed. Berova et al., 2000).

Aromatic chromophores: The near UV-CD spectrum reports on the chiral environment of aromatic residues such as phenylalanine, tryptophan and tyrosine and their characteristic bands help in detecting changes in the environment of the aromatic residues due to conformational changes in the protein (Sreerama and Woody, 2004). In addition to near-UV absorption, aromatic residues in close proximity have often been shown to absorb in the far-UV region. For instance, the excitonic coupling of paired

tryptophan side chains has been shown to give rise to a positive band around ~229 nm (Grishina and Woody, 1994). This unique feature of the tryptophan residues will be used in Chapter 8 to measure the thermodynamic stability of β hairpin peptides.

2.1.2 Infrared Spectroscopy

Infrared (IR) absorption originates from the interaction of electromagnetic waves with molecular vibrations. As a protein contains several normal modes of vibration, the IR spectra of a protein can be quite complex with many overlapping bands. However, as will be discussed below, it is still possible to use infrared spectroscopy to analyze the structure and conformation of a protein (Surewicz et al., 1993). The backbone amide groups and amino acid side chains produce IR active vibrations in the mid-IR region.

The amide moiety of the peptide linkage gives rise to characteristic IR absorption bands, namely, amide A, B and I-VII (Krimm *et al.* 1986). However, for secondary structure determination the vibrational mode that is most extensively used is the amide I vibrational mode ($1600 - 1700 \text{ cm}^{-1}$) which arises mainly from the C=O stretching vibration with some contributions from the out-of-phase CN stretch, the CCN deformation, and the NH in-plane bend. The predominant localization of the amide I mode to the C=O stretch allows practical analysis of this vibrational band for conformational studies and is much less complicated than the other modes mentioned above. More importantly, the fundamental property that renders the amide I vibration useful as a conformational probe is its dependence on structure-sensitive factors such as transition dipole coupling (TDC) and the absorption frequency is sensitive to hydrogen bonding and through bond coupling (Krimm and Bandekar, 1986; Barth and Zscherp,

2002). TDC is a resonance interaction between the oscillating dipoles of neighboring amide groups and it depends on the relative orientations and separation distance between the dipoles and thus provides information about the geometrical arrangement of the peptide groups in a protein. TDC gives rise to two effects, namely exciton transfer (Hamm et al., 1998) and band splitting (Abe and Krimm, 1972). TDC is responsible for the large splitting observed for the amide I band of anti-parallel beta sheet structures; a spectral feature that will be used to explain the experimental results presented in Chapters 4 and 6. Furthermore, formation of intermolecular hydrogen bonds with solvent molecules can also significantly affect the amide I frequency of a given secondary structural element. Water-backbone hydrogen bonding results in the reduction of the force constant of the corresponding amide C=O stretching vibration, thereby leading to a shift of the amide I transition to a lower frequency. For example, it is well known that fully hydrated monomeric helices exhibit an amide I band centered at $\sim 1630\text{ cm}^{-1}$, whereas helices buried in the interior of a protein absorb at $\sim 1650\text{ cm}^{-1}$ (Barth and Zscherp, 2002; Walsh et al., 2003; Wang et al., 2004; Mukherjee et al., 2007b). This sensitivity of the amide I band to hydration will be used to explain the results obtained in Chapters 3-5.

Different secondary structures give rise to characteristic absorption frequency of the amide I band. Following are some of the general observations regarding the amide I band positions of different protein secondary structures. Solvated and buried α -helical amides typically absorb at 1630 and 1650 cm^{-1} respectively; parallel β -sheets absorb at $\sim 1630\text{ cm}^{-1}$, anti-parallel β -structures exhibit band splitting which yields two bands at

1620 and 1680 cm^{-1} and unstructured amides typically yield a broad absorbance at $\sim 1645 \text{ cm}^{-1}$ (Susi and Byler, 1987; Surewicz et al., 1993; Haris and Chapman, 1994; Barth and Zscherp, 2002; Walsh et al., 2003). Since the amide I bands of the different secondary structures are highly overlapping, a broad featureless spectrum is usually recorded for proteins with many different secondary structures. Therefore, resolution enhancement methods such as Fourier self-deconvolution and second derivative analysis is frequently done to identify and assign the dominate bands in the protein spectra (Surewicz et al., 1993).

The IR absorption of amino acid side chain (Barth, 2001; Barth and Zscherp, 2002) provides information regarding the local environment of a particular side chain such as the protonation state, coordination of cations and hydrogen bonding. For example, the carbonyl group of protonated carboxyl groups absorb at 1710-1790 cm^{-1} . Such a diagnostic band for protonation of carboxyl groups which is free from overlapping backbone IR absorption bands will be useful for studying proton pathways in proteins (Rothschild, 1992; Maeda, 1995).

In order to gain site-specific conformational information for positions throughout the protein sequence, isotope (^{13}C) labeling of individual residues can be done because incorporation of ^{13}C -labeled carbonyl into a peptide backbone causes the amide I band of that residue to shift to a lower frequency by $\sim 40 \text{ cm}^{-1}$, thereby creating a new spectral feature in the IR spectrum (Fabian et al., 1996; Ludlam et al., 1996; Decatur and Antonic, 1999; Cheng et al., 2001; Huang et al., 2001a; Decatur, 2006). Furthermore, non-natural amino acid such as *p*-cyano-phenylalanine can be incorporated in the protein sequence as

useful local probes of environment (e. g. hydrogen bonding environment) (Huang et al., 2003a; Tucker et al., 2004b). In Chapter 4, we have taken advantage of *p*-cyano-phenylalanine to probe the location of peptides in reverse micelles.

Water (H₂O) is one of the most ideal solvent for dissolving proteins. However, the bending vibration of water yields a strong IR absorbance band centered at 1643 cm⁻¹ with an molar absorptivity of 21.8 M⁻¹ cm⁻¹ (Veniaminov and Prendergast, 1997) which overlaps with the amide I band arising from the polypeptide backbone. To minimize the solvent interference, deuterated water (D₂O) is used instead. The combination mode of stretching and bending modes of D₂O absorbs at 1650 cm⁻¹, but the molar absorptivity is only 1.4 M⁻¹ cm⁻¹ and hence the solvent interference is much less than that of H₂O (Veniaminov and Prendergast, 1997). The amide I band measured in D₂O is designated as amide I' and the amide I' band positions are typically red-shifted by 5–10 cm⁻¹ due to deuteration of backbone hydrogens. Regardless of whether H₂O or D₂O is used, the solvent contribution to the infrared spectrum should be subtracted in order to measure the IR spectra of the protein itself. In order to achieve this we have used a two-compartment IR cell (described below) which allows us to take the IR spectra of the sample and background solutions under identical conditions. This has been done for all the IR spectra reported in this thesis.

Later in this Chapter we will discuss the application of IR spectroscopy in temperature-jump relaxation experiments. Other applications include attenuated total reflectance (Tucker et al., 2004b), stopped-flow IR spectroscopy (Tang and Gai, 2006), and two-dimensional IR spectroscopy (Hamm et al., 1999).

2.1.3 Transmission Electron Microscopy

Transmission electron microscopy (TEM) is an important technique widely used for material characterization and also for visualizing biological samples. The advantage of using TEM over light microscope is that it allows one to visualize the specimen at a higher resolution due to the small de Broglie wavelength of electrons. In a transmission electron microscope, a thin specimen (0.5 μm or less) is irradiated with electron beam of uniform current density. The electrons travel through the specimen and interact strongly with the atoms of the specimen and some of the electrons passing through the specimen are scattered. The electron-intensity distribution behind the specimen is focused and imaged with a system of electromagnetic lenses onto a fluorescence screen or recorded by direct exposure to a photographic film or detected by a sensor such as a charge couple device (CCD) camera. Contrast in this technique depends on the atomic number of the atoms present in the specimen because electron dense regions of the specimen will scatter more electrons, therefore those regions will appear dark in the image thereby increasing the contrast. Since biological specimens are composed of atoms of very low atomic number (mainly carbon, oxygen, nitrogen and hydrogen), to increase the contrast the samples are stained/shadowed with electron dense material like salts of heavy metals. For isolated macromolecules like DNA or large proteins, a thin film of heavy metal such as platinum is sprayed is evaporated onto the dried sample to enhance contrast and this procedure is called shadowing and is used to study the surface of a specimen by TEM. To observe finer details, negative staining is used. In this procedure the specimen is supported on a thin film of carbon on a copper grid and is washed with heavy metal salt

such as uranyl acetate. After drying the sample, a thin film of the metal covers the carbon film except where the adsorbed macromolecule is present. Since, the macromolecule allows more electrons to pass through in comparison to that of the surrounding heavy metal stain, a reversed or negative image of the molecule is formed (Williams and Carter, 1996; Sigle, 2005). In Chapter 6, we will use TEM to visualize the aggregates formed by peptides derived from amyloid β peptides.

2.1.4 Dynamic Light Scattering

Dynamic light scattering (DLS) (also known as Quasi Elastic Light Scattering [QELS] and Photon Correlation Spectroscopy [PCS]) is a laser based scattering technique that can be used to characterize the size distribution profile of particles (e.g. proteins, polymers, micelles, carbohydrates, nanoparticles, etc.) dispersed or dissolved in a liquid. It is an attractive technique used for size characterization of particles because it is non-invasive, data processing is fast and there is no need for extensive sample preparation. If the size of the particles (< 250 nm) is smaller than the wavelength of the light, then the light beam will be scattered uniformly in all directions (Raleigh scattering). When a laser light is passed through a solution containing the particles, it is possible to observe time-dependent fluctuations in the scattered intensity using a suitable detector. The fluctuations are due to constructive and destructive interference of light scattered by neighboring particles undergoing Brownian motion in the solution. Since, the fluctuations originate from particle motion; it contains information about the dynamic properties of the particles. Analysis of the time-dependent intensity fluctuations can provide information regarding the diffusion coefficient of the particle. If the viscosity of the

medium is known, then using the Stokes Einstein equation, the hydrodynamic radius of the particles can be calculated. In order to analyze the time dependence of the intensity fluctuations, a digital correlator is used and the resulting autocorrelation function can be analyzed in terms of particle size distribution by numerically fitting the data with calculations based on assumed distributions (Berne and Pecora, 1976; Schurr, 1977; Chu, 1992). In Chapter 5 we will use DLS to characterize the size distribution of reverse micelles.

2.2 Time Resolved Spectroscopic Measurements

2.2.1 Time-Resolved Laser-Induced T-jump Infrared Spectroscopy

A protein ensemble exists in an equilibrium between folded and unfolded states and this equilibrium shifts with temperature. A sudden rapid increase in temperature can therefore initially leave the protein ensemble in a conformational distribution that does not correspond to the equilibrium distribution at the new temperature. The resulting relaxation to the new, higher temperature equilibrium contains kinetic information regarding folding and unfolding. If a two state model is assumed (i.e. only folded or unfolded state exists), then the observed relaxation rate (k_R) is equal to the sum of the folding (k_F) and unfolding (k_U) rates, which can be separately determined via the temperature dependent equilibrium constant ($K_{eq} = k_F/k_U$) (Eigen and deMaeyer, 1963).

For initiating protein folding/unfolding reactions, laser-induced temperature jump (*T*-jump) technique can be implemented. Heating is accomplished by the excitation of the vibrational combination band of D₂O which is centered at ~1900 nm. The 1900 nm *T*-jump pulse can be provided by hydrogen Raman shifting the fundamental (1064 nm) of a

Nd:YAG Q-switched laser (Figure 2.1). Although the heating of the solvent is achieved in 10-20 picosecond, the time-resolution of the set-up is determined by both the laser pulse width and the detector rise time. For instance, the IR set-up depicted in the following section and used in experiments described in Chapters 7 and 8 possesses a time-resolution of ~20 ns which is ultimately determined by the rise time of the MCT detector.

The *T*-jump initiation method is advantageous in that it is generally applicable to all proteins and does not require significant amounts of protein sample. For example, a typical *T*-jump IR experiments in our lab requires 15 μ L of protein sample at a concentration of ~1 mM. Furthermore, the initiation is reversible; heat dissipation facilitates complete cooling in 0.1 seconds (Figure 2.2), thereby allowing repeated averaging for a specific initial temperature (and jump) as well as experiments at multiple initial temperatures. The *T*-jump technique has been used in conjunction with fluorescence spectroscopy (Ballew et al., 1996), in which the conformational probe is usually Trp, and IR spectroscopy (Dyer et al., 1998b), in which transient absorption changes are usually monitored at 1630 cm^{-1} where solvated helices and β -hairpin absorbs.

2.3 Materials and Experimental Methods

2.3.1 Peptide Synthesis and Purification

All the peptides that are used in the studies described in the remaining Chapters were synthesized using standard Fmoc-protocol on a PS-3 synthesizer (Protein Technologies Inc., MA) and cleaved using a 95% trifluoroacetic acid, 2.5% triisopropylsilane, and 2.5% water cleavage cocktail. The identities of all samples were

verified by electrospray mass spectroscopy or matrix-assisted laser desorption ionization (MALDI) mass spectroscopy.

2.3.2 Sample Preparation

For all peptide samples, multiple rounds of lyophilization were performed to remove the trifluoroacetic acid (TFA) from peptide purification and also the exchangeable protons of the peptide. For CD and IR experiments, the solution was prepared by directly dissolving the lyophilized samples in either D₂O/H₂O or 20 mM Phosphate buffers. The concentration of each sample was determined optically by using a Lambda 25 UV-Vis spectrometer (Perkin Elmer, MA) with a 1 cm pathlength cuvette. The extinction coefficient of a particular protein was calculated based on the specific protein sequence and the presence of either phenylalanine or tryptophan or tyrosine. For peptides without chromophores, specifically NTL9:41:74 and NTL9:48-64, the concentrations of the peptide samples were determined by comparing CD results to those of Raleigh and coworkers (Kuhlman et al., 1997).

The reverse micelles solutions were prepared in the following way. Sodium bis(2-ethylhexyl) sulfosuccinate (AOT) and isooctane (IO) were purchased from Sigma Chemical Co. (St. Louis, MO). Isooctane was used as received. AOT was purified by dissolving it in methanol and stirring it overnight in the presence of activated charcoal. Subsequent filtration and removal of methanol by distillation under vacuum produced AOT that was used in all the studies presented in this thesis. For prolong storage the purified AOT was kept in the dry box at room temperature. The purified AOT was dried under vacuum overnight before use. 50/100/300 mM AOT/IO solution was prepared by

dissolving the appropriate mass of AOT in isooctane and the resultant solution was vortexed for 3 minutes and then sonicated for 10 minutes in a bath sonicator. To prepare the peptide-AOT/IO solution, lyophilized peptide solid was first dissolved in D₂O/H₂O (pH* ~ 3-4, pH meter reading), and then an appropriate aliquot of this peptide solution was added to the above AOT/IO solution to achieve the desired w_0 value following the injection method (Luisi, 1985). For example, to prepare 1 ml of 50 mM AOT/IO reverse micelles at $w_0 = 6$, 5.4 μ L of H₂O or peptide-H₂O solution will be added. Before use, this solution was further stirred for 30 minutes and then centrifuged for 15 minutes to remove any precipitates. IR reference samples (i.e., AOT/IO/D₂O solutions) were prepared in the same manner except that no peptide was added. The final peptide concentration of the peptide-AOT/IO samples was determined optically.

2.3.3 Circular Dichroism Spectroscopy

Wavelength scan and thermal melting CD curves were collected on an Aviv 62A DS circular dichroism spectrometer (Aviv Associate, NJ) using a 1 mm sample cuvette. The mean residue ellipticity, $[\theta]$, was calculated using $[\theta] = (\theta_{\text{obs}}/10lc)/N$, where θ_{obs} is the measured ellipticity in millidegrees, l is the optical path length of the sample cell (cm), c is the molar concentration of the peptide, and N is the number of residues. The folding/unfolding thermodynamics were obtained by fitting the CD thermal melting transition to the following two-state model:

$$\theta(T) = \frac{\theta_F(T) + K_{eq}(T) \times \theta_U(T)}{1 + K_{eq}(T)} \quad (2.1)$$

$$K_{eq}(T) = \exp(-\Delta G(T)/RT) \quad (2.2)$$

$$\Delta G(T) = \Delta H_m + \Delta C_p \cdot (T - T_m) - T \cdot [\Delta S_m + \Delta C_p \cdot \ln(T/T_m)] \quad (2.3)$$

where $\theta_F(T)$ is the folded CD baseline, $\theta_U(T)$ is the unfolded CD baseline, $K_{eq}(T)$ is the equilibrium constant for unfolding, $T_m = \Delta H_m/\Delta S_m$ is the thermal melting temperature, ΔH_m and ΔS_m are the enthalpy and entropy changes at T_m , respectively, and ΔC_p is the heat capacity change associated with unfolding, which has been assumed here to be temperature independent. In the fit, $\theta_F(T)$ and $\theta_U(T)$, were treated as linear functions of temperature.

2.3.4 Fourier Transform Infrared Spectroscopy

Static FTIR spectra were collected on a Magna-IR 860 spectrometer (Nicolet, WI) equipped with a HgCdTe detector using 2 cm^{-1} resolution. A customized CaF_2 sample cell that was divided into two compartments with a Teflon spacer and mounted on a programmable translation stage was used to allow separate measurements of the sample and the reference under identical conditions. Due to the low water content in the AOT reverse micelle samples, we were able to use a sample cell with a relatively long optical path length ($390 \text{ }\mu\text{m}$). Consequently, this allowed us to use peptide samples in the sub-millimolar concentration range. For experiments using bulk D_2O as solvent, the path length of the sample cell was either $50 \text{ }\mu\text{m}$ or $100 \text{ }\mu\text{m}$. Temperature control with $\pm 0.2 \text{ }^\circ\text{C}$ precision was obtained by a thermostated copper block. Typically, 256 scans were averaged to generate one spectrum, except for results presented in Chapter 6 where 1024 scans were averaged.

2.2.5 Transmission electron microscopy (TEM):

The transmission electron microscopy was performed by the Biomedical Imaging Core of the University of Pennsylvania School of Medicine. TEM images were recorded using a JEOL JEM-1010 electron microscope operating at 80 kV and equipped with a Hamamatsu ORCA digital camera using AMT Advantage image capture software. TEM samples were prepared by first depositing samples to Formvar coated 300 mesh copper grids. These grids were then negatively stained with 2% uranyl acetate in water. Any excess fluid was blotted off immediately. The grids were then allowed to dry in air for 10 minutes.

2.3.6 Dynamic Light Scattering

The particle size distribution of the reverse micelles with or without the peptide were measured by light-scattering photon correlation spectroscopy (Zetasizer 3000HSA, Malvern Instruments, Malvern, UK) utilizing a 10-mW He-Ne laser operating at 633 nm and a detector angle of 90°. Measurements were made at 25 °C. The solutions were filtered using a surfactant-free cellulose acetate filter (size: 0.2 µm) before making any measurements. The CONTIN algorithm was used to analyze the autocorrelation function.

2.3.7 T-Jump Infrared Spectroscopy

The time-resolved *T*-jump IR apparatus (Figure 2.1) used in the studies presented in this thesis has been described in detail elsewhere (Huang et al., 2002a). Briefly, a 1.9 µm laser pulse, generated via Raman shifting of the fundamental output of a Q-Switched Nd:YAG laser in H₂, was used to generate a 8-10 °C *T*-jump, and the *T*-jump induced

transient absorbance changes were measured by a continuous wave (CW) IR diode laser in conjunction with a 50 MHz HgCdTe (or MCT) detector and a digital oscilloscope. As in the static IR measurements, a thermostated, two-compartment sample cell with 52/100 μm path length was used to allow the separate measurements of the sample and reference under identical conditions. The measurements on reference compartment provide information for both background subtraction and also T -jump amplitude determination (Williams et al., 1996). The latter was achieved by using the T -jump induced absorbance change of the D_2O buffer solution at the probing frequency ν , $\Delta A(\Delta T, \nu)$, and the following equation: $\Delta A(\Delta T, \nu) = a(\nu) \cdot \Delta T + b(\nu) \cdot \Delta T^2$, where ΔT corresponds to the difference between the final (T_f) and initial (T_i) temperatures, and $a(\nu)$ and $b(\nu)$ are constants that were determined by analyzing the temperature dependence of the FTIR spectra of the buffer.

Figure 2.1 Time-resolved laser-induced temperature-jump infrared set-up. The T -jump pulse is generated via Raman shifting the injection-seeded Q-switched Nd:YAG fundamental (1064 nm) in pressurized H_2 gas. A CW lead salts diode laser serves as the infrared probe and is tunable in the region from 1550-1800 cm^{-1} . Changes in the transient absorbance of the probe as a result of the temperature-jump are detected by a 50 MHz MCT detector.

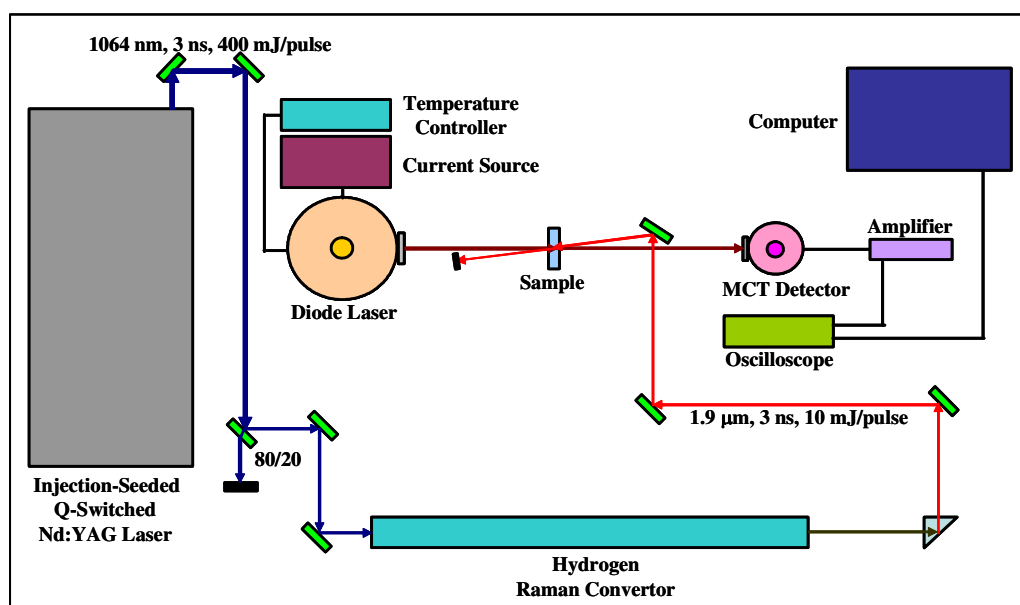
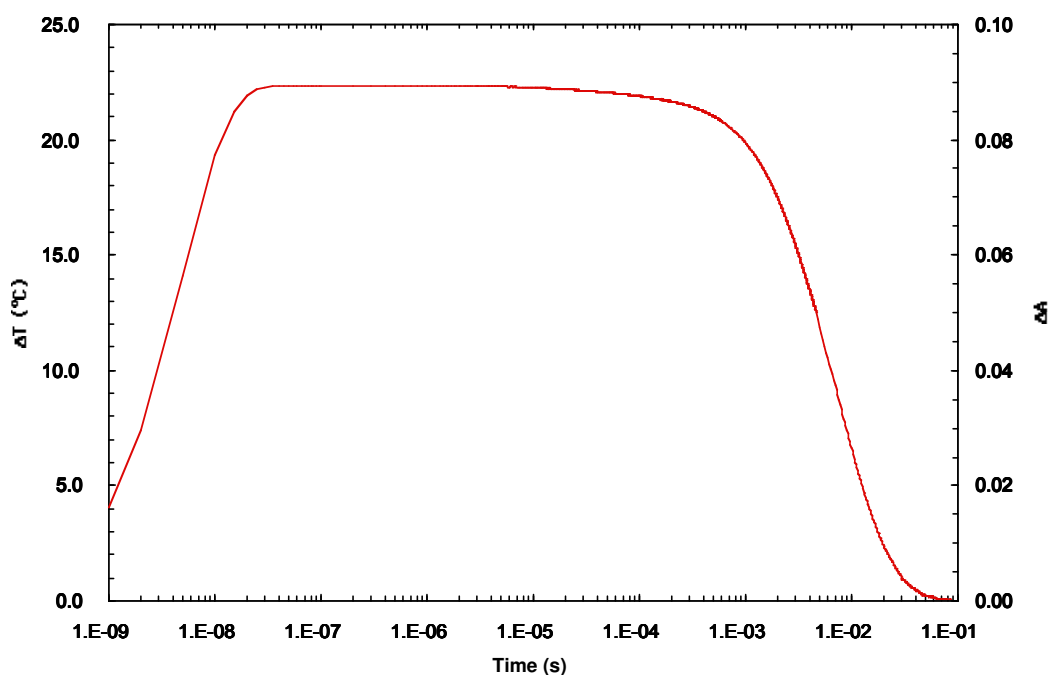


Figure 2.2 The time-resolved absorption profile of D₂O after a temperature-jump. The absorption change is monitored at 1632 cm⁻¹ (right axis) and used along with temperature-dependent equilibrium IR measurements of D₂O to calculate the temperature change (left axis) for a 100 μm D₂O sample as a function of time. This profile indicates the time window accessible to the *T*-jump IR set-up, namely ~20 ns – 1ms.



Chapter 3: Effect of Hydration on the Amide I band of Helical Peptides

This work has been published as a part of: S. Mukherjee, P. Chowdhury and F. Gai. *J. Phys. Chem. B* 2007 **111**, 4596-4602.¹

S. M. collected and analyzed the data. S. M., P. C. and F. G. wrote the paper.

The amide I' band of a polypeptide is sensitive not only to its secondary structure content but also to its environment. In this study we show how degrees of hydration affect the underlying spectral features of the amide I' band of two alanine-based helical peptides. This is achieved by solubilizing these peptides in the water pool of sodium bis(2-ethylhexyl) sulfosuccinate reverse micelles with different water contents or w_0 values. In agreement with several earlier studies, our results show that the amide I' band arising from a group of dehydrated helical amides is centered at $\sim 1650\text{ cm}^{-1}$, whereas hydration shifts this frequency towards lower wavenumbers.

¹ Reproduced with permission from [S. Mukherjee, P. Chowdhury and F. Gai. *J. Phys. Chem. B* 2007 **111**, 4596-4602.] Copyright (2007), the American Chemical Society.

3.1 Introduction

The amide I band of a polypeptide arises mainly from its backbone amide C=O stretching vibrations and, due to its sensitivity to various structural determinants, has been extensively used as a conformational reporter (Krimm and Bandekar, 1986; Heimbürg et al., 1996; Gilmanishin et al., 1997; Volk et al., 1997; Yoder et al., 1997; Dyer et al., 1998a; Decatur, 2006) of peptides and proteins. For example, it has been used in the study of peptide folding dynamics (Petty and Volk, 2004; Vu et al., 2004; Du and Gai, 2006) as well as structural determination of small peptides via nonlinear IR methods (Zanni et al., 2001; Mukherjee et al., 2006a; Sul et al., 2006; Wang et al., 2006; Zhuang et al., 2006). The fundamental property that renders the amide I vibration useful as a conformational probe is its dependence on structure-sensitive factors such as couplings among neighboring amide oscillators, intramolecular hydrogen bonding, and local electric fields (Krimm and Bandekar, 1986). Furthermore, formation of intermolecular hydrogen bonds with solvent molecules can also significantly affect the amide I frequency of a given secondary structural element. For example, it is well known that fully hydrated monomeric helices exhibit an amide I' band centered at a frequency lower than that arising from helices buried in the interior of a protein (Martinez and Millhauser, 1995). Therefore, the degree of exposure of the amide groups of a peptide or protein to the surrounding solvent is expected to have a profound influence on the frequency of its amide I band. Despite its importance, however, there are only a few experimental efforts attempting to directly and quantitatively assess how hydration affects the amide I frequency. For instance, Vanderkooi and co-workers have employed an isotope-editing

technique in conjunction with molecular dynamics simulation to distinguish between the amide I' bands of interior and solvent-exposed residues in a GCN4 coiled-coil (Manas et al., 2000) and a de novo designed three-helix bundle protein (Walsh et al., 2003). Their results confirmed that water-backbone hydrogen bonding results in the reduction of the force constant of the corresponding amide C=O stretching vibration, thereby leading to a shift of the amide I' transition to a lower frequency. Consistently, Decatur and coworkers (Starzyk et al., 2005) have recently shown that upon addition of 2,2,2-trifluoroethanol (TFE), a reagent commonly used to induce helix formation in short peptides, the amide I' band of an alanine rich peptide shifts to a higher frequency due to the alleviation of the D₂O-helix backbone hydrogen bonding interactions. While using a co-solvent like TFE allows one to probe various effects of peptide backbone dehydration, this method nevertheless suffers from the disadvantage that the interaction between the co-solvent and the solute as well as that between the co-solvent and water have to be considered when interpreting the experimental results. Herein, we have attempted to use AOT reverse micelles with different water loadings as platforms to directly test how degrees of hydration affect the amide I' band of helical peptides.

The advantage of using AOT reverse micelles is that one can, in a fairly controllable fashion, vary the amount of water available to guest molecules solubilized inside the micellar core, thus allowing a systematic study of how degrees of hydration affect the physical properties of interest. In practice, this can be achieved by preparing reverse micelles with different w_0 values, a parameter defined as the ratio of the molar concentration of water to that of the surfactant ($[\text{water}]/[\text{AOT}]$). Variation in w_0 is not

only associated with changes in the number of water molecules inside the micellar core but is also accompanied by variation of the physicochemical properties of the entrapped water (Maitra, 1984; Luisi, 1985; Chowdhury et al., 2000; Senapati and Chandra, 2001; Freda et al., 2002; Levinger, 2002). Hence AOT reverse micelles provide a unique platform for examining the effect of hydration on the IR spectrum of a peptide.

3.2 Experimental Methods

Materials. AOT and isooctane were purchased from Sigma Chemical Co. (St. Louis, MO).

Peptide synthesis and purification. The AKA_n peptides (n = 2 and 6) have the following sequence, YGAKAAAA(KAAAA)_nG. These peptides and a pentapeptide (SPEAA) were synthesized, identified and purified as detailed in Chapter 2. The residual trifluoroacetic acid (TFA) from peptide synthesis was removed as outlined in Chapter 2. The amide hydrogen was further exchanged to deuterium by dissolving the peptide solids in D₂O followed by lyophilization.

Sample preparation. 50 mM AOT/IO solution was prepared as described in Chapter 2. To prepare the peptide-AOT/IO solution, lyophilized peptide solid was first dissolved in D₂O, and then an appropriate aliquot of this peptide solution was added to the above AOT/IO solution to achieve the desired w_0 value. Before use, this solution was further stirred for 30 minutes and then centrifuged for 15 minutes to remove any precipitates. IR reference samples (i.e., AOT/IO/D₂O solutions) were prepared in the same manner except that no peptide was added. The final peptide concentration of the AKA_n-AOT/IO samples

was determined optically by the single tyrosine absorbance at 276 nm using $\epsilon_{276} = 1450 \text{ cm}^{-1} \text{ M}^{-1}$ and was found to be in the range of 50-120 μM .

FTIR measurements. Fourier transform infrared (FTIR) spectra were collected as described in Chapter 2. For all reported FTIR spectra, a background arising from imperfect subtraction of AOT signals was subtracted.

3.3 Results

As shown in Figure 3.1, the AKA₆ peptide in D₂O shows an amide I' band that is dominated by a spectral feature centered at $\sim 1629 \text{ cm}^{-1}$, in agreement with previous studies indicating that fully D₂O-solvated α -helices absorb around this frequency (Heimburg et al., 1996; Reisdorf and Krimm, 1996; Manas et al., 2000; Huang et al., 2001b; Walsh et al., 2003; Gnanakaran and Garcia, 2005). However, when dissolved in the D₂O pool of AOT reverse micelles of $w_0 = 6$ the amide I' band of AKA₆ becomes significantly broadened, due to the existence of two apparent, overlapping spectral components centered at ~ 1634 and 1650 cm^{-1} , respectively. While the amide I' band of the AKA₂ peptide is also composed of two major spectral features, the 1650 cm^{-1} component becomes less pronounced, owing to the apparent blue-shift of the lower frequency component (Figure 3.1). We have shown in a CD study that both peptides adopt predominantly helical structures under the same experimental conditions (Mukherjee et al., 2006b). Thus, these two spectral components can be assigned to helical amide groups that experience distinctly different environments arising from differential hydration inside the reverse micellar core. Since buried helical amides in proteins frequently exhibit an amide I' band centered around $\sim 1650 \text{ cm}^{-1}$ (Manas et al., 2000), we

therefore attribute the 1650 cm^{-1} component to dehydrated helical amides, whereas the lower frequency component is ascribed to helical amides that are either fully or partially hydrated. While this study alone does not allow us to pinpoint the exact hydration status of individual amide groups along the peptide backbone, these results nevertheless indicate that the amide I' band of helical peptides exhibits a strong dependence on the degree of backbone hydration.

Consistent with the above assignments, the amide I' band of a pentapeptide (SPEAA), which does not form any detectable helical conformations in D_2O and AOT reverse micelles (based on CD results, data not shown), is broad and exhibits a maximum at $\sim 1644\text{ cm}^{-1}$ in D_2O and $\sim 1647\text{ cm}^{-1}$ in reverse micelles of $w_0 = 6$, respectively (Figure 3.2). Apparently, this blue-shift (as much as 8 cm^{-1} when comparing the edges of the two spectra) arises from the change in hydration status of the peptide due to the limited supply of water molecules in AOT reverse micelles. In other words, these results indicate that the hydrogen bond formed between amide carbonyls and water molecules in reverse micelles is weaker than that in bulk water. Thus, this result further strengthens the notion that dehydration leads to an increase in the amide I' vibrational frequency of polypeptides.

To gain a better understanding of the effect of hydration on the amide I' band of these AKA_n peptides, we further measured the FTIR spectra of the AKA_2 and AKA_6 peptides in AOT/ D_2O /IO reverse micelles at higher w_0 values. As shown (Figure 3.3a), at w_0 of 10 and at $4.0\text{ }^\circ\text{C}$ the amide I' band of AKA_2 is dominated by a single spectral feature centered at $\sim 1634\text{ cm}^{-1}$, indicating that increasing w_0 leads to an increase in the

degree of hydration of the peptide backbone whereas for AKA₆ there is still a prominent component at $\sim 1650\text{ cm}^{-1}$. At w_0 of 20, the amide I band of AKA₂ (Figure 3.3b) becomes almost identical to that obtained in D₂O, suggesting that the overall hydration in both cases is similar. However, for AKA₆ at w_0 of 20 the $\sim 1634\text{ cm}^{-1}$ (Figure 3.3b) component becomes more pronounced due to more backbone hydration of the peptide at w_0 of 20, although the 1650 cm^{-1} component is still present, albeit smaller. Thus, these results corroborate the above assignment that the 1650 cm^{-1} component arises primarily from dehydrated helical amides.

3.4 Discussion

It is well established that water plays an important role in many chemical and biological processes. However, in many cases it has been difficult to evaluate the net effect of hydration on the physical and/or chemical properties of the molecular system of interest simply because a systematic variation of the degree of hydration of the solute molecule in question is not easily achievable (except in the gas phase where it has been shown that solute-water complexes with a limited, but well-defined number of water molecules can be created, for example, for peptides (Jarrold, 2000; Massi and Straub, 2003; Wyttenbach et al., 2005)). While using a co-solvent can sometimes allow one to probe how dehydration affects a specific physical observable (Starzyk et al., 2005), such a method may encounter added complexity that renders the experimental results difficult to interpret. Herein, we have attempted to use AOT reverse micelles in conjunction with FTIR spectroscopy to provide further understanding of how hydration affects their amide

I' band, an infrared marker extensively used in protein and peptide conformational studies.

Due to its sensitivity to various structural determinants, the amide I' band of polypeptides are being increasingly used in a wide variety of applications, including studies concerning protein folding dynamics (Petty and Volk, 2004; Vu et al., 2004; Du and Gai, 2006), protein secondary structure determination (Krimm and Bandekar, 1986; Heimbürg et al., 1996; Gilmanishin et al., 1997; Volk et al., 1997; Yoder et al., 1997; Dyer et al., 1998a), peptide-membrane interaction (Wytténbach et al., 2005), enzymatic reaction (Arrondo and Goni, 1999), and ligand binding in proteins (Callender and Dyer, 2006), among others. In D₂O solution, the amide I' band of a polypeptide is inadvertently broadened by various homogeneous and inhomogeneous mechanisms, thereby rendering a quantitative interpretation of the spectrum difficult. Among those factors that affect the frequency and width of the amide I' band, interactions between the polypeptide and surrounding water molecules seem to be uniquely important but nevertheless are less studied. For instance, while it has long been recognized that hydration of an α -helix induces a shift in its amide I' band to lower wavenumbers (Martinez and Millhauser, 1995; Chen and Spiro, 2002), the most convincing experimental evidence comes only recently from studies involving the use of isotope-editing and molecular dynamics simulation techniques (Manas et al., 2000; Walsh et al., 2003). Herein, we seek to provide a direct, albeit complementary, assessment of how degrees of hydration affect the amide I' band of helical peptides by using AOT/D₂O/IO reverse micelles with different w_0 values.

As expected (Figure 3.1), the amide I' bands of AKA₂ and AKA₆ obtained in AOT reverse micelles of $w_0 = 6$ are distinctly different from those obtained in D₂O. For example, in D₂O a single spectral feature centered at $\sim 1629\text{ cm}^{-1}$ dominates the amide I' region of the FTIR spectrum of AKA₆, whereas in AOT reverse micelles its amide I' band consists of two overlapping but distinguishable spectral components, centered at around 1634 and 1650 cm^{-1} , respectively. The FTIR spectrum of AKA₂ in the amide I' region shows similar characteristics although the separation between the two corresponding spectral components becomes less distinct due to the apparent blue-shift of the low frequency component. These results can be rationalized based on the fact that at w_0 of 6 there are only about 300-325 water molecules inside each micellar core (Chowdhury et al., 2000), of which about 32% is considered as 'free' and is capable of interacting with other guest molecules (Maitra, 1984). Therefore, this limitation in supplying free water molecules creates a scenario wherein some of the helical amide groups are only partially solvated (or hydrated) or not solvated at all and, as a result, giving rise to two distinct amide I' bands. Apparently, the low frequency component arises from those helical amides that are hydrogen bonded with D₂O molecules, whereas the high frequency band most likely corresponds to dehydrated helical amides. This assignment is consistent with the results of several earlier studies which suggest that water-exposed amide groups of a protein can form bifurcated helical hydrogen bonds due to the formation of an additional hydrogen bond between an helical amide carbonyl and the surrounding water molecules (Heimburg et al., 1996; Reisdorf and Krimm, 1996; Arrondo and Goni, 1999). The FTIR spectra collected at higher w_0 values also support such an assignment. For example, at w_0

of 10 the amide I' band of AKA₂ at 4 °C (Figure 3.3a) is already very similar to that in D₂O (data not shown), owing to the increased number of free D₂O molecules. Nonetheless, compared to that obtained in D₂O, the hydrated helical band of AKA₆ and AKA₂ in AOT reverse micelles shows a clear blue-shift (Figure 3.1), suggesting that on average the hydrogen bond formed between an amide unit and water is weakened under such conditions. In agreement with this picture, it has been shown that in AOT reverse micelles of low w_0 values the confined water molecules experience weaker hydrogen bonding (Parrish and Blout, 1972; Venables et al., 2001). Consistently, the amide I' band of an unstructured pentapeptide in AOT reverse micelles of $w_0 = 6$ also shows a blue-shift compared to that obtained in D₂O (Figure 3.2). Quite different from those of the AKA_n peptides, however, the overall bandwidth of the amide I' profile of this pentapeptide is approximately constant irrespective of the 'solvent' used. Thus, the latter result suggests that the broadening of the spectrum is mainly due to the large repertoire of conformations sampled by this peptide.

Another interesting feature regarding the spectra presented in Figure 3.1 is the apparent red-shift of the hydrated helical amide I' band of AKA₆ (~1634 cm⁻¹) compared to that (~1638 cm⁻¹) of AKA₂. Since AKA₆ is much longer, one would expect that for the same number of water molecules it will experience on average a lesser degree of hydration and consequently give rise to a more blue-shifted hydrated helical amide I' band. Support for this notion is established from the results of FTIR spectra of these two peptides at higher w_0 values where the AKA₆ peptides still contains some dehydrated amide groups even at $w_0 = 20$, which is not observed for AKA₂ (Figure 3.3 a and b).

Therefore, the observed trend indicates that the microscopic hydration details are different for these two peptides. While the current experimental approach does not allow us to reveal this difference, we hypothesize that it is caused by the change in peptide chain length as well as the inhomogeneous distribution of the water molecules inside the polar core of the AOT reverse micelles (Maitra, 1984). It probably adopts a compact conformation with a decreased mean helicity. Thus, it is conceivable that the helical stretch of this peptide incidentally locates in a region where the free water is relatively abundant, leading to a more red-shifted (hydrated) helical amide I' band. While any further speculation on the detail of the location of the peptide inside the water pool of the reverse micelles is beyond the scope of our present study, we do believe that the complex interplay of effects arising from geometric distortions of both the micelles and peptide leads to the observed but not anticipated trend. Further simulation studies (Abel et al., 2006) may help provide a more decisive description.

3.5 Conclusion

Using infrared spectroscopy and AOT reverse micelles, we have studied how degrees of hydration might affect the amide I' vibrational transitions of two alanine-based helical peptides at low temperatures. Our results show that the dehydrated helical amide groups give rise to an amide I' band centered around $\sim 1650\text{ cm}^{-1}$, whereas hydration shifts this band towards lower frequencies.

Figure 3.1 FTIR spectra (in the amide I' region) of AKA₂ (pink) and AKA₆ (blue) in AOT/D₂O/IO reverse micelles of $w_0 = 6$. Also shown are the FTIR spectra of AKA₂ (green) and AKA₆ (red) in D₂O. All the spectra were collected at 4 °C and have been normalized with respect to that of AKA₂ in $w_0 = 6$ to facilitate comparison.

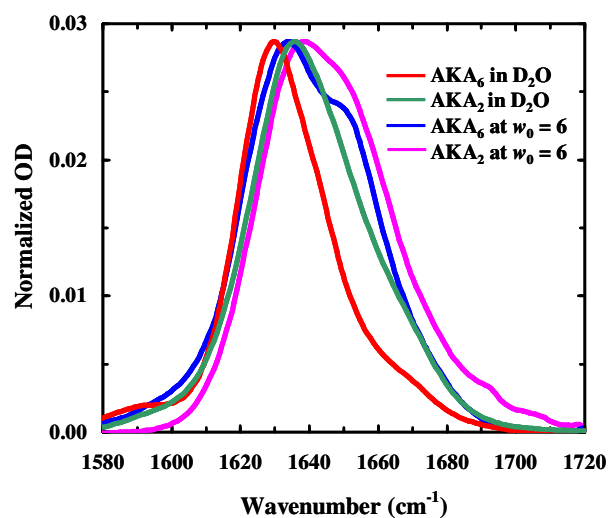


Figure 3.2 FTIR spectra (in the amide I' region) of SPEAA in D₂O (red) at 2.6 °C and AOT/D₂O/IO reverse micelles of $w_0 = 6$ (blue) at 4.1 °C. The spectrum obtained in D₂O has been normalized with respect to that obtained in reverse micelles.

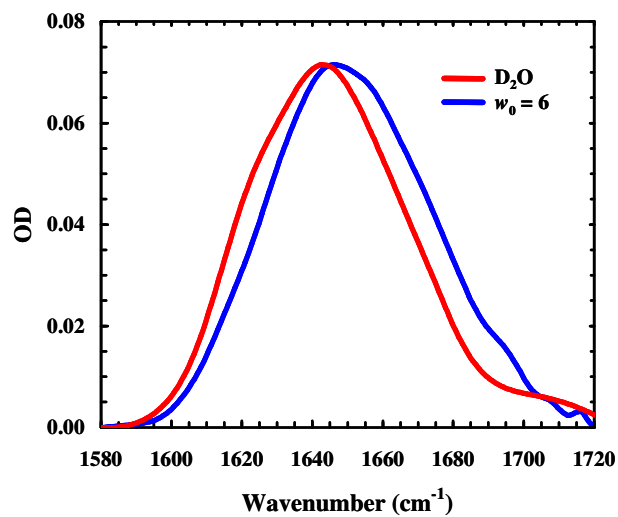
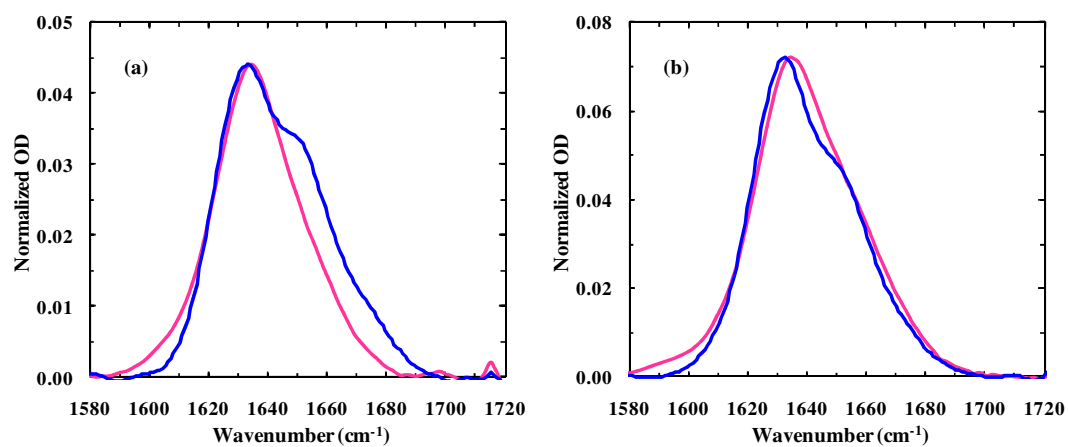


Figure 3.3 FTIR spectra (in the amide I' region) of AKA₂ (pink) and AKA₆ (blue) in AOT/D₂O/IO reverse micelles of $w_0 = 10$ (a) and 20 (b).



Chapter 4: Probing the Site-Specific Hydration Status of a Peptide Inside a Membrane-Mimetic Environment

This work has been published: Site-specific hydration status of an amphipathic peptide in AOT reverse micelles. S. Mukherjee, P. Chowdhury, W. F. DeGrado, and F. Gai. *Langmuir* 2007 **23**, 11174-11179.²

S. M. collected and analyzed the data. W.F.D provided some of the peptide samples. S. M, P. C. and F. G. wrote the paper.

Reverse micelles formed by sodium bis(2-ethylhexyl) sulfosuccinate (AOT) in isooctane (IO) and water have long been used as a means to provide a confined aqueous environment for various applications. In particular, AOT reverse micelles have often been used as a template to mimic membrane-water interfaces. While earlier studies have shown that membrane-binding peptides can indeed be incorporated into the polar cavity of AOT reverse micelles where they mostly fold into an α -helical structure, the underlying interactions leading to the ordered conformation are however not well understood. Herein, we have used circular dichroism (CD) and infrared (IR) spectroscopies in conjunction with a local IR marker (i.e., the C \equiv N group of a non-natural amino acid, *p*-cyano-phenylalanine) and a global IR reporter (i.e., the amide I' band of the peptide backbone) to probe the conformation as well as the hydration status of an antimicrobial peptide, mastoparan x (MPx), in AOT reverse micelles of different

² Reproduced with permission from [S. Mukherjee, P. Chowdhury, W. F. DeGrado, and F. Gai. *Langmuir* 2007 **23**, 11174-11179.] Copyright (2007), the American Chemical Society.

water contents. Our results show that at, $w_0 = 6$, MPx adopts an α -helical conformation with both the backbone and hydrophobic side chains mostly dehydrated, whereas its backbone becomes partially hydrated at $w_0 = 20$. In addition, our results suggest that the amphipathic α -helix so formed orients itself in such a manner that its positively charged, lysine-rich, hydrophilic face points toward the negatively charged AOT head groups, while its hydrophobic face is directed toward the polar interior of the water pool. This picture is in marked contrast to that observed for the binding of MPx to phospholipid bilayers wherein the hydrophobic surface of the bound α -helix is buried deeper into the membrane interior.

4.1 Introduction

Reverse micelles, formed by the self-assembly of various amphiphilic molecules in organic solvents, have been used in a wide variety of applications (Pileni, 1993; De and Maitra, 1995; Wand et al., 1998). One of the most well-characterized reverse micellar systems is that formed by sodium bis(2-ethylhexyl) sulfosuccinate (AOT) in isooctane (IO) wherein the hydrocarbon chains of the AOT molecules extend into the nonpolar solvent while the negatively charged sulfosuccinate head groups aggregate to form a polar core. The latter is known to solubilize water and, therefore, has been widely used as a fairly controllable means of providing a confined aqueous environment or cavity, the size of which depends on w_0 , i.e., the ratio of the molar concentration of water to that of AOT (Luisi, 1985). For example, we have recently taken advantage of this particular feature of AOT reverse micelles and have studied how degrees of hydration affect the amide I' band as well as the aggregation properties of alanine-based helical peptides (Mukherjee et al., 2007b).

Moreover, it has been suggested that AOT reverse micelles with low w_0 values (e.g., $w_0 = 6$) could be used to mimic the membrane-water interface because the confined water molecules, especially those at the interfacial region, are non-bulk-like, resulting in a low dielectric environment at the interface (Belletete et al., 1990; Riter et al., 1998b; Bhattacharyya, 2003; Dokter et al., 2006). Indeed, previous studies have shown that a number of membrane-binding proteins/peptides, such as myelin basic protein (MBP) (Nicot et al., 1985), synthetic adrenocorticotropin (Gallay et al., 1987), and melittin (Raghuraman and Chattopadhyay, 2003), can be incorporated into AOT reverse micelles

wherein they appear to fold into their biologically functional α -helical (MBP, melittin) or β -sheet (adrenocorticotropin) structures as opposed to a predominantly disordered conformation found in aqueous solution. However, in these early studies either tryptophan fluorescence (Nicot et al., 1985; Gallay et al., 1987; Raghuraman and Chattopadhyay, 2003), which is known to be most sensitive to the immediate environment of the indole fluorophore, and/or titration of ϵ -amino groups of lysine residues and tryptophan with water-soluble reagents (Nicot et al., 1985), were used to probe the hydration status of the peptide of interest, thus falling short of providing a more comprehensive picture regarding how other side chains as well as the peptide backbone are solvated. Herein, we attempt to use infrared (IR) spectroscopy in combination with a non-natural amino acid IR probe (i.e., *p*-cyano-phenylalanine) (Getahun et al., 2003) to obtain site-specific hydration information on a membrane-binding peptide, mastoparan x (MPx) (Hirai et al., 1979), in AOT reverse micelles. MPx is an amphipathic peptide isolated from wasp venom and has been shown to be involved in a range of biological actions (Higashijima et al., 1990; Matsuzaki et al., 1996).

Recently, Getahun et al. (Getahun et al., 2003) have shown that nitrile-containing amino acids, especially *p*-cyano-phenylalanine (Phe_{CN}), could be used as IR markers of the local environment of peptides and proteins, due to the sensitivity of the C \equiv N stretching vibration to hydrogen bonding (Huang et al., 2003b) and local electrical field (Suydam and Boxer, 2003). For example, the frequency of the C \equiv N stretching vibration of Phe_{CN} in water is centered at 2237.2 cm⁻¹ whereas in tetrahydrofuran (THF), the dielectric constant of which is similar to that of a protein's interior, the frequency of this

vibration shifts to 2228.5 cm^{-1} (Getahun et al., 2003). Tucker et al. have further shown that this IR probe is particularly useful in probing the local environment of a specific residue in a membrane-bound peptide (Tucker et al., 2004a). Herein, we aim to extend the application of this IR probe to assess the site-specific hydration status of amphipathic peptides in AOT reverse micelles. As an example, we have studied a series of mutants of MP_x, each containing a single Phe_{CN} residue at different positions along the peptide sequence. Our results show that with the use of nitrile-containing amino acids it is indeed possible to provide a site-specific interrogation of the hydration status of the peptide in question, thus providing a better understanding of the overall environment of the peptide. In addition, our results suggest that the AOT reverse micelle is quite different from other model membrane systems, such as phospholipid bilayers, in that the former induces an amphipathic peptide to form an α -helix at its interfacial region through the combined effects of electrostatic interaction and dehydration.

4.2 Experimental Methods

Materials. AOT and IO was purchased from Sigma Chemical Co. (St. Louis, MO). Phe_{CN} was purchased from Bachem (CA) and was used as received.

Peptides. The sequences of the peptides used (or discussed) in the current study are listed below:

MP_x: INWKGIAAMAKKLL

MP_x-CN5: INWK-Phe_{CN}-IAAMAKKLL

MP_x-CN6: INWKG-Phe_{CN}-AAMAKKLL

MP_x-CN7: INWKGI-Phe_{CN}-AMAKKLL

MP_x-CN₉: INWKGIAA-Phe_{CN}-AKKLL

MP_x-CN₁₅: INWKGIAAMAKKLL-Phe_{CN}

AKA₁: YGAKAAAAKAAAAG

AKA₂: YGAKAAAA(KAAAA)₂G

The MP_x-CN_y peptides were synthesized, purified and its masses verified as described in Chapter 2.

Sample Preparation. The AOT/IO solution was prepared as discussed in Chapter 2. To prepare the peptide-AOT/IO/H₂O solutions, lyophilized peptide was first dissolved in Millipore water, and then an appropriate aliquot of this peptide solution (pH 3–4, pH meter reading) was added to the above AOT/IO solution to achieve the desired w_0 values of 6, 20, and 30, the polar core of which have diameters of 28, 70, and 102 Å, respectively (Maitra, 1984). Before use, this solution was further stirred for 30 min and then centrifuged for 15 min to remove any undissolved peptides. AOT samples for background measurements were prepared in a similar manner except with no peptide being added to the AOT/IO/H₂O solution. The final peptide concentration was determined optically (Tucker et al., 2005) using $\epsilon_{280} = 6450 \text{ cm}^{-1} \text{ M}^{-1}$ and was found to be in the range of 48–100 μM for the reverse micellar solutions. The peptide-AOT/IO/D₂O samples used for the amide I' measurements were prepared following similar procedures, the details of which have been described in Chapter 2. Similarly, the Phe_{CN}-AOT/IO/H₂O solutions were prepared according to the above protocols, and the final Phe_{CN} concentration, determined optically using $\epsilon_{280} = 850 \text{ cm}^{-1} \text{ M}^{-1}$ (Tucker et al., 2005), was found to be in the range of 0.5–1.4 mM.

FTIR Spectroscopy. Fourier transform infrared (FTIR) spectra were collected as described in Chapter 2 at 4 and 25 °C. For all reported FTIR spectra, a background arising from imperfect subtraction of AOT signals was subtracted.

CD Spectroscopy. The far-UV CD data were collected as described in Chapter 2 at 4 and 25 °C. The mean residue ellipticity, $[\theta]$, was calculated as described in Chapter 2.

4.3 Results and Discussion

We have carried out CD and IR experiments at 4 and 25 °C, respectively. Since the results obtained at these temperatures are rather similar, below we report and discuss only those collected at 4 °C.

CD studies. The secondary structure content of the MPx-CN_y peptides in aqueous solution and AOT reverse micelles was assessed by CD spectroscopy. Consistent with previous studies involving native MPx (Higashijima et al., 1983; Wakamatsu et al., 1992), the far-UV CD spectrum of MPx-CN5 indicates that it exists in a largely disordered conformation in aqueous solution (Figure 4.1). However, incorporation of this peptide into AOT reverse micelles of $w_0 = 6$ results in a drastic conformational change, leading to the formation of a predominantly α -helical ensemble (Figure 4.1). Other mutants used in this study show similar behaviors (data not shown). Thus, these results are in agreement with previous studies, suggesting that AOT reverse micelles, especially at low w_0 values, could be used to mimic the membrane–water interface (Nicot et al., 1985; Gallay et al., 1987; Raghuraman and Chattopadhyay, 2003). The fact that an alanine-rich peptide having an equal number of residues (i.e., AKA₁) does not show

appreciable helicity under the same conditions (Mukherjee et al., 2006b) further corroborates this idea. Moreover, in agreement with an earlier study involving similar MPx-CNy peptides bound to POPC phospholipid bilayers (Tucker et al., 2004a), these results show that mutation of a single residue with Phe_{CN} does not perturb in any significant manner the helical content as well as the amphipathic nature of MPx. Furthermore, compared to that obtained at $w_0 = 6$, the mean residue helicity of MPx-CN5 in AOT reverse micelles of $w_0 = 20$ is decreased. Since for monomeric α -helices water molecules often act as “denaturants” by competing for hydrogen-bonding partners with the helical amide groups, this result therefore suggests that the peptide backbone in the current case becomes more solvated at higher w_0 values, a picture consistent with the FTIR results (see below). Previous CD studies on other membrane-binding peptides in AOT reverse micelles have also shown that increasing the water content can, depending upon the peptide, minimally (Nicot et al., 1985; Raghuraman and Chattopadhyay, 2003) or significantly (Gallay et al., 1987) perturb the folded conformation. Thus, to provide further insight into the effect of hydration, we have employed IR spectroscopy as an additional tool to probe the hydration status of the MPx-CNy peptides under different conditions.

C \equiv N stretching vibration of Phe_{CN}. It has been shown that the C \equiv N stretching vibration of Phe_{CN} is sensitive to solvent or the local environment it samples in a protein (Getahun et al., 2003). However, to show that this IR mode can indeed be used as a probe of local hydration status of peptides inside reverse micelles, we first collected FTIR spectra of Phe_{CN} in AOT reverse micelles of different w_0 values. As shown (Figure 4.2), the C \equiv N

stretching vibration of Phe_{CN} is indeed sensitive to the amount of water present inside the reverse micelles and is therefore expected to be useful for probing the local hydration status of a peptide solubilized in AOT reverse micelles. For example, in AOT reverse micelles of $w_0 = 6$ the Phe_{CN} molecules exhibit a dominant C≡N stretching band centered at $\sim 2229\text{ cm}^{-1}$, whereas at higher w_0 values (e.g., 20 and 30) a new spectral feature centered at $\sim 2237\text{ cm}^{-1}$ becomes evident. Interestingly, the position and width of the C≡N band obtained at $w_0 = 6$ are almost identical to those obtained in THF (Getahun et al., 2003), indicating that under this condition the C≡N group is not hydrogen-bonded to water molecules. Therefore, this result suggests that in AOT reverse micelles of low w_0 values the Phe_{CN} molecules preferentially locate at the interfacial region of the micelles, with the cyano-benzene ring likely protruding into a hydrophobic environment where the C≡N moiety is free from any hydrogen-bonding interactions. On the other hand, the center frequency of the 2237 cm^{-1} band observed at higher w_0 values is the same as that measured for fully hydrated Phe_{CN} molecules (Getahun et al., 2003). However, the width of this band ($\sim 16\text{ cm}^{-1}$) is much larger than that observed for Phe_{CN} in water ($\sim 9.8\text{ cm}^{-1}$), indicative of a much larger heterogeneous broadening. Taken together, these results therefore suggest that this spectral feature arises from an ensemble of Phe_{CN} molecules whose cyano groups experience different degrees of hydration, a picture which is not only consistent with the heterogeneous nature of water distribution inside reverse micelles (Maitra, 1984; Onori and Santucci, 1993; Venables et al., 2001; Nucci and Vanderkooi, 2005) but also demonstrates the utility of the C≡N stretching vibration as a local IR probe.

Moreover, it is evident that the integrated area of the 2237 cm^{-1} band increases with increasing w_0 , indicating that the population of the (partially and/or fully) solvated Phe_{CN} molecules increases with increasing water content. This result is interesting in that it shows that solvation of Phe_{CN} by water molecules becomes more favorable at higher w_0 values, which correlates well with the fact that the number of “free water” molecules available to interact with any guest molecules not only increases with increasing w_0 but also become more bulk like. Therefore, a probable explanation for the observation that the Phe_{CN} molecules prefer a “dry” state (namely, the $\text{C}\equiv\text{N}$ moiety is not hydrated) at low w_0 values (e.g., $w_0 = 6$) is due to the non-bulk-like nature of the entrapped “free water” molecules (Maitra, 1984; Onori and Santucci, 1993; Venables et al., 2001; Nucci and Vanderkooi, 2005; Dokter et al., 2006). The current results thus suggest that these water molecules interact with each other in such a manner that breaking up the water hydrogen-bonding network, to solvate the Phe_{CN} molecule, is free-energetically unfavorable. While previous studies (Leodidis and Hatton, 1990; Adachi et al., 1991) have shown that both phenylalanine (Phe) and tyrosine (Tyr) exhibit high affinity toward the interfacial region of AOT reverse micelles (e.g., even at $w_0 > 40$, the reported partition coefficients (Leodidis and Hatton, 1990) for Phe and Tyr are 90 and 9 at $25\text{ }^\circ\text{C}$, respectively, favoring the AOT bound state), the current results nevertheless indicate that Phe_{CN} , which likely exhibits a hydrophobicity smaller than that of Phe but larger than that of Tyr, interacts less strongly with the AOT molecules. For example, assuming that the cross section is the same for both the free (or dehydrated) and hydrogen-bonded $\text{C}\equiv\text{N}$ moieties, we estimated

the relative population of the dehydrated Phe_{CN} at $w_0 = 30$ to be only about 50%, using the integrated areas of the 2229 and 2237 cm^{-1} spectral components in Figure 4.2c.

C \equiv N stretching vibration of MP_x-CN_y peptide. To probe the local or site-specific hydration status of the MP_x peptide entrapped in AOT reverse micelles, we have studied the C \equiv N stretching vibration of a series of Phe_{CN} mutants of MP_x at $w_0 = 6$. As shown (Figure 3 and Table 1), the C \equiv N stretching frequencies of these peptides show small but measurable variations, ranging from 2228.5 to 2231.0 cm^{-1} . Therefore, these results indicate that the C \equiv N groups in these peptides experience a rather “hydrophobic” environment, as a fully hydrated Phe_{CN} residue in a peptide environment has been shown to exhibit a C \equiv N vibrational frequency of $\sim 2237 \text{ cm}^{-1}$ (Getahun et al., 2003). While we cannot determine the exact location of the peptide molecules, these results nevertheless suggest that at low w_0 values they locate in the interfacial region of the AOT reverse micelles where very few “free water” molecules remain available (Maitra, 1984; Onori and Santucci, 1993; Venables et al., 2001; Nucci and Vanderkooi, 2005; Dokter et al., 2006) to interact with any guest molecules. In agreement with this picture, the amide I' band of MP_x-CN5 in AOT reverse micelles of $w_0 = 6$ is centered at $\sim 1650 \text{ cm}^{-1}$ (Figure 4), a band position often assigned to dehydrated helical amides (Manas et al., 2000; Walsh et al., 2003) and also observed for helical peptides in LPC micelles and phospholipid membrane systems (Haris and Chapman, 1994). More convincingly, the amide I' band of MP_x-CN5 exhibits a narrow bandwidth ($\sim 20 \text{ cm}^{-1}$), indicating that the amide carbonyls sample a rather homogeneous environment. Thus, the peptide backbone of MP_x-CN5 is mostly desolvated or dehydrated in AOT reverse micelles of $w_0 = 6$.

Measurements on other MPx-CNy peptides yielded similar results (data not shown). On the other hand, under the same conditions an alanine-rich peptide (AKA₂) exhibits a much broader amide I' band, primarily due to the coexistence of hydrated and dehydrated helical amide groups (Mukherjee et al., 2007b). Interestingly, increasing w_0 to a value of 20 induces an appreciable broadening in the amide I' band of MPx-CN5. In particular, the spectral feature arising from the hydrated helical amides (Mukherjee et al., 2007b), which absorb at $\sim 1634\text{ cm}^{-1}$, becomes more distinct. In contrast, the amide I' profile of AKA₂ does not show any substantial changes when increasing w_0 from 6 to 20 (Mukherjee et al., 2007b), a finding further corroborating the idea that alanine-based peptides sample a more heterogeneous environment even in reverse micelles of low w_0 values. Taken together, these results underscore the necessity for further studies, perhaps computer simulations (Garcia et al., 1997; Im and Brooks, 2005; Nymeyer et al., 2005; Abel et al., 2006), that can help provide much needed molecular insights into these systems.

As a model system, the binding of MPx to various membranes and membrane mimicking systems has been extensively studied using bicelles, SDS micelles, and phospholipid bilayers of different compositions (Higashijima et al., 1983; Wakamatsu et al., 1992; Hori et al., 2001; Whiles et al., 2001; Tucker et al., 2004a; Todokoro et al., 2006). For example, NMR studies have shown that when bound to anionic phospholipid bilayers, MPx folds into an amphipathic α -helix whose hydrophobic face, composed of residues, W3, I6, M9, L13, and L14, tends to insert deeper into the hydrophobic region of the membrane bilayers (Todokoro et al., 2006). Indeed, using the same MPx-CNy peptides and IR spectroscopy, Tucker et al. (Tucker et al., 2004a) have shown that both

positions 6 and 9 sample on average a more hydrophobic environment when the corresponding MPx-CN_y peptide is bound to a POPC phospholipid bilayer. However, in AOT reverse micelles, the C≡N stretching vibration of both MPx-CN6 and MPx-CN9 shows a frequency that is blue-shifted compared to that of other MPx-CN_y peptides, suggesting that in both cases the Phe_{CN} residue (therefore I6 and M9 in MPx) samples a less hydrophobic environment. Moreover, we found that increasing w_0 to 20 has a negligible effect on the C≡N stretching vibration of MPx-CN5, MPx-CN9, and MPx-CN15 (data not shown), suggesting that even in an environment where more “free water” molecules are available (Maitra, 1984; Onori and Santucci, 1993; Venables et al., 2001; Nucci and Vanderkooi, 2005), the Phe_{CN} side chain in these peptides is not hydrated.

These findings are intriguing and interesting at the same time because they suggest a different mechanism underlying the interaction between an amphipathic peptide and AOT reverse micelles, especially at low w_0 values. When interacting with membranes, such as anionic phospholipid bilayers, an amphipathic peptide (e.g., MPx) often aligns itself in a manner such that the hydrophilic surface faces the more water-exposed region (i.e., the phospholipid head groups) while the residues on the hydrophobic side orient themselves toward the alkyl chains of the lipids (Todokoro et al., 2006). However, in the case of AOT reverse micelles our results suggest that the hydrophobic face of the MPx α -helix is actually directed toward the center of the polar core of the micelles. Since the sulfosuccinate head groups, lining the interfacial region of AOT reverse micelles, are negatively charged and therefore can interact favorably with any positively charged groups, we hypothesize that electrostatic interactions play a key

role in stabilizing the amphipathic α -helix formed by the MPx peptide in AOT reverse micelles. Since the hydrophilic side of the MPx α -helix consists mostly of lysine residues, which are positively charged under the current conditions, it is therefore very likely that this side faces the head groups of the AOT molecules (Figure 4.5) to maximize the favorable electrostatic interactions (Dong and Zhou, 2006). Consequently, residues located at positions 6 and 9, which constitute part of the hydrophobic face of the MPx α -helix, will point toward the water pool (Figure 4.5). As a result, the cyano moiety at these positions will show a slightly higher C \equiv N stretching frequency, due to a modest increase in the polarity of the environment it samples. Alternatively, these higher frequencies may be attributed to intramolecular hydrogen bond formation, for example, between the C \equiv N group and the side chain of nearby asparagine and/or lysine residues. However, a closer inspection of the NMR structure (Todokoro et al., 2006) of MPx largely rules out this possibility. Consistent with this argument, our previous study has shown that the C \equiv N stretching frequency of both MPx-CN6 and MPx-CN9, when bound to a phospholipid bilayer (Tucker et al., 2004a), is indistinguishable from those of other MPx-CN_y peptides. What is surprising, however, is that even at $w_0 = 20$, none of the Phe_{CN} side chains in either MPx-CN5, MPx-CN9, or MPx-CN15 show any evidence of increased degrees of hydration (as judged by both the position and width of the C \equiv N band). This implies that solvating such hydrophobic side chains by water molecules is an unfavorable process (Garcia et al., 1997), a picture that is obvious but rarely tested by experiments. It is well-known that in the interfacial (or head group) region of AOT reverse micelles very few “free water” molecules are available to interact with any guest molecules, thus

entailing this region hydrophobic-like for the entrapped molecular species (Maitra, 1984; Onori and Santucci, 1993; Venables et al., 2001; Nucci and Vanderkooi, 2005). In this respect it is therefore of interest to revisit the commonly accepted notion that the AOT reverse micelles can be used as a reliable membrane-mimicking system. While indeed this inverted micellar system has been shown to exhibit membrane-like characteristics, including the slowdown of the interfacial water solvation dynamics (Riter et al., 1998a; Dokter et al., 2006) and promotion of α -helix formation for membrane-binding peptides (Nicot et al., 1985; Gallay et al., 1987; Raghuraman and Chattopadhyay, 2003), results from the current study nevertheless suggest that the mechanism of interaction between MPx and AOT reverse micelles is different from that between MPx and lipid bilayers.

4.4 Conclusion

Using the $\text{C}\equiv\text{N}$ stretching vibration of *p*-cyano-phenylalanine and the amide I' band of the peptide backbone as a local and global IR reporter, respectively, we have examined the hydration status of an amphipathic peptide, mastoparan x, in AOT reverse micelles. Our results show that at $w_0 = 6$ the peptide adopts an α -helical conformation and is mostly dehydrated, as judged from both the $\text{C}\equiv\text{N}$ stretching and the amide I' vibrational transitions, suggesting that mastoparan x preferentially binds to the interfacial region of the AOT reverse micelles where “free water” molecules are scarce. Furthermore, our results suggest that the positively charged, hydrophilic side of the mastoparan x α -helix faces the negatively charged sulfosuccinate head groups, indicating that electrostatic interactions, together with the hydrophobic-like environment near the interfacial region of the AOT reverse micelles, provide the major driving forces for folding.

Table 4.1 Band position (ν) and full width at half-maximum ($\Delta\nu$) of the stretching vibration of $\text{C}\equiv\text{N}$ in MPx-CNy peptides.

Phe _{CN} Position	5	6	7	9	15
ν (cm ⁻¹)	2229.0	2230.7	2228.6	2230.9	2228.5
$\Delta\nu$ (cm ⁻¹)	7.7	6.9	7.7	7.6	6.8

Figure 4.1 Far-UV CD spectra of MPx-CN5 in water (x) and AOT reverse micelles at w_0 = 6 (o) and 20 (Δ), respectively. These data were collected at 4 °C.

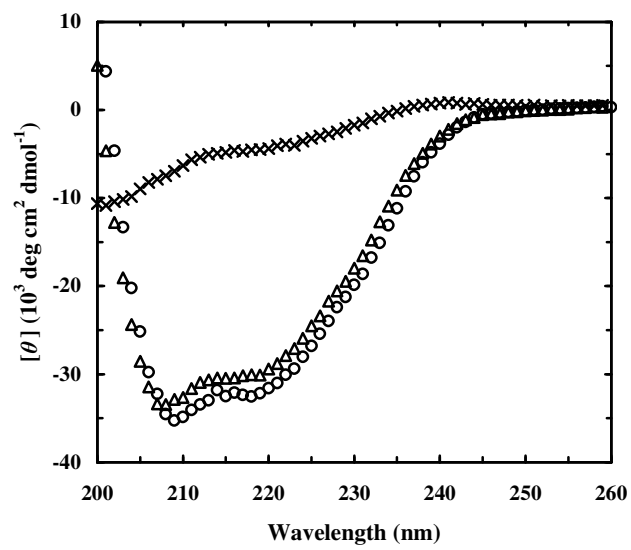


Figure 4.2 FTIR spectra (in the $\text{C}\equiv\text{N}$ stretching region) of Phe_{CN} in AOT reverse micelles of (a) $w_0 = 6$, (b) $w_0 = 20$, and (c) $w_0 = 30$. These data were collected at 4 °C and the concentrations are about 0.5, 1.1 and 1.4 mM for (a), (b) and (c), respectively. Similar results were obtained for Phe_{CN} concentrations in the range of 60-200 μM . The smooth line in (a) corresponds to a Lorentzian with $\nu = 2229.1 \text{ cm}^{-1}$ and $\Delta\nu = 7.4 \text{ cm}^{-1}$. The smooth lines in (b) and (c) correspond to a sum of two Lorentzians with $\nu_1 = 2229.1 \text{ cm}^{-1}$, $\Delta\nu_1 = 6.9 \text{ cm}^{-1}$, $\nu_2 = 2236.9 \text{ cm}^{-1}$ and $\Delta\nu_2 = 16.9 \text{ cm}^{-1}$ for (b) and $\nu_1 = 2229.4 \text{ cm}^{-1}$, $\Delta\nu_1 = 6.9 \text{ cm}^{-1}$, $\nu_2 = 2236.6 \text{ cm}^{-1}$ and $\Delta\nu_2 = 15.4 \text{ cm}^{-1}$ for (c), respectively.

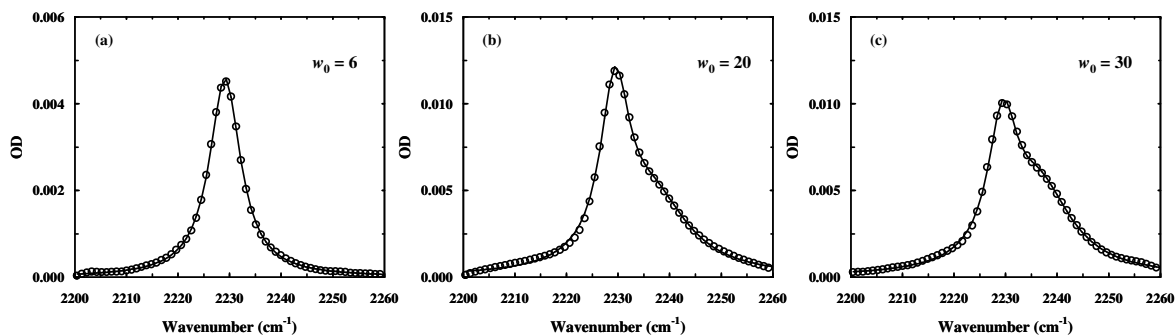


Figure 4.3 FTIR spectra (in the $\text{C}\equiv\text{N}$ stretching region) of MPx-CNy peptides in AOT reverse micelle of $w_0 = 6$, as indicated in the plot. These spectra were collected at 4 °C and have been offset for clarity. The solid lines are fits to a Lorentzian function and the corresponding fitting parameters are listed in Table 4.1.

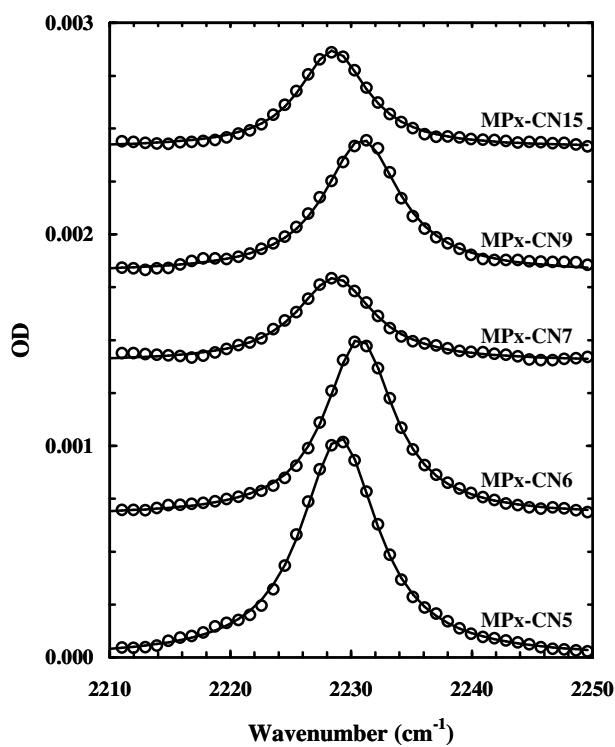


Figure 4.4 FTIR spectra (in the amide I' region) of MPx-CN5 in AOT/IO/D₂O reverse micelles of $w_0 = 6$ (red) and 20 (blue), respectively. These data were collected at ~ 4 °C and the spectrum obtained at $w_0 = 6$ has been normalized with respect to that obtained at $w_0 = 20$ for easy comparison. Also shown (thin black line) is the normalized amide I' band of the AKA₂ peptide in AOT/IO/D₂O reverse micelles of $w_0 = 6$.

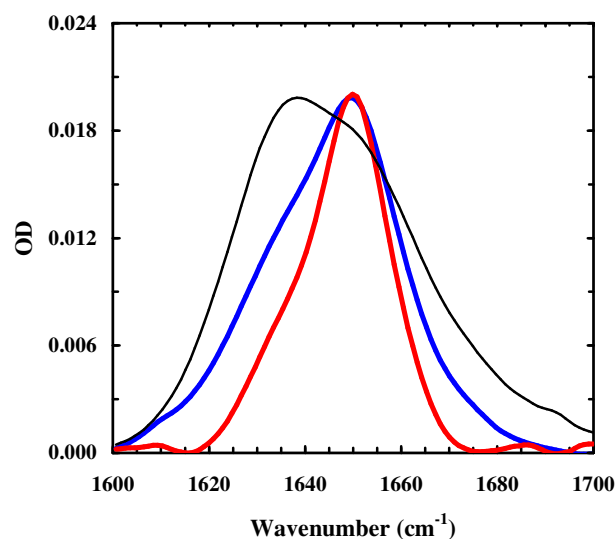
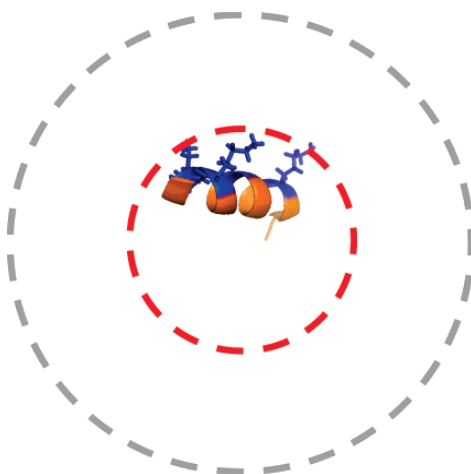


Figure 4.5 An illustrative representation of the proposed orientation and location of the MPx peptide inside an AOT reverse micelle of $w_0 = 6$, where the red and gray circles are intended to represent the inner and outer surfaces of the reverse micelle, respectively. While the lysine side chains are also shown (blue), it is worth noting that the dimensions of the peptide are not drawn to proportion.



Chapter 5: Effect of Hydration on the Helicity and Aggregation Properties of Five Alanine-Based Peptides

This work is part of the following publications: S. Mukherjee, P. Chowdhury, and F. Gai. *J. Phys. Chem. B* 2006 **110**, 11615-11619. S. Mukherjee, P. Chowdhury, and F. Gai. *J. Phys. Chem. B* 2007 **111**, 4596-4602.³

S. M. collected and analyzed the data. S. M, P. C. and F. G. wrote the paper.

We show that the helicity of alanine-based peptides can be tuned by varying the degrees of backbone hydration. The latter was achieved by solubilizing the peptides in the water pool of sodium bis(2-ethylhexyl) sulfosuccinate (AOT) reverse micelles with different water contents or w_0 values. Far-UV circular dichroism measurements on a series of alanine-rich peptides indicate that the helicity of short peptides is significantly increased in AOT reverse micelles at low w_0 values, as compared to the corresponding helical content in buffer at 4 °C. This result therefore corroborates the previous simulation studies suggesting that desolvation of backbone CO and NH groups increases the stability of monomeric helices. Temperature-dependent infrared studies further show that these helical peptides undergo a thermally induced conformational transition in reverse micelles of low w_0 values (e.g., $w_0 = 6$), resulting in soluble peptide aggregates rich in antiparallel β -sheets. Interestingly, however, increasing w_0 or water content leads to an increase in the onset temperature at which such β -aggregates begin to form. Therefore,

³ Reproduced with permission from [S. Mukherjee, P. Chowdhury, and F. Gai. *J. Phys. Chem. B* 2006 **110**, 11615-11619. S. Mukherjee, P. Chowdhury, and F. Gai. *J. Phys. Chem. B* 2007 **111**, 4596-4602.] Copyright (2006, 2007), the American Chemical Society.

these results provide strong evidence suggesting that limited hydration facilitates aggregate formation and that removal of water imposes a free energy barrier to peptide association and aggregation, a feature that has been suggested in recent simulation studies focusing on the mechanism of β -amyloid formation.

5.1 Introduction

It is widely known that the conformation that a polypeptide chain assumes is dependent on the particular environment in which the folding process takes place. Given the importance of water in mediating the process of protein folding (Levy and Onuchic, 2006), we sought to examine how degrees of hydration will affect the conformation of a polypeptide chain. Although, it is well established that water plays an important role in many chemical and biological processes, however, in many cases it has been difficult to evaluate the net effect of hydration on the physical and/or chemical properties of the molecular system of interest simply because a systematic variation of the degree of hydration of the solute molecule in question is not easily achievable (except in the gas phase where it has been shown that solute-water complexes with a limited, but well-defined number of water molecules can be created, for example, for peptides (Jarrold, 2000; Wyttenbach et al., 2005)). While using a co-solvent can sometimes allow one to probe how dehydration affects a specific physical observable (Starzyk et al., 2005), such a method may encounter added complexity that renders the experimental results difficult to interpret. In this regard, AOT reverse micelles might prove especially useful because it has been shown that the water in the polar core of AOT reverse micelles is well defined and its content can be tuned by varying the ratio of the molar concentration of water to that of the surfactant or w_0 value (Maitra, 1984). In addition, the influence of geometrical confinements (Zhou et al., 2008) on the structure and stability of a biological molecule of interest encapsulated within the polar core of the reverse micelles could also be studied (Peterson et al., 2004).

Alanine-based helical peptides have been widely used in experimental studies aimed at understanding the folding dynamics of monomeric helices (Williams et al., 1996; Thompson et al., 1997; Volk et al., 1997; Clarke et al., 1999b; Lednev et al., 1999b; Huang et al., 2001b; Huang et al., 2001c; Jas et al., 2001; Huang et al., 2002b; Werner et al., 2002; Wang et al., 2003; Wang et al., 2004; Bredenbeck et al., 2005; Balakrishnan et al., 2007). Typically, the sequence of such peptides contains XAAAA repeats, with X being a polar or charged amino acid (e.g., lysine and arginine). While Marqusee and Baldwin (Marqusee and Baldwin, 1987; Marqusee et al., 1989) originally used such amino acids to increase the solubility of alanine-based peptides in aqueous solution, recent simulation studies nevertheless suggest that the side chain of such residues may play an unexpected role in stabilizing the helical conformation. For example, using conformational energy calculations, Scheraga and co-workers (Vila et al., 2000; Vila et al., 2001) have shown that a lysine side chain can effectively desolvate several amide NH and CO groups, thereby strengthening the corresponding helical hydrogen bonds. As a result, the α -helix is stabilized. Furthermore, using an explicit solvent model, Garcia and co-workers (Garcia and Sanbonmatsu, 2002; Ghosh et al., 2003) have obtained similar results indicating that such side chain-shielding effects are indeed stabilizing. Moreover, Jarrold and co-workers have demonstrated that alanine-rich peptides can form very stable helical conformations in vacuo (Hudgins and Jarrold, 1999). Taken together, these studies thus indicate that water molecules actually act as denaturants toward the helical conformation by competing for hydrogen bonds with the amide CO and NH groups. Therefore, alanine-rich peptides can serve as an excellent

model system to examine how degrees of hydration affect the conformation of a peptide. Specifically, we investigated the conformational properties of five alanine-based peptides used by Wang et al. (Wang et al., 2004) by solubilizing these peptides in the aqueous core of AOT reverse micelles at different water contents.

Consistent with previous simulation studies (Vila et al., 2000; Vila et al., 2001; Garcia and Sanbonmatsu, 2002; Ghosh et al., 2003), our CD results indicate that at low temperatures, dehydrating the backbone CO and NH groups of alanine-based peptides results in an increase in its overall helicity. The CD results also indicate that the alanine-based peptides undergo a sharp thermal unfolding transition in AOT reverse micelles of $w_0 = 6$. To provide a better understanding of how alanine-based peptides are hydrated in AOT reverse micelles and why they undergo such unusual temperature-dependent conformational changes, we examined the thermodynamic properties of two alanine peptides by examining their amide I' (amide I vibration measured in D₂O) vibrational transitions as a function of water loading inside the polar core of the reverse micelles and temperature. These infrared (IR) measurements not only allowed us to directly probe how the degree of hydration affects the amide I' bands of α -helices, but they also revealed that limited hydration promotes formation of aggregates rich in antiparallel β -sheets. The latter finding has important implication for the mechanism of amyloid formation and protein aggregation in general (Dobson, 1999).

5.2 Experimental Methods

Materials. AOT and isooctane were purchased from Sigma Chemical Co. (St. Louis, MO). AOT was purified using standard procedures outlined in Chapter 2. Isooctane was used without further purification.

Peptide Synthesis and Purification. The peptides used in the current study have the following sequence, YGAKAAAA(KAAAA)_nG (i.e., AKA_n peptide with n = 1, 2, 3, 5, and 6), and were synthesized by employing the standard Fmoc protocol and purified by reverse phase HPLC. The identity of the samples was further verified by electrospray-ionization mass spectroscopy.

Preparation of Samples. 50 mM AOT/isooctane solution was prepared as outlined in Chapter 2. To prepare the peptide-AOT/IO solutions, lyophilized peptide solid was first dissolved in Millipore water and then an appropriate aliquot of this peptide solution was added to the above AOT/IO solution to achieve the desired w_0 values. Before use, this solution was further stirred for 30 min and then centrifuged for 15 min to remove any precipitates. Similarly, the peptide/buffer solution was prepared by directly dissolving lyophilized peptide solid into phosphate buffer (50 mM, pH 7). The final peptide concentration of all of the samples was determined optically by the single tyrosine absorbance at 276 nm using $\epsilon_{276} = 1450 \text{ cm}^{-1} \text{ M}^{-1}$ and was found to be in the range 30–123 μM . Assuming that peptide incorporation does not affect the characteristic micellar distributions, a simple stoichiometric calculation (Chowdhury et al., 2000) indicates that the peptide to micelle ratio is $\sim 1:20$ for $w_0 = 6$ and 50 μM peptide.

CD Spectroscopy. The far-UV CD data were collected on an AVIV 62DS spectrometer (Lakewood, NJ) using a 1 mm quartz cell.

FTIR Measurements. FTIR spectra were collected on a Nicolet Magna-IR 860 spectrometer using 2 cm^{-1} resolution. The two-compartment sample cell, temperature control, and data averaging protocols have been described in Chapter 2. Due to the low water content in the AOT reverse micelle samples, we were able to use a sample cell with a relatively long optical path length (390 μm , determined interferometrically). Consequently, this allowed us to use peptide samples in the sub-millimolar concentration range. For all the spectra shown, a background arising from imperfect subtraction of AOT signals was subtracted.

Dynamic Light Scattering Measurements. The size distribution of AOT reverse micelles at $w_0 = 6, 10$ and 20 with or without the AKA₃ peptide was measured as outlined in Chapter 2.

5.3 Results and Discussion

Previous studies (Freda et al., 2002) have shown that at low w_0 values (e.g., below 10) most of the water molecules are hydrogen bonded to the negatively charged sulfosuccinate headgroups of the AOT molecules and, thus, very few free water molecules are available to interact with any guest molecule entrapped inside the water pool of the reverse micelles. For example, at $w_0 = 6$, there are about 300-325 water molecules per water cavity (Chowdhury et al., 2000), of which only a small fraction (~32%) is considered as free while the rest remains bound to the AOT headgroups (Maitra, 1984). Since water plays an essential role in determining the structure, stability,

and dynamics of biological molecules, it is expected that this limited supply of water molecules will affect the conformational properties of proteins and peptides solubilized inside the water pool of AOT reverse micelles (Raghuraman and Chattopadhyay, 2003). For instance, it is expected that AOT reverse micelles with low water content will promote alanine-based peptides to adopt helical conformations because the intrahelical hydrogen bonds in such an environment will be strengthened, owing to the simultaneous decrease in the overall dielectric constant and degrees of backbone hydration (Vila et al., 2001; Ghosh et al., 2003; Abel et al., 2006). Consistent with this expectation (Figure 5.1), the helicity of the AKA₁ peptide, which lacks significant helical content in aqueous solution, undergoes a dramatic increase in helicity when introduced into AOT reverse micelles at $w_0 = 6$. While geometrical confinement exerted by the finite size of the aqueous cavity of the AOT reverse micelle could also lead to structural changes (see discussion below), we believe in the current case the confinement effect is negligible because the diameter of the water pool at $w_0 = 6$ is approximately 28 Å (Maitra, 1984), much longer than the helix length of AKA₁ (~14 Å estimated by assuming that only the KAAAKAAAA segment can form a helical conformation). Furthermore, we found that the AKA₁ peptide (and also other AKA_n peptides used in the current study) is insoluble in both isooctane and AOT-isooctane mixtures (without water) and the increase in helicity is independent of peptide concentration. Therefore, we attributed the increased helicity of the AKA₁ peptide in AOT reverse micelles to alleviated peptide backbone hydration. Apparently, results obtained in earlier simulation studies (Vila et al., 2000; Vila et al., 2001; Garcia and Sanbonmatsu, 2002; Ghosh et al., 2003) of alanine-rich peptides in

water and reverse micelles (Abel et al., 2006) corroborate such a conclusion. This finding is also consistent with the fact that fluorinated alcohols, such as 2,2,2-trifluoroethanol (TFE) (Guo and Karplus, 1994; Cammers-Goodwin et al., 1996; Rajan and Balaram, 1996; Luo and Baldwin, 1997; Kentsis and Sosnick, 1998; Hong et al., 1999; Roccatano et al., 2002) and 1,1,1,3,3,3-hexafluoro-propan-2-ol (HFIP) (Andersen et al., 1999; Hong et al., 1999; Roccatano et al., 2005), can promote helix formation in aqueous solution. While several microscopic mechanisms have been proposed, this helix-promoting ability of fluorinated alcohols could be regarded as a consequence of alcohol-water and/or alcohol-peptide interactions, which have been suggested to help reduce the degree of hydrogen bonding between peptide amide groups and water molecules (Guo and Karplus, 1994; Cammers-Goodwin et al., 1996; Rajan and Balaram, 1996; Luo and Baldwin, 1997; Kentsis and Sosnick, 1998; Andersen et al., 1999; Hong et al., 1999; Roccatano et al., 2002).

While the above result suggests that the water pool formed in AOT reverse micelles at $w_0 = 6$ preferentially stabilizes the helical conformation of short alanine-based peptides, the mean residue ellipticity of AKA₁ at 222 nm (i.e., $[\theta]_{222}$, which is a commonly used indicator of the overall helicity of proteins and peptides (Berova et al., 2000)) and 4 °C is only about 14 000 deg cm² dmol⁻¹, indicating that the peptide conformation is far from being fully helical (Luo and Baldwin, 1997). Therefore, to provide a better understanding of how degrees of hydration affect the conformation of peptides, we further studied (a) the helicity of the AKA₃ peptide in AOT reverse micelles

with different w_0 values and (b) the thermal unfolding transitions of a series of AKA_n peptides in AOT reverse micelles at $w_0 = 6$.

Dynamic light scattering measurements confirmed that the incorporation of the AKA₃ peptide did not statistically affect the size distribution of the empty reverse micelles (Figure 5.2). As shown (Figure 5.3), the far-UV CD spectra of AKA₃ collected at different water concentrations indicate that its overall helical content in AOT reverse micelles is significantly increased compared to its buffer counterpart, as judged by the value of $[\theta]_{222}$. While these results further support the idea that decreasing degrees of backbone hydration stabilizes the helical conformation of alanine-based peptides, the net effect of a reverse micelle is somewhat complicated and depends on w_0 . For example, the $[\theta]_{222}$ value of AKA₃ at $w_0 = 4$ is smaller than those obtained at larger w_0 values, suggesting that a different effect, which is destabilizing in nature, also exists. Quite likely, this destabilization effect arises from the fact that the peptide molecules can only sample a limited and confined space in reverse micelles and, as a result, the longest helical conformation that can exist in a certain water cavity is limited by the size of the latter. For AKA₃, this “geometric confinement effect” would become more pronounced for water pools formed in AOT reverse micelles at $w_0 = 4$ because the diameter of the latter is approximately 20 Å (Maitra, 1984), whereas the length of the fully helical structure formed by an AKA₃ peptide is ~29 Å (estimated by assuming that only the KAAAA(KAAAA)_n segment can adopt a helical conformation). While it has been shown that confinement or crowding generally leads to an increase in the stability of proteins or even induces unstructured polypeptide chains to fold (Eggers and Valentine, 2001b; Zhou

and Dill, 2001; Peterson et al., 2004; Zhou et al., 2008), the consequence of confinement on a helix is exactly the opposite because it prefers to adopt a linear structure. Consistent with our result, a similar confinement effect has also been observed for DNA molecules entrapped in the water cavities of reverse micelles (Budker et al., 2002). Taken together, the CD data presented in Figure 5.3 therefore signify the net result of two competing effects, namely, confinement and backbone dehydration, on the helicity of the AKA₃ peptide.

To gain a better understanding of the confinement effect discussed above, the thermal unfolding transitions of five AKA_n peptides were compared at a fixed w_0 value (i.e., $w_0 = 6$). As shown (Figure 5.4), the CD thermal unfolding curves of these peptides exhibit rather interesting but different thermal melting behaviors when encapsulated inside the water pool of AOT reverse micelles at $w_0 = 6$. First, all peptides, except AKA₁, exhibit a major and also rather sharp unfolding transition. However, the midpoint of the transition occurs at different temperatures for different peptides. Second, the overall helicity of these peptides at low temperatures (e.g., 4 °C), as judged by their mean residue ellipticity, first increases with an increase of the peptide chain length (i.e., from AKA₁ to AKA₃) and then decreases as the peptide chain is further lengthened (i.e., from AKA₃ to AKA₆). Since a monotonic increase in helicity with increasing chain length has been observed for this set of peptides in aqueous solution (Wang et al., 2004), these results therefore reinforce the idea that the effect of reverse micelles at a specific w_0 value on helical peptides is a balance of two opposing effects, namely, (a) stabilization resulting from backbone dehydration and (b) destabilization arising from geometrical confinement.

Both AKA₂ and AKA₆ peptides undergo a sharp thermal unfolding transition in AOT reverse micelles of $w_0 = 6$. To help elucidate the nature of such transition and also to investigate how temperature affects the hydration and hence the amide I' vibrational transitions of α -helices, we further studied the temperature dependence of the amide I' band of both peptides in AOT/D₂O/IO reverse micelles of $w_0 = 6$. While w_0 should remain constant with increasing temperature, previous studies have shown that temperature does have an effect on the size of the micelles. However, such effect has been shown to be minimal for AOT reverse micelles with low w_0 values (e.g., $w_0 = 6$) (Zulauf and Eicke, 1979). Interestingly, AKA₂ and AKA₆ show rather similar behavior at $w_0 = 6$ in the context that their spectra display a drastic change above a characteristic onset temperature. For example, for AKA₂ increasing the temperature from 4.3 to about 53.2 °C causes the hydrated helical amide I' absorbance to diminish, which is accompanied by the concomitant increase in the intensity of the dehydrated helical amide I' band (Figure 5.5a). A further increase in temperature, however, significantly changes the overall shape of the amide I' band, indicative of a conformational change occurring at higher temperatures (see below). Similarly, the amide I' band of AKA₆ undergoes an initial modest change when the temperature is increased from 4.3 to 25.3 °C, followed by a drastic change with further increase in temperature (Figure 5.5b). Since our CD results (Figure 5.4) show that under the current micellar conditions the AKA₂/AKA₆ peptide does not undergo a distinct conformational transition below ~45/35 °C, the spectral changes taking place at relatively low temperatures could then be attributed to a dehydration process wherein the initially hydrated sites progressively become less

hydrated or completely dehydrated. Consequently, the dehydrated helical amide I' absorbance (i.e., the band centered at 1650 cm^{-1} , see Chapter 3 for more information) also shows a gain in intensity (Figure 5.5b), albeit small, with increasing temperature at the expense of the hydrated helical band, a feature supporting the idea that the spectral changes observed at relatively low temperatures in both cases arise at least in part from the interconversion between two discrete subsets of amide carbonyls, i.e., hydrated and dehydrated helical amides. To gain a better understanding of the effect of hydration on the amide I' band of these AKA_n peptides as well as their aggregation properties, we further measured the temperature-dependent FTIR spectra of the AKA₂ and AKA₆ peptides in AOT/D₂O/IO reverse micelles at higher w_0 values. As shown (Figure 5.6a), at w_0 of 10 and low temperatures (e.g., $4.0\text{ }^{\circ}\text{C}$) the amide I' band of AKA₂ is dominated by a single spectral feature centered at $\sim 1634\text{ cm}^{-1}$, indicating that increasing w_0 leads to an increase in the degree of hydration of the peptide backbone. At $w_0 = 20$, the amide I' band of AKA₂ (Figure 5.6b) becomes almost identical to that obtained in D₂O, suggesting that the overall hydration in both cases is similar. Thus, these results corroborate the above assignment that the 1650 cm^{-1} component arises primarily from dehydrated helical amides. In principle, spectral decomposition can be used to provide further quantitative information regarding the constituent and resolvable spectral features underlying the amide I' profile (Zhu et al., 2004b). However, a simple Fourier self-deconvolution (FSD) analysis revealed that at least five overlapping bands are required to fit these amide I' spectra. Therefore, we did not attempt to quantitatively assess how these bands vary as a function of w_0 and temperature.

Taken together, the aforesaid temperature-dependent studies suggest that increasing temperature can lead to either weakening or breaking of the hydrogen bonds formed between the amide groups and water molecules, consequently resulting in a blue shift in the amide I' vibrational transitions of the corresponding amide carbonyls. This finding can be used to rationalize the so-called fast relaxation phase observed in laser-induced temperature-jump IR experiments of peptides and proteins (Huang et al., 2001b; Huang et al., 2002b; Zhu et al., 2003; Bredenbeck et al., 2005; Xu et al., 2006). In such experiments, one frequently observes a *T*-jump induced kinetic phase in the amide I' region that occurs on a time scale that is too fast to be resolved by a nanosecond *T*-jump apparatus. While other conformational processes may also contribute to this fast phase (Huang et al., 2001b), the current results nevertheless suggest that the temperature-induced spectral shift in the amide I' band will definitely give rise to a fast *T*-jump relaxation signal provided such shift takes place on the picosecond time scale, as recently observed by Hamm and co-workers (Bredenbeck et al., 2005).

The temperature-dependent FTIR spectra of these peptides indicate that above a certain onset temperature two new spectral features, which are narrow and centered at ~ 1620 and $\sim 1687\text{ cm}^{-1}$, respectively, begin to develop (Figure 5 a and b). These spectral features are characteristic of peptide aggregates rich in multistranded antiparallel β -sheets (Byler and Susi, 1986; Dong et al., 1990; Surewicz et al., 1993; Haris and Chapman, 1995). Since the peptide to micelle ratio was estimated to be less than 1 (see Experimental Methods), the current results can be explained on the basis of an early study indicating that reverse micelles are dynamic in nature and can coalesce and/or

exchange contents among themselves (Luisi, 1985). Since the onset temperature for each peptide coincides with the temperature wherein its CD signal starts to decrease in a cooperative manner, these FTIR results thus suggest that the sharp thermal unfolding transitions obtained in our CD studies (Figure 5.4) arise from an aggregation process. Interestingly, however, our FTIR data show that this aggregation process depends on both the water content and peptide chain length, i.e., the degree of peptide hydration, providing strong implication for the mechanism of peptide self-association in aqueous solution.

The temperature at which the characteristic IR spectral features of aggregates become observable is ~ 32.3 °C for AKA₆ and ~ 60.3 °C for AKA₂, respectively, at $w_0 = 6$ (Figure 5.5 a and b). Moreover, since the AKA₆ peptide in D₂O does not show any detectable aggregates even at 77 °C and at a molar concentration that is 25-50 times larger than that used in the reverse micellar studies, these results thus suggest that the limited supply of water molecules found inside the polar cavity of AOT reverse micelles presents an environment conducive to peptide aggregation. Consistent with this notion, the AKA₆ peptide, which is much longer and therefore less hydrated, exhibits a lower onset aggregation temperature. Taken together, these results suggest that the process of dehydration plays an important role in peptide and protein aggregation.

To provide further evidence supporting this notion, we have studied the aggregation behaviors of both peptides in AOT reverse micelles of higher w_0 values. If dehydration is indeed one of the important factors governing the thermodynamics of the aggregation process, one would expect the extent of aggregation of these peptides to

decrease with increasing w_0 . As expected (Figure 5.6 a and b), in the temperature range studied the AKA₂ peptide shows no aggregation in reverse micelles of $w_0 = 10$ and 20. Results obtained with the AKA₆ peptide (Figure 5.6 c and d) further strengthen the conclusion drawn above that dehydration facilitates aggregation as indicated by the fact that at $w_0 = 10$ the characteristic IR peaks of AKA₆ aggregates only become prominent at 40.4 °C, higher than that observed at $w_0 = 6$, whereas increasing the value of w_0 to 20 abolishes the aggregation process (in the temperature range studied). Taken together, these results therefore provide the strongest evidence, suggesting that hydration/dehydration plays a key role in mediating polypeptide aggregation and that hydration helps prevent aggregate formation. The latter notion becomes quite apparent if a desolvation barrier has to be overcome prior to peptide self-assembly. Moreover, these results further indicate that dehydration rather than temperature-induced unfolding is responsible for the formation of aggregate in reverse micelles.

Finally we would like to discuss our results in the perspective of other relevant studies concerning the conformational transition from α -helix to β -sheet, a hallmark associated with amyloid formation. Hall and co-workers have shown using discontinuous molecular dynamics simulations that a polyalanine-based peptide (Ac-KA₁₄K-NH₂) prefers either the α -helix or β -structure depending on the solvent condition (i.e., the value of a hydrophobic strength parameter “ R ”) (Nguyen et al., 2004). While at low R values the peptide interconverts between predominantly α -helix and random coil-like structures depending on temperature, at very high values of R the peptide takes up a β -sheet-like structure, a precursor for β -aggregate formation. Furthermore, Carpenter and co-workers

have shown that for poly-l-lysine the preferred conformation in the dried state (lyophilized peptide) is β -sheet irrespective of the structure the peptide might adopt in solution (Prestrelski et al., 1993), which is in agreement with our observation that dehydration promotes the formation of peptide aggregates rich in β -sheets. Additionally, Tarus et al. (Tarus et al., 2005; Tarus et al., 2006) have recently shown through simulation that the initial dimerization/oligomerization between A β peptides might involve the formation of contacts between hydrophobic clusters, a process requiring expulsion of interfacial water molecules. However, as the authors have suggested, the latter event may encounter an effective free energy barrier because it requires a cooperative rearrangement of ordered water molecules. In a related study concerning a β -amyloid peptide and its mutant, Massi and Straub have also shown that desolvation is an important step in peptide aggregation.⁴⁶ Moreover, Fernandez and Scheraga have shown through simulations that removal of water from regions of proteins having underdehydrated hydrogen bonds (UDHB) is an important factor in defining protein-protein interactions and subsequent amyloidogenic β -sheet association (Fernandez and Scheraga, 2003). Taken together, these studies all suggest that hydration imposes a free energy barrier for two protein or peptide molecules to associate. Therefore, our study provides direct experimental evidence supporting this notion. Finally, our findings are particularly interesting from a comparative point of view because the water stored in the polar core of reverse micelles has been suggested to mimic the water found in the nanopores of cellular compartments (Levinger, 2002).

5.5 Conclusions

Using circular dichroism and infrared spectroscopy and AOT reverse micelles, we have studied how degrees of hydration can affect the conformation of alanine-rich peptides. Our results show that desolvation of the peptide backbone increases the stability of the helical conformation. Moreover, our results indicate that, in an environment where the number of water molecules is insufficient to completely solvate the peptide, self-association that leads to the formation of β -aggregates can become thermodynamically more favorable. In other words, dehydration facilitates the formation of peptide aggregates.

Figure 5.1 Far-UV CD spectra of AKA₁ peptide in pH 7 phosphate buffer (open triangles) and AOT reverse micelle at $w_0 = 6$ (open circles). These data were collected at 4 °C.

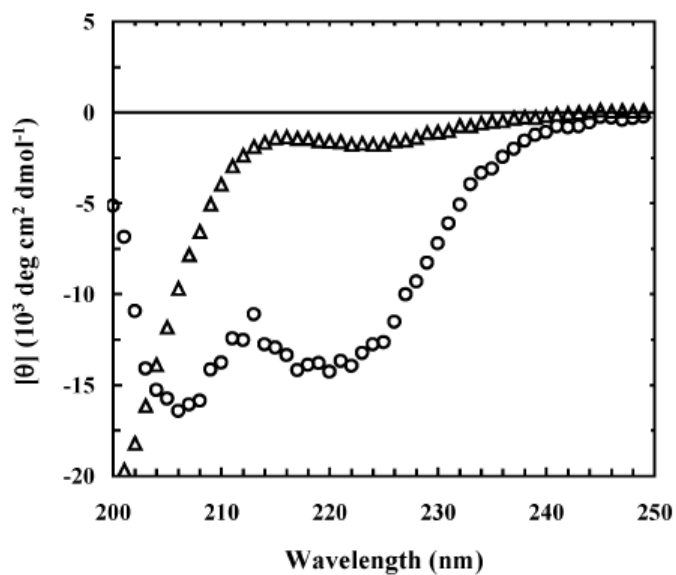


Figure 5.2 Size distribution of reverse micelles at $w_0 = 6, 10$ and 20 with (red) or without (blue) AKA₃ peptides. These data were collected at 25 °C.

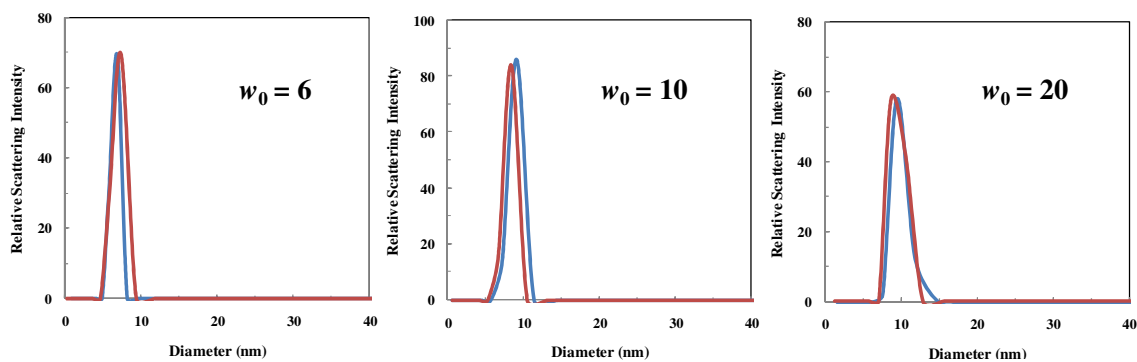


Figure 5.3 Far-UV CD spectra of AKA₃ peptide collected at 4 °C and in pH 7 phosphate buffer and AOT reverse micelles at $w_0 = 4, 6, 10$, and 20, as indicated.

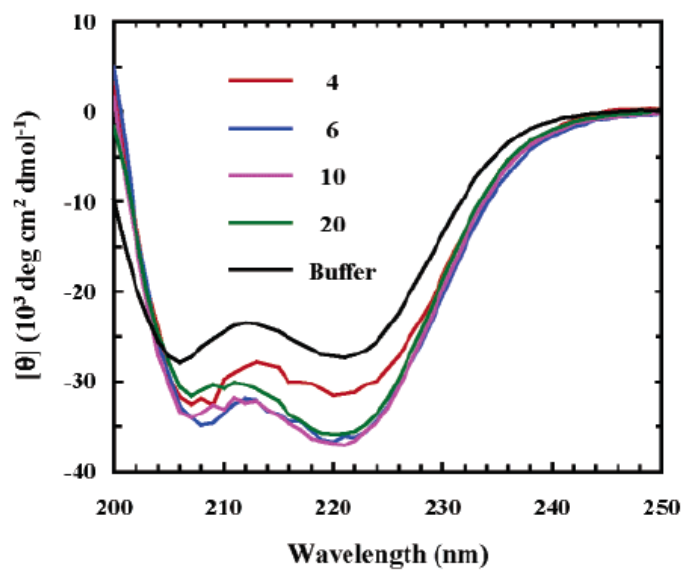


Figure 5.4 CD thermal melting curves of AKA_n peptides (n = 1, 2, 3, 5, and 6) in AOT reverse micelles at $w_0 = 6$.

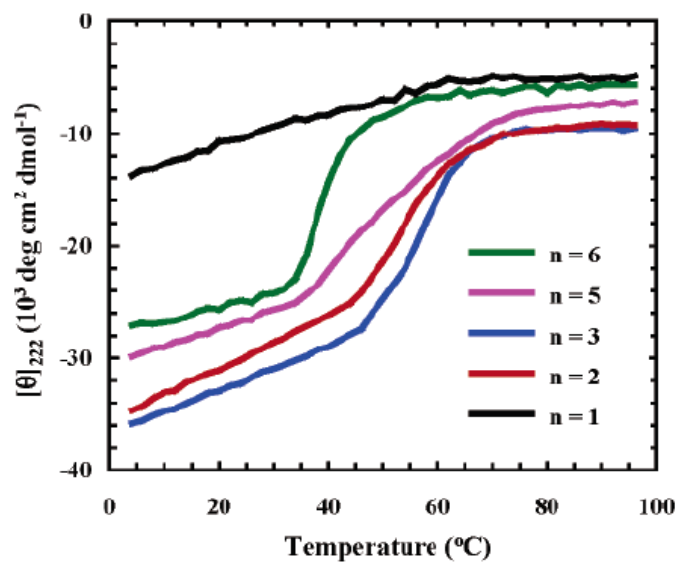


Figure 5.5 Temperature-dependent FTIR spectra (in the amide I' region) of AKA₂ (a) and AKA₆ (b) in AOT/D₂O/IO reverse micelles of $w_0 = 6$. Also shown in c are the FTIR spectra of AKA₆ in D₂O. The temperature (°C) at which each spectrum was collected is indicated in the figure.

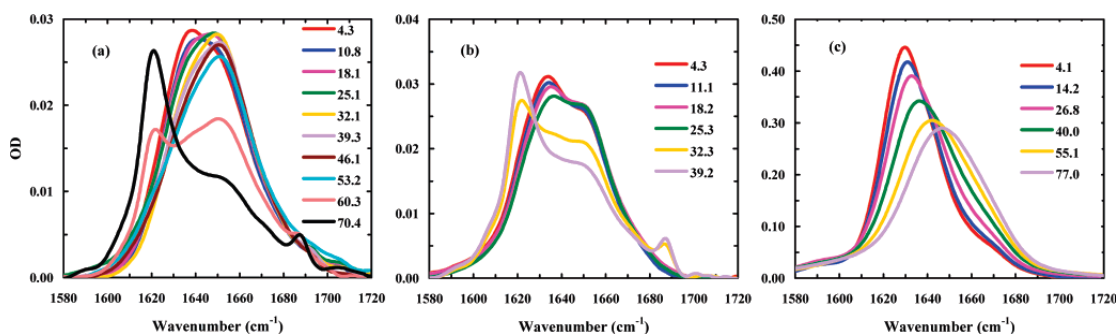
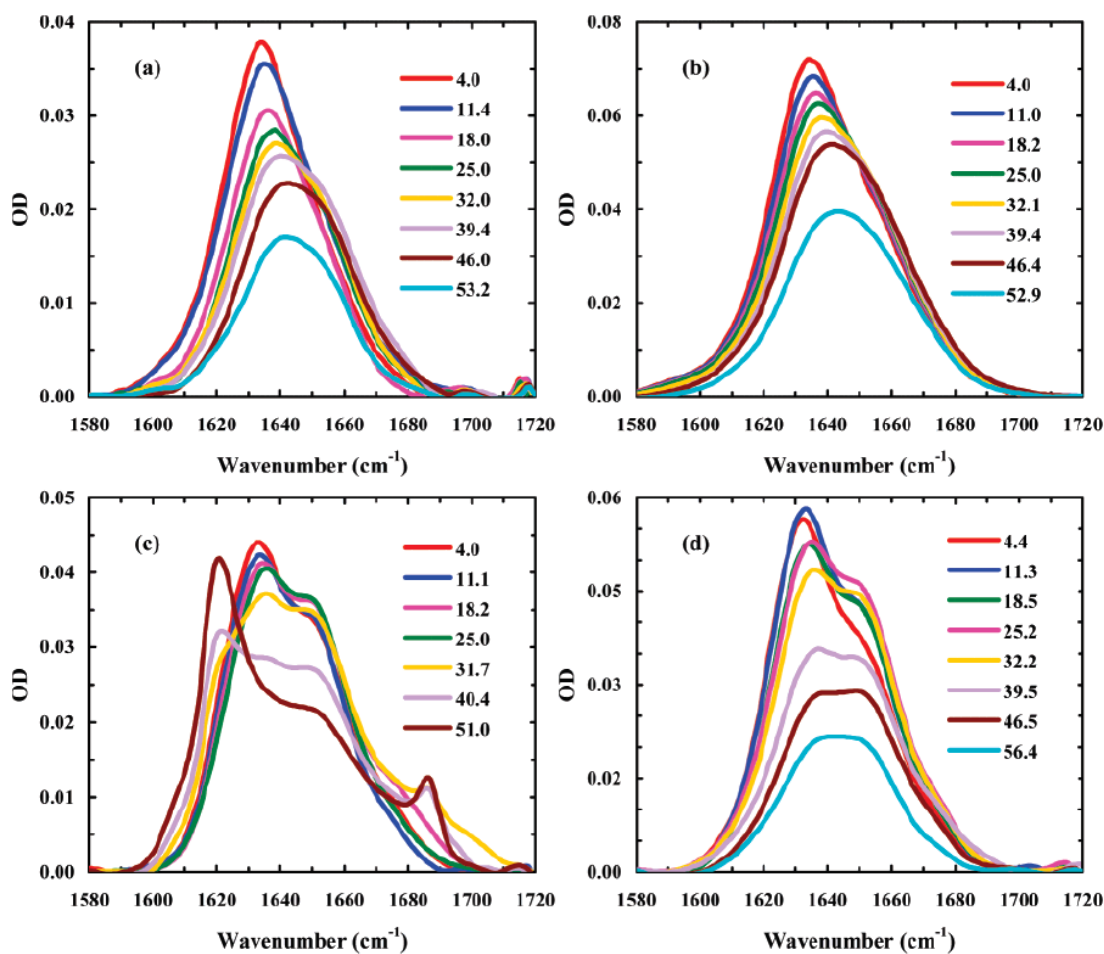


Figure 5.6 Temperature-dependent FTIR spectra (in the amide I' region) of AKA₂ and AKA₆ in AOT/D₂O/IO reverse micelles at different w_0 values, i.e., (a) AKA₂ at $w_0 = 10$, (b) AKA₂ at $w_0 = 20$, (c) AKA₆ at $w_0 = 10$, and (d) AKA₆ at $w_0 = 20$. The temperature (°C) at which each spectrum was collected is indicated in the figure.



Chapter 6: Effect of Limited Hydration on the Aggregation

Kinetics of Two Amyloidogenic Peptide

This work has been published: S. Mukherjee, P. Chowdhury, and F. Gai. *J. Phys. Chem. B* 2009 **113**, 531-535.⁴

S. M. collected and analyzed the data. S. M, P. C. and F. G. wrote the paper.

It is well known that water plays a crucial role in the folding, dynamics and function of proteins. Here we provide further evidence showing that the aggregation kinetics of peptides also depend strongly on their hydration status. Using reverse micelles as a tool to modulate the accessible number of water molecules and infrared spectroscopy and transmission electron microscopy as means to monitor aggregate formation, we show that the rate of aggregation of two amyloid forming peptides increases significantly under conditions where limited hydration of the peptide molecule is expected to occur. These results are in accord with recent computer simulations indicating that the expulsion of interfacial water molecules is a key event in the dimerization/oligomerization of amyloid β (A β) peptides.

⁴ Reproduced with permission from [S. Mukherjee, P. Chowdhury, and F. Gai. *J. Phys. Chem. B* 2009 **113**, 531-535.] Copyright (2009), the American Chemical Society.

6.1 Introduction

Amyloidosis is associated with a variety of human pathological conditions (Soto, 2001; Chiti and Dobson, 2006). Thus, recent years have seen a remarkable increase in the number of studies aimed at understanding the molecular mechanism(s) underlying amyloid formation both *in vitro* and *in vivo* using various techniques (Kelly, 1998; Soto, 2001; Dobson, 2003; Thirumalai et al., 2003; Tycko, 2003; Chiti and Dobson, 2006; Teplow et al., 2006; Chen et al., 2007; Haass and Selkoe, 2007; Bieschke et al., 2008; Kim et al., 2008; Shashilov and Lednev, 2008; Strasfeld et al., 2008). While previous studies have shown that various factors, including solvent, temperature, pH, concentration, and sequence, can significantly affect the rate of aggregation and amyloid formation (Jarrett et al., 1993; Shen and Murphy, 1995; Wood et al., 1996; Harper and Lansbury, 1997; Nielsen et al., 2001; Gorman et al., 2003; Marek et al., 2007; Wolf et al., 2008), the precise role of water, the most abundant substance in the living cell, however, is yet to be fully ascertained. Herein, we attempt to assess the effect of dehydration, by varying the available number of water molecules, on the aggregation kinetics of two well-studied peptides, A β ₁₆₋₂₂ (sequence: KLVFFAE) and Sup35₇₋₁₃ (sequence: GNNQQNY), which despite their short chain lengths have been shown to exhibit significant amyloidogenic propensity (Balbach et al., 2000; Balbirnie et al., 2001). In addition, both peptides form dehydrated oligomer/amyloid structures (Balbirnie et al., 2001; Klimov and Thirumalai, 2003; Lipfert et al., 2005; Esposito et al., 2006; Zheng et al., 2006), implying that expulsion of water is an obligatory step along the course of aggregation and fibrillization.

In the current study, modulation of the amount of water accessible to the peptide molecules of interest is achieved by solubilizing them in the water pool of reverse micelles. The reverse micelles were prepared from sodium bis(2-ethylhexyl) sulfosuccinate (AOT), isooctane (IO) and water. Many studies have shown that the number of ‘free’ water molecules confined in the polar core of a specific AOT reverse micelle system is determined by its w_0 value (i.e., [water]/[AOT]) (Luisi, 1985). For example, there are approximately 96, 473, and 4273 free water molecules available to interact with the solute molecules in the core of reverse micelles with w_0 values of 6, 10, and 20, respectively. Thus, the hydration status of an entrapped peptide can be tuned by simply varying the molar ratio of water to surfactant in the reverse micelle (Mukherjee et al., 2007b). In addition, the use of AOT reverse micelles may also prove to be beneficial for the current study because the water confined in the micellar cores has often been proposed to mimic that found in the nanopores of cellular compartments (Levinger, 2002). Our results show that both A β ₁₆₋₂₂ and Sup35₇₋₁₃ peptides form soluble aggregates in AOT reverse micelles of low w_0 values at a rate that is much faster than that in bulk water.

6.2 Experimental Methods

Materials. AOT and isooctane were purchased from Sigma Chemical Co. (St. Louis, MO). AOT was further purified by dissolving it in methanol and stirring the solution overnight in the presence of activated charcoal. Subsequent filtration and removal of methanol by distillation under vacuum yielded the AOT used in the current study.

Isooctane was used without further purification. D₂O (D, 99.96%) was purchased from Cambridge Isotope Laboratories, Inc. (Andover, MA).

Peptide synthesis and purification. A β ₁₆₋₂₂ and Sup35₇₋₁₃ peptides were synthesized and the identity of the samples was further verified as outlined in Chapter 2. Hydrogen to deuterium exchange as well as removal of residual trifluoroacetic acid from peptide synthesis were accomplished by two rounds of lyophilization against a 0.1 M DCl solution at a peptide concentration of ~50-75 μ M. The deuterated peptide was immediately used in the FTIR experiments.

Sample preparation. The purified AOT was dried under vacuum overnight before use. Then 50, 100, and 300 mM AOT/IO solutions were prepared by dissolving an appropriate mass of AOT in isooctane, which were used to prepare micelle solutions of $w_0 = 6, 10$ and 20, respectively. The resultant solutions were first vortexed for 3 minutes and then sonicated for 10 minutes in a bath sonicator, followed by stirring for one hour. The reference solution used in the FTIR experiments with a desired w_0 value was prepared by adding an appropriate amount of D₂O to one of the above AOT/IO solutions. The resultant solution was further stirred for 30 minutes before use. Similarly, the peptide-micelle solution of a desired w_0 value was prepared by directly mixing appropriate amounts of the pre-prepared AOT/IO/D₂O solution and lyophilized peptide solid. This mixture was then incubated under room temperature for 30 minutes with slight vortexing every 10 minutes. Assuming that peptide incorporation does not affect the characteristic micellar distributions, a simple stoichiometric calculation indicates that the peptide to

micelle ratio is about 1:5 for all of the AOT reverse micelles used, with the final peptide concentration being $\sim 200 \mu\text{M}$ in each case. The peptide/D₂O solution was prepared by directly dissolving lyophilized peptide solid in D₂O (pH* = 2, pH meter reading) and the peptide concentration is $\sim 200 \mu\text{M}$. In all cases, the peptide concentration was determined optically by either the phenylalanine absorbance at 257.4 nm using $\epsilon = 197 \text{ M}^{-1} \text{ cm}^{-1}$ for A β_{16-22} or by the tyrosine absorbance at 276 nm using $\epsilon = 1450 \text{ M}^{-1} \text{ cm}^{-1}$ for Sup35₇₋₁₃. Because of the small molar absorptivity of phenylalanine and also interference of the peptide backbone absorbance the reported concentrations for A β_{16-22} peptide are expected to have a large uncertainty and are in the range of 100 - 300 μM .

FTIR measurements. FTIR spectra were collected at 25 °C as outlined in Chapter 2. For measurements in bulk D₂O, an optical path length of 100 μm was used, whereas for those in AOT reverse micelles, a longer optical path length (390 μm) was used. For all the spectra measured in AOT reverse micelles, a background arising from imperfect subtraction of AOT signals was further estimated and subtracted. Because of such baseline correction, all reported spectra should be viewed as only semi-quantitative.

Circular dichroism (CD) measurements. Far-UV CD data were collected on an Aviv 62A DS circular dichroism spectrometer (Aviv Associate, NJ) using a 1 mm sample cuvette. Mean residue ellipticity was calculated as outlined in Chapter 2.

Transmission electron microscopy (TEM) measurements. TEM images were recorded as described in Chapter 2. Samples used for TEM experiments are identical to those used in the corresponding IR measurements (i.e., A β_{16-22} + AOT reverse micelle solution of $w_0 =$

6). TEM samples were prepared by first depositing an aliquot ($\sim 5 \mu\text{L}$) of the $\text{A}\beta_{16-22}$ -AOT reverse micelle solution of $w_0 = 6$, which has been incubated for either 24 hours or 9 days, to Formvar coated 300 mesh copper grids. These grids were then negatively stained with 2% uranyl acetate in water. Any excess fluid was blotted off immediately. The grids were then allowed to dry in air for 10 minutes. Grids used for collecting the image of the reference solution (i.e., the AOT reverse micelle solution of $w_0 = 6$) were prepared identically.

6.3 Results and Discussion

Aggregate formation was monitored by the amide I' band of the peptides because of its proven sensitivity to conformational changes. As shown (Figure 6.1a), the amide I' bands of $\text{A}\beta_{16-22}$ and Sup35_{7-13} in bulk D_2O ($\text{pH}^* = 2$), collected 1 hour after the peptide solution was prepared, show typical characteristics of disordered peptides (Barth and Zscherp, 2002). Consistent with this observation, far-UV CD measurements also show that these peptides are predominantly unstructured in solution (Figure 6.1b). In addition, these spectra (both CD and IR) did not show any appreciable changes even after three days of incubation (data not shown), indicating that when fully hydrated these peptides aggregate rather slowly under the current experimental conditions.

However, incorporation of $\text{A}\beta_{16-22}$ and Sup35_{7-13} in the D_2O pool of AOT reverse micelles of $w_0 = 6$ leads to a drastic enhancement in their aggregation rate. As shown (Figure 6.2), the amide I' band of $\text{A}\beta_{16-22}$, also collected 1 hour after the peptide sample was prepared, is now characterized by spectral features of soluble peptide aggregates rich

in antiparallel β -sheets (Balbach et al., 2000; Barth and Zscherp, 2002; Ma and Nussinov, 2002; Klimov and Thirumalai, 2003; Favrin et al., 2004; Petty and Decatur, 2005), namely, the sharp bands centered at ~ 1620 and ~ 1687 cm^{-1} respectively, indicating that significant peptide aggregation has occurred within the dead time (ca. 1 hour) of the current method. Similarly, the amide I' band of the Sup35₇₋₁₃ peptide (Figure 6.2), obtained under the same conditions, indicates that it also aggregates at a rate that is too fast to be resolved by the current method. However, the soluble aggregates formed by Sup35₇₋₁₃ are instead rich in parallel β -sheets, as evident from the lack of the characteristic high-frequency component (i.e., the peak around ~ 1687 cm^{-1}) of antiparallel β -sheets in its amide I' band. These results are consistent with several previous studies (Balbach et al., 2000; Balbirnie et al., 2001; Ma and Nussinov, 2002; Klimov and Thirumalai, 2003; Favrin et al., 2004; Nelson et al., 2005; Petty and Decatur, 2005), showing that the fundamental spectral characteristics of the corresponding aggregation process of these peptides remain unaltered in the presence of AOT reverse micelles. While many factors have been shown to affect the rate of peptide or protein aggregation (see below) (Jarrett et al., 1993; Shen and Murphy, 1995; Wood et al., 1996; Harper and Lansbury, 1997; Gorman et al., 2003; Marek et al., 2007; Wolf et al., 2008), the current results are nonetheless interesting in that they were obtained in an environment wherein only about 96 free water molecules are available per micellar core (Maitra, 1984). Thus, it is expected that the hydration status of the entrapped peptide molecule is significantly different from that in bulk water (Mukherjee et al., 2007a; Mukherjee et al., 2007b), leading to changes in its physical and/or chemical properties. A

similar idea has also been put forward based on the modulation of water activity in a confined environment (Zhou, 2007). Hence, we propose that the observed increase in the rate of peptide aggregation in AOT reverse micelles arises primarily from dehydration or limited hydration of the peptide molecules of interest.

If the above assertion of kinetic enhancement based on the assumption of dehydration is valid, then one would expect the aggregation rate of these peptides to decrease with an increase in the number of free water molecules inside the polar core of the reverse micelles (i.e., an increase in the w_0 value) (Maitra, 1984). Indeed, the aggregation rate of Sup35₇₋₁₃ in AOT reverse micelles of $w_0 = 10$, as judged by the evolution of its amide I' band as a function of incubation time (Figure 6.3), becomes slower. These data clearly show that unlike that of $w_0 = 6$, no detectable aggregation has occurred 1 hour after the peptide sample was prepared, with the detectable sign of aggregation starting to develop only after ~6 hours of incubation, as judged by the appearance of the characteristic aggregation band centered at ~1624 cm⁻¹. The latter becomes the dominant spectral feature after 24 hours of incubation, indicating that at this time a significant portion of the peptide molecules has assembled into soluble aggregates. Further incubation of this sample for an extended period of time led to the formation of insoluble aggregates, indicative of the dynamic nature of this system (Luisi, 1985). As expected, increasing the w_0 value to 20 suppresses the rate of Sup35₇₋₁₃ aggregation to a further extent (Figure 6.4). It is evident in this case that even after 24 hours of incubation the AOT-peptide sample does not show detectable aggregates. Interestingly, however, the amide I' band of A β ₁₆₋₂₂ in AOT reverse micelles of $w_0 = 10$ (Figure 6.3) is very similar

to that obtained at $w_0 = 6$, indicating that under such conditions aggregation has already taken place to an appreciable extent during the dead time of the current method. On the other hand, the amide I' band of A β_{16-22} in AOT reverse micelles of $w_0 = 20$, also measured after 1 hour of incubation, is dominated by spectral features of disordered peptide monomers (Figure 6.4), thereby suggesting significant alleviation of peptide aggregation under conditions where the peptide molecules are expected to be extensively hydrated. However, after 24 hours of incubation, an appreciable amount of A β_{16-22} peptide was found to form insoluble aggregates that remained suspended in solution and thus, no further attempt was made to measure its FTIR spectrum under this condition.

Taken together, the above results indeed support the idea that the degree of hydration is an important determinant of the rate of peptide aggregation, and that the actual effect of dehydration on aggregation depends on the sequence. For example, in reverse micelles of $w_0 = 10$, A β_{16-22} aggregates faster than Sup35₇₋₁₃. Previous studies have shown that the major driving force for the oligomerization of A β_{16-22} , which contains the crucial central hydrophobic cluster (Wu et al., 2007) essential for the polymerization of the full length peptide,⁴¹ is hydrophobic interaction (Balbach et al., 2000), whereas the aggregates formed by the hydrophilic peptide Sup35₇₋₁₃ are primarily stabilized by interstrand backbone-backbone and side chain-side chain hydrogen bonds (Balbirnie et al., 2001; Lipfert et al., 2005; Nelson et al., 2005; Zheng et al., 2006; Strodel et al., 2007). Therefore, it is not surprising that A β_{16-22} exhibits a faster aggregation rate than Sup35₇₋₁₃ under conditions wherein only limited hydration is possible. This is because under such conditions most of the available water molecules are involved in

preferential solvation of the polar or charged groups, leaving the hydrophobic side chains relatively dehydrated (Garcia et al., 1997; Mukherjee et al., 2007a). As a result, the free energy barrier encountered in peptide-peptide association via the mechanism of hydrophobic interaction is expected to be greatly reduced for A β ₁₆₋₂₂.

Furthermore, it is well established that the rate of peptide aggregation is highly concentration dependent (Xue et al., 2008). Thus, the first concern in the interpretation of the current data is that whether the observed enhancement in the aggregation rate of both peptides is due to an incidental increase in local peptide concentration as a result of confinement in the water pool of the reverse micelles. In order to minimize this possibility, all AOT experiments were carried out under conditions where the ratio of micellar core to peptide was maintained at 5:1. In other words, the percentage of micelles initially containing more than one peptide molecule is fairly small. Thus, the faster aggregation rate of these peptides in AOT reverse micelles, compared to that in bulk water, is unlikely to result from the concentration effect. In addition, previous studies have shown that interactions with lipid membranes play an important role in the aggregation of a number of amyloidogenic peptides (Yip and McLaurin, 2001; Dante et al., 2002; Murphy, 2007). Thus, the second concern is whether the enhanced aggregation rate we observe in the current case arises from interactions of these two peptides with the surfactant-water interface of the reverse micelle. While we cannot entirely rule out this possibility, the overall enhancement is unlikely to have resulted solely from such interactions because the rate of aggregation for both peptides changes as a function of w_0 value. In fact, such interactions in the current case may even slow down aggregation by

preventing peptide molecules to diffuse through different water pools, an event necessary for self-association. Based on these arguments and the data acquired at different w_0 values, we therefore attribute the drastically enhanced aggregation rate observed for both $A\beta_{16-22}$ and $Sup35_{7-13}$ in AOT reverse micelles primarily to peptide dehydration. Consistent with this picture, several earlier studies (Balbirnie et al., 2001; Petty and Decatur, 2005) have suggested that peptide self-association encounters a substantial desolvation free energy barrier. Of particular interest is a recent MD simulation study wherein water expulsion has been associated with the formation of protofilaments of aggregating $A\beta_{16-22}$ peptides (Krone et al., 2008). Indeed, dewetting is a common phenomenon observed in the self-association of hydrophobic surfaces and biological molecules (Hummer and Garde, 1998; Lum et al., 1999; Liu and Chan, 2005; MacCallum et al., 2007). Moreover, it is worth mentioning that the above results also indicate that these reverse micelles must be dynamic in nature (Luisi, 1985), allowing the entrapped solute molecules to move from one polar core to another so that peptide-peptide association or aggregation can take place.

While the current study focuses mainly on probing the effects of dehydration on the early stages of the kinetics of peptide aggregation, to confirm that the peptide aggregates formed in AOT reverse micelles can further assemble into larger oligomeric structures we have also performed TEM measurements on the $A\beta_{16-22}$ -AOT reverse micelle system. As shown (Figure 6.5 a and b), the transmission electron micrograph of negatively stained deposits obtained from $A\beta_{16-22}$ -AOT reverse micelle solution of $w_0 = 6$, which has been incubated for either 24 hours or 9 days, revealed annular aggregates

whereas such structures were distinctly absent from the micrograph obtained from the reference AOT reverse micelle solution (Figure 6.5c). Such annular-like structures have also been observed in other amyloidogenic systems (e.g., A β peptides, α -synuclein, human hormone calcitonin, immunoglobulin light chain, and ABri peptides) (Lashuel et al., 2002; Srinivasan et al., 2004; Zhu et al., 2004a; Avidan-Shpalter and Gazit, 2006; Zheng et al., 2008). Thus, this result not only substantiates the notion that in AOT reverse micelles of low w_0 value the aggregation rate of A β_{16-22} is enhanced, but it also suggests that AOT reverse micelles may play an important role in controlling the morphology of the aggregates formed in such systems.

The aggregation results obtained in D₂O and AOT reverse micelles of different water contents combined thus provide strong evidence indicating that the degree/extent of hydration plays an important but often understated role in the kinetics of aggregate formation of amyloid peptides, a notion that so far has only been implied in other studies. For example, it has been shown that amyloid fibrils formed from the sequential stacking of β -sheets are primarily anhydrous (Balbirnie et al., 2001) in nature, suggesting that expulsion of water molecules is an obligatory step during aggregate formation and subsequent fibrillization. In particular, a recent molecular dynamics study (Tarus et al., 2005) on A β_{10-35} has shown that formation of contacts between hydrophobic clusters of aggregating peptides encounters an appreciable free energy barrier arising from the removal of water molecules solvating the interacting interfaces/domains. Additionally, differences in spatial distribution of solvent (water) molecules around a protein can influence its interaction with other proteins and/or self-association (Fernandez and

Scheraga, 2003; De Simone et al., 2005). Moreover, studies involving the diastereomeric assembly of polylysines (Dzwolak et al., 2004) and the effect of osmolytes (Yang et al., 1999) on the morphology of aggregates and the amyloidogenic pathways of the A β peptide also suggest that hydration can indeed be a key factor in controlling the thermodynamics as well as the kinetics of such processes, even though the aggregation process in reverse micelles could be mechanistically quite different from that in aqueous solutions.

6.4 Conclusions

In summary, we have studied the aggregation properties of two amyloidogenic peptides, A β ₁₆₋₂₂ and Sup35₇₋₁₃, in D₂O and AOT reverse micelles of different w_0 values. Our results show that the aggregation rates of these peptides are greatly enhanced when solubilized in the water pool of AOT reverse micelles of $w_0 = 6$ and 10 wherein the number of free water molecules interacting with the peptide molecules are quite limited. Thus, these experimental results provide strong indication that dehydration promotes aggregate formation by reducing the free energy barrier arising from desolvation or removal of water molecules from the interfacial region.

Figure 6.1. The amide I' bands (a) and CD spectra (b) of A β ₁₆₋₂₂ (blue) and Sup35₇₋₁₃ (red) peptides in D₂O.

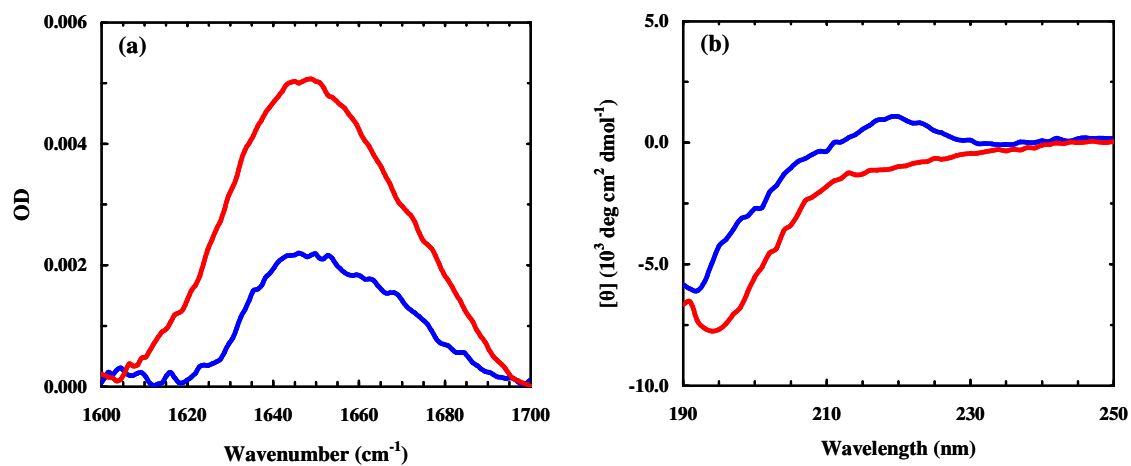


Figure 6.2. The amide I' bands of A β ₁₆₋₂₂ (blue) and Sup35₇₋₁₃ (red) peptides in AOT reverse micelles of $w_0 = 6$. These data were collected after 1 hour of sample incubation.

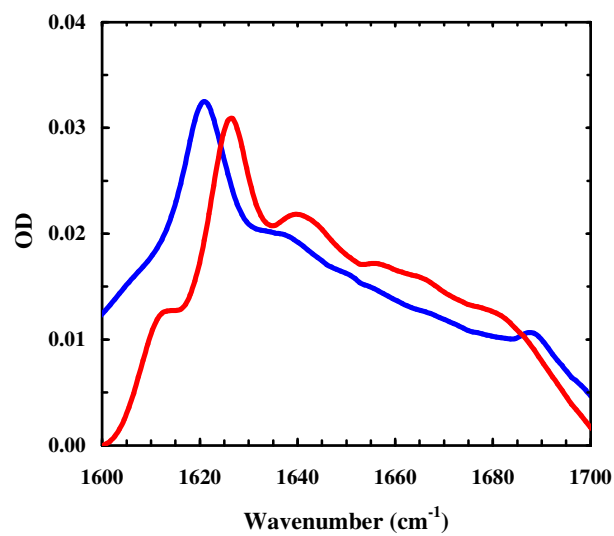


Figure 6.3 The amide I' bands of Sup35₇₋₁₃ in AOT reverse micelles of $w_0 = 10$ collected after different incubation times, i.e., 1 hour (pink), 6 hours (green), and 24 hours (red). Also shown in blue is the amide I' band ($\times 5$) of A β ₁₆₋₂₂ in AOT reverse micelles of $w_0 = 10$, collected after 1 hour of incubation.

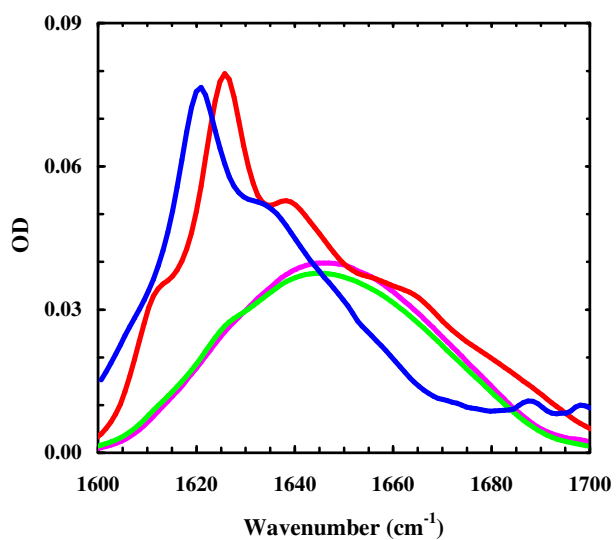


Figure 6.4 The amide I' bands of Sup35₇₋₁₃ (red) and A β ₁₆₋₂₂ (blue) peptides in AOT reverse micelles of $w_0 = 20$. The Sup35₇₋₁₃ spectrum was collected after 24 hours of incubation, while that of A β ₁₆₋₂₂ was measured after 1 hour of incubation.

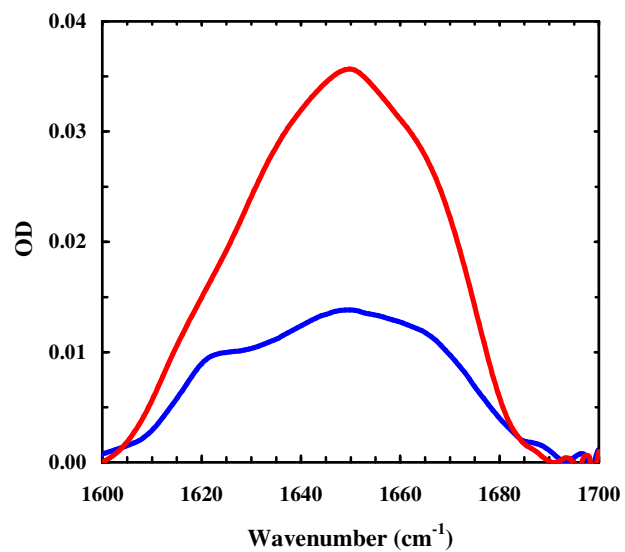
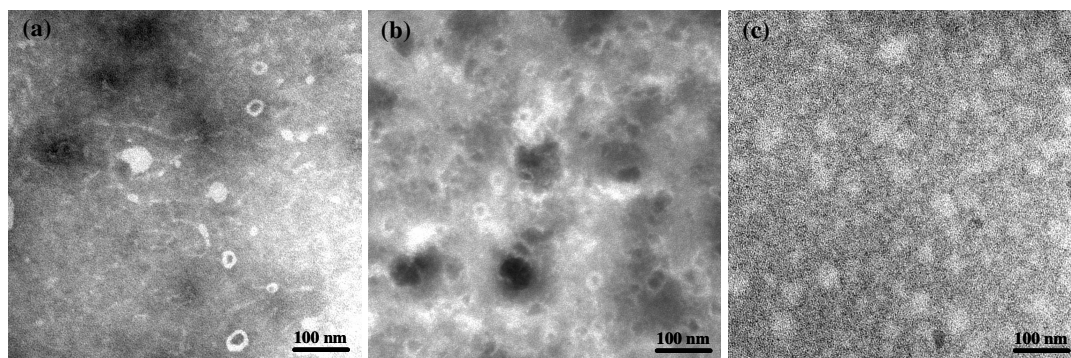


Figure 6.5 TEM images of the $A\beta_{16-22}$ -AOT reverse micelle sample at $w_0 = 6$ after (a) 24 hours incubation and (b) 9 days incubation. Also shown in (c) is the TEM image of the AOT reverse micelle solution of $w_0 = 6$.



Chapter 7: Folding Kinetics of Naturally Occurring

Helical Peptide

This work has been published: Folding kinetics of a naturally occurring helical peptide: implication of the folding speed limit of helical proteins. S. Mukherjee, P. Chowdhury, M. R. Bunagan and F. Gai. *J. Phys. Chem. B* 2008 **112**, 46-50.⁵

S. M. and P. C. collected and analyzed data and contributed equally to the paper. S. M., P. C., M. R. B. and F. G. wrote the paper.

The folding mechanism and dynamics of a helical protein may strongly depend on how quickly its constituent α -helices can fold independently. Thus, our understanding of the protein folding problem may be greatly enhanced by a systematic survey of the folding rates of individual α -helical segments derived from their parent proteins. As a first step, we have studied the relaxation kinetics of the central helix (L9:41-74) of the ribosomal protein L9 from the bacterium *Bacillus stearothermophilus*, in response to a temperature-jump (*T*-jump) using infrared spectroscopy. L9:41-74 has been shown to exhibit unusually high helicity in aqueous solution due to a series of side chain-side chain interactions, most of which are electrostatic in nature, while still remaining monomeric over a wide concentration range. Thus, this peptide represents an excellent model system not only for examining how the folding rate of naturally occurring helices differs from

⁵ Reproduced with permission from [S. Mukherjee, P. Chowdhury, M. R. Bunagan and F. Gai. *J. Phys. Chem. B* 2008 **112**, 46-50.] Copyright (2008), the American Chemical Society.

that of the widely studied alanine-based peptides, but also for estimating the folding speed limit of (small) helical proteins. Our results show that the T -jump induced relaxation rate of L9:41-74 is significantly slower than that of alanine-based peptides. For example, at 11 °C its relaxation time constant is about 2 μ s, roughly seven times slower than that of SPE₅, an alanine-rich peptide of similar chain length. In addition, our results show that the folding rate of a truncated version of L9:41-74 is even slower. Taken together, these results suggest that individual α -helical segments in proteins may fold on a time scale that is significantly slower than the folding time of alanine-based peptides.

8.1 Introduction

Helices are not only ubiquitous in proteins, but are also known to sample a wide variety of sequences. However, previous experimental studies on the folding dynamics of monomeric α -helices have focused mainly on alanine-based peptides (Williams et al., 1996; Thompson et al., 1997; Volk et al., 1997; Clarke et al., 1999b; Lednev et al., 1999b; Huang et al., 2001b; Huang et al., 2001c; Jas et al., 2001; Huang et al., 2002b; Werner et al., 2002; Wang et al., 2003; Wang et al., 2004; Bredenbeck et al., 2005; Balakrishnan et al., 2007), of which, most are composed of AAAXA repeats (Williams et al., 1996; Thompson et al., 1997; Volk et al., 1997; Clarke et al., 1999b; Lednev et al., 1999b; Huang et al., 2001b; Huang et al., 2001c; Jas et al., 2001; Huang et al., 2002b; Werner et al., 2002; Wang et al., 2003; Wang et al., 2004; Bredenbeck et al., 2005; Balakrishnan et al., 2007) with X being a charged residue such as lysine or arginine. Since such alanine-rich sequences are rarely encountered in proteins, it is thus imprudent to assume that naturally occurring α -helices would show similar folding rates as those of alanine-rich peptides. In fact, our recent study on the folding kinetics of a neuroactive α -helical peptide, Conantokin-T (Con-T), found in the venom of the piscivorous cone snail *Conus tulipa*, shows that it folds slower than alanine-based peptides of similar chain length (Du et al., 2007). In addition, several simulation studies (Hummer et al., 2001; Sorin and Pande, 2005; Van Giessen and Straub, 2006) also indicate that the folding rate of individual α -helices in proteins is sequence dependent and that the folding of those segments having low intrinsic helical propensity is initiated by side chain interactions through the formation of salt-bridges or hydrophobic contacts (Scott et al., 2006). Akin to

the role of folding nucleus in the nucleation-condensation model of protein folding (Fersht, 1995), such side chain contacts, either native or nonnative, could provide a scaffold for further growth of the native structure. On the other hand, those segments with higher helical propensity may fold independently, thereby providing a framework for further constructing the native tertiary structure. Thus, in light of the important role of secondary structure formation in existing protein folding models (Kim and Baldwin, 1982; Fersht, 1995; Daggett and Fersht, 2003), there is a strong need for further investigation of the sequence-dependence of α -helix folding kinetics. Herein, we have studied the relaxation kinetics of a naturally occurring α -helical peptide (Kuhlman et al., 1997), L9:41-74 from the bacterium *Bacillus stearothermophilus*, in response to a laser-induced *T*-jump using infrared (IR) spectroscopy.

The study of the folding dynamics of naturally occurring α -helices has been hampered mainly due to the low conformational stability of isolated protein helical fragments as well as their tendency to aggregate in absence of stabilizing tertiary contacts. However, Raleigh and co-workers (Kuhlman et al., 1997) have shown that L9:41-74, which corresponds to the central α -helix of ribosomal protein L9 (Figure 7.1), a multidomain protein from the bacterium *B. stearothermophilus*, is not only monomeric but is also highly helical in aqueous solution (the fractional helicity is ~68% at 25 °C). Thus, this peptide is ideally suited for both equilibrium and kinetic IR studies. L9:41-74 is composed of 34 amino acids and its helical structure is mainly stabilized by favorable side chain-side chain interactions (Kuhlman et al., 1997).

Our results show that L9:41-74 folds in about 1.7 μ s at 20.0 $^{\circ}$ C, which is indeed comparable to the folding times of several ultrafast folding helical proteins (Mayor et al., 2000; Zhu et al., 2003; Kubelka et al., 2004; Zhu et al., 2004b; Bunagan et al., 2006). In addition, our results show that the folding rate of L9:41-74 is approximately seven times slower than that of alanine-based peptides of similar chain length (Wang et al., 2004), consistent with our earlier observation that formation of salt-bridges in the rate-limiting step slows down protein folding (Du et al., 2007). Interestingly, shortening L9:41-74 to only 17 residues leads to an even longer folding time. Taken together, these results thus suggest that the folding time of α -helices in proteins is strongly dependent on sequence and chain length.

8.2 Experimental Methods

Peptide Samples. L9:41-74 and L9:48-64 (sequence: Ac-⁴⁸EAQKQKEQRQ⁵⁸AAEELAN-NH₂) were synthesized based on standard Fmoc-protocols on a PS3 automated peptide synthesizer (Protein Technologies, Inc., Woburn, MA) and purified by reverse-phase chromatography. The identity of the peptide sample was further verified by matrix assisted laser desorption ionization mass spectroscopy. Multiple rounds of lyophilization against a 0.1 M DCl/D₂O solution were used to remove the exchangeable hydrogens and also the residual trifluoroacetic acid from the peptide synthesis. Peptide solutions used in both CD and IR measurements were prepared by directly dissolving lyophilized peptide solids in 20 mM phosphate buffer (pH 7). The final peptide concentrations of the peptide samples were determined by comparing CD results to those

of Raleigh and coworkers (Kuhlman et al., 1997) and were about 40–95 μM and 1.5 mM for CD and IR samples, respectively.

CD and FTIR Measurements. The CD data were collected on an Aviv 62A DS circular dichroism spectrometer (Aviv Associate, NJ) using a 1 mm sample cuvette. Mean residue ellipticity was calculated using the equation $[\theta] = (\theta_{\text{obs}}/10lc)/N$, where θ_{obs} is the ellipticity in millidegrees, l is the optical path length in cm, c is the concentration of the peptide in M, and N is the number of residues. Static FTIR spectra with 2 cm^{-1} resolution were collected on a Magna-IR 860 spectrometer (Nicolet, WI) equipped with a HgCdTe detector. A two-compartment CaF_2 sample cell with a 52 μm Teflon spacer was used to allow separate measurements of the sample and the reference under identical conditions. Temperature control with $\pm 0.2\text{ }^\circ\text{C}$ precision was obtained by a thermostatted copper block. Typically, 256 scans were averaged to yield the spectrum reported.

Infrared T-jump Apparatus. The time-resolved *T*-jump IR apparatus has been described in detail in Chapter 2. Briefly, a 3 ns laser pulse centered at $\sim 1.9\text{ }\mu\text{m}$ was used to quickly raise the temperature of the sample solution by 7–11 $^\circ\text{C}$, and the *T*-jump induced transient kinetics were measured by a continuous wave IR diode laser and a 50 MHz HgCdTe detector in conjunction with a digital oscilloscope.

8.3 Results

CD Studies. As shown (Figure 7.2), the far-UV CD spectrum of L9:41-74 at 4.0 $^\circ\text{C}$ and pH 7 exhibits the characteristic double minima of α -helices at 208 and 222 nm, respectively, indicating that the α -helical conformation is significantly populated under this condition. Compared to that observed for other monomeric α -helical peptides,

however, the CD thermal unfolding transition of L9:41-74 measured at 222 nm is less broad (Figure 7.2b) (Huang et al., 2001b; Wang et al., 2003). In fact, its unfolding transition is similar to that of small helical proteins. The fractional helicity (f_H) of L9:41-74 was further estimated using the following relationship (Luo and Baldwin, 1997),

$$f_H = \frac{[\theta]_{222} - [\theta]_C}{[\theta]_H - [\theta]_C} \quad (1)$$

with,

$$[\theta]_H = -44,000 \times (1 - 2.5/n) + 100 \times T \quad (2)$$

and,

$$[\theta]_C = 640 - 45 \times T \quad (3)$$

where $[\theta]_{222}$ is the measured mean residue ellipticity at 222 nm, $[\theta]_H$ is the mean residue ellipticity at 222 nm of an ideal peptide with 100% helicity, $[\theta]_C$ is the mean residue ellipticity at 222 nm of a coil, n is the length of the potential helical region, and T is the temperature in °C. The fractional helicity of L9:41-74 at 4.0 °C was estimated to be ~87%, and the temperature at which the average helicity reaches 50% is ~32.0 °C. These results are in excellent agreement with those of Raleigh and co-workers (Kuhlman et al., 1997).

Static FTIR Studies. As indicated (Figure 7.3a), the amide I' band of L9:41-74, which arises mainly from backbone C=O stretching vibrations in D₂O, is centered around 1632 cm⁻¹ at the lowest temperature studied (4.0 °C) and shifts toward higher frequencies with increasing temperature. The underlying spectral changes as a function of temperature are better discerned when these data are presented as difference spectra, generated by

subtracting the spectrum at 4.0 °C from those obtained at higher temperatures. As shown (Figure 7.3b), the FTIR difference spectra of L9:41-74 exhibit a negative feature centered around 1630 cm^{-1} , resulting primarily from loss of α -helical conformations with increasing temperature, and a positive feature centered around 1665 cm^{-1} , arising primarily from the concurrent formation of nonhelical conformations (Huang et al., 2001b). Since temperature-induced variations in backbone solvation also shift the amide I' band of α -helical peptides toward a higher frequency (Manas et al., 2000; Mukherjee et al., 2007b), no further attempt was made to analyze these difference spectra to extract quantitative information regarding the thermal unfolding transition of the peptide.

T-Jump Induced Relaxation Kinetics. The relaxation kinetics of L9:41-74 in response to a *T*-jump were probed at 1631 cm^{-1} where solvated α -helices absorb (Figure 7.3) (Manas et al., 2000; Mukherjee et al., 2007b). As shown (Figure 7.4), the *T*-jump induced relaxation proceeds in two distinct and well-separated phases, in agreement with our previous studies on alanine-based peptides (Huang et al., 2001c; Huang et al., 2002b; Wang et al., 2004). The fast phase is too fast to be resolved by the current IR setup and is attributed to the aforementioned temperature-induced shift of the amide I' band (Mukherjee et al., 2007b). On the other hand, the slow phase, which is well-resolved in the temperature range of the current study, is attributed to a conformational redistribution process occurring between helical and nonhelical conformations in response to the *T*-jump. While nonexponential relaxation kinetics have been observed for alanine-based peptides (Huang et al., 2002b), in the current case the slow phase can be modeled with a single-exponential function (Figure 7.4), and the resultant relaxation rate constants thereby

obtained exhibit Arrhenius temperature dependence with an apparent activation energy of about 10.2 kcal/mol (Figure 7.5). Compared to that of alanine-based peptides of similar chain length, these data indicate that the *T*-jump induced relaxation rate of L9:41-74 is significantly slower. For example, at 20 °C the relaxation rate constant of L9:41-74 is $(1.17 \pm 0.15 \text{ } \mu\text{s})^{-1}$, whereas a 34-residue alanine-based peptide (SPE₅) relaxes in about $(200 \text{ ns})^{-1}$ in response to a *T*-jump (Figure 7.5) (Wang et al., 2004).

4.4 Discussion

Alanine-based α -helical peptides have been extensively studied in order to understand the kinetics/mechanism of the helix-coil transition (Williams et al., 1996; Thompson et al., 1997; Clarke et al., 1999a; Lednev et al., 1999a; Mitsutake and Okamoto, 2000; Buchete and Straub, 2001; Huang et al., 2001b; Huang et al., 2001c; Hummer et al., 2001; Jas et al., 2001; Levy et al., 2001; Wu and Wang, 2001; Baumketner and Shea, 2003; Chowdhury et al., 2003; Peng et al., 2003; Takano et al., 2003; Doshi and Munoz, 2004; Gnanakaran et al., 2004; Nguyen et al., 2004; Sorin and Pande, 2005; Couch et al., 2006; Morozov and Lin, 2006; Yang and Cho, 2007). However, it is not clear as to what extent the folding dynamics of these peptides are representative of those of naturally occurring α -helices wherein alanine is seldom the most abundant residue. Thus, in light of the critical role of secondary structure formation in several protein folding models (Kim and Baldwin, 1982; Fersht, 1995), studying the folding kinetics of model α -helical peptides derived from proteins is not only interesting but also necessary. However, examples of kinetic studies on naturally occurring α -helical peptides are rare because such peptides are usually unstable and/or prone to aggregation

when isolated from their parent proteins. In this regard, the finding that the peptide corresponding to the central α -helix of ribosomal protein L9 from the bacterium *B. stearothermophilus* can fold into a highly α -helical structure in aqueous solution is significant.

Consistent with the results of Raleigh and co-workers (Kuhlman et al., 1997), our equilibrium CD and IR studies indicate that L9:41-74 exhibits an unusually high helicity at ambient temperatures and also remains monomeric over a large concentration range. Thus, this peptide is ideally suited for *T*-jump IR studies because this technique requires peptide samples of relatively high concentration. In addition, Raleigh and co-workers have shown that the α -helical conformation of L9:41-74 is primarily stabilized by a series of side chain-side chain interactions, most of which form salt-bridges, while other factors, such as acetylation and the N-capping effect (Chakrabartty et al., 1993; Viguera and Serrano, 1999), can also contribute to the stability of the folded state. Previously, we have shown that the folding rate of the neuroactive peptide Con-T, whose α -helical conformation is also stabilized by a series of salt-bridges, is significantly slower than that of alanine-based peptides of similar chain length, suggesting that salt-bridges play an important role in determining the folding rate of α -helical peptides (Du et al., 2007). However, the sequence of Con-T is rather unique in that it contains 4 γ -carboxyglutamic acid residues which are less commonly encountered in nature. Thus, the general role of salt-bridge formation in the folding kinetics of α -helical peptides composed of natural amino acids needs to be further examined, and in this regard, L9:41-74 would be a good model system.

The *T*-jump induced relaxation kinetics of L9:41-74 were probed by monitoring the absorbance change at 1632 cm^{-1} , a characteristic vibrational frequency of solvated α -helical amides (Manas et al., 2000; Mukherjee et al., 2007b). As shown (Figure 7.5), compared to that of alanine-based peptides (Williams et al., 1996; Thompson et al., 1997; Lednev et al., 1999a; Huang et al., 2001b; Huang et al., 2001c; Jas et al., 2001; Huang et al., 2002b; Wang et al., 2003; Wang et al., 2004; Balakrishnan et al., 2007), the relaxation rate of L9:41-74, in response to a *T*-jump, is distinctly slower. For example, at $11.0\text{ }^{\circ}\text{C}$ the relaxation time constant of L9:41-74 is $2.0 \pm 0.2\text{ }\mu\text{s}$, whereas a 34-residue alanine-rich peptide, SPE₅, relaxes in about $0.3\text{ }\mu\text{s}$ (Wang et al., 2004). Since the helicities of these two peptides are quite similar at this temperature, these results thus indicate that the folding rate of L9:41-74 is approximately seven times slower than that of SPE₅. As noted by Raleigh and co-workers (Kuhlman et al., 1997), there are 10 possible stabilizing side chain-side chain interactions in L9:41-74, including seven Lys·Glu pairs (*i*, *i* + 4; Lys₆₆·Glu₇₀, Lys₆₉·Glu₇₃, Lys₇₄·Glu₇₀ and *i*, *i* + 3; Lys₄₅·Glu₄₈, Lys₅₁·Glu₄₈, Lys₅₁·Glu₅₄, Lys₆₇·Glu₇₀), one Arg₅₆·Glu₆₀ pair, and two Gln·Glu pairs (Gln₅₀·Glu₅₄ and Gln₅₇·Glu₆₁), through the formation of either a salt-bridge or a hydrogen bond. Thus, these results further suggest that side chain-side chain interactions having stringent orientation/geometrical positioning requirements (Kumar and Nussinov, 1999), such as those leading to the formation of salt-bridges, play an important role in determining the folding rate of α -helical peptides. Due to the higher entropic penalty associated with the formation of such well-aligned interactions, they are likely to slow down folding if formed in the transition state or rate-limiting steps, as observed in the current case.

However, to explicitly determine the individual kinetic role of these interacting pairs or any other structural motifs, further mutational studies are required (Huang et al., 2001b).

Since the typical helical stretch in proteins is about 14 residues (Fersht, 1999), we have further studied the *T*-jump induced relaxation kinetics of the 17-residue peptide L9:48-64, which is a truncated version of L9:41-74. As expected, this peptide has a much lower helicity than L9:41-74 (Figure 7.2) at 4.0 °C due to its shorter sequence (Kuhlman et al., 1997). However, its single-exponential relaxation rate is similar to that of L9:41-74 in the temperature range studied (Figure 7.5). For example, at 11.4 °C the *T*-jump induced relaxation time constant of L9:48-64 is $1.5 \pm 0.2 \mu\text{s}$, comparable to that ($\sim 2.0 \mu\text{s}$) of L9:41-74. Since the helicity of L9:48-64 is only ca. 24% at this temperature, these results indicate that the folding rate of L9:48-64 is slower than that of L9:41-74 because the helicity of the latter is ca. 78%. Indeed, using a two-state analysis (Wang et al., 2003) we estimated the helical folding times to be about 6.1 and 2.4 μs for L9:48-64 and L9:41-74, respectively, at 11.4 °C. These results are particularly interesting because they indicate that the α -helix folding rate depends on chain length, following the relation that shorter peptides fold slower. A similar trend has also been observed for the folding rates of a series of alanine-based peptides (Wang et al., 2004).

Finally, given the large number of theoretical and simulation studies carried out on alanine-based peptides (Mitsutake and Okamoto, 2000; Hummer et al., 2001; Levy et al., 2001; Wu and Wang, 2001; Baumketner and Shea, 2003; Chowdhury et al., 2003; Peng et al., 2003; Takano et al., 2003; Nguyen et al., 2004; Gnanakaran and Garcia, 2005; Sorin and Pande, 2005; Couch et al., 2006; Morozov and Lin, 2006; Yang and Cho,

2007), L9:41-74 would indeed prove to be a good model system for further computational studies and subsequent comparison.

4.5 Conclusion

In conclusion, we have studied the relaxation kinetics of two naturally occurring α -helices, L9:41-74 and L9:48-64, in response to a laser-induced T -jump using IR spectroscopy. Both peptides are derived from the central helix of ribosomal protein L9 from the bacterium *B. stearothermophilus*. The longer peptide (i.e., L9:41-74) exhibits unusually high α -helicity at room temperature due to a series of stabilizing side chain to side chain salt-bridges and/or hydrogen bonds, making it an ideal model for investigating how such side chain-side chain interactions influence the folding rate of monomeric α -helices. Our results show that the folding rate of L9:41-74 is $(1.7 \pm 0.2 \mu\text{s})^{-1}$ at 20 °C and is therefore distinctly slower than that of the commonly studied alanine-based α -helical peptides, which typically fold on the nanosecond time scale. Taken together, these results suggest that formation of side chain-side chain interactions that need to be spatially disposed/aligned in a proper manner increases the folding free energy barrier, thereby resulting in a decrease in the rate at which the peptide folds. Furthermore, our results show that the folding rate of L9:48-64 is slower than that of L9:41-74. This result is especially interesting in the context of protein folding because the chain length of individual α -helical segments in proteins is typically about 14 amino acid long (Fersht, 1999).

Figure 7.1 Ribbon representation of the structure of ribosomal protein L9 (PDB ID: 1div). The sequence of L9:41-74 is: Ac-⁴¹PANLKALEAQ ⁵¹KQKEQRQAAE ⁶¹ELANAKKLKE ⁷¹QLEK-NH₂.

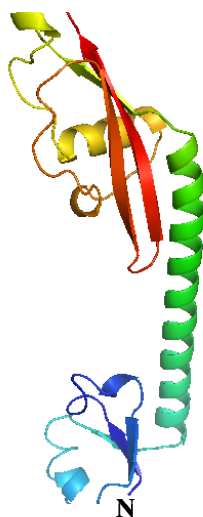


Figure 7.2 (a) Far-UV CD spectra of L9:41-74 (blue) and L9:48-64 (red) at 4.0 °C. (b) Mean residue ellipticities of L9:41-74 (blue) and L9:48-64 (red) at 222 nm as a function of temperature.

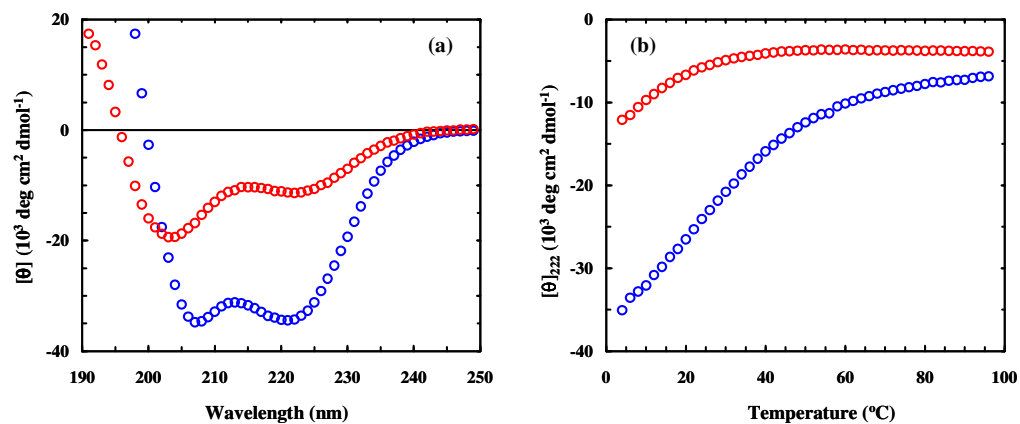


Figure 7.3 (a) FTIR spectra of L9:41-74 (in the amide I' region) at 4.0 (blue), 39.0 (green), and 83.1 °C (red), respectively. (b) Difference FTIR spectra generated by subtracting the spectrum collected at 4.0 °C from those collected at higher temperatures, as indicated.

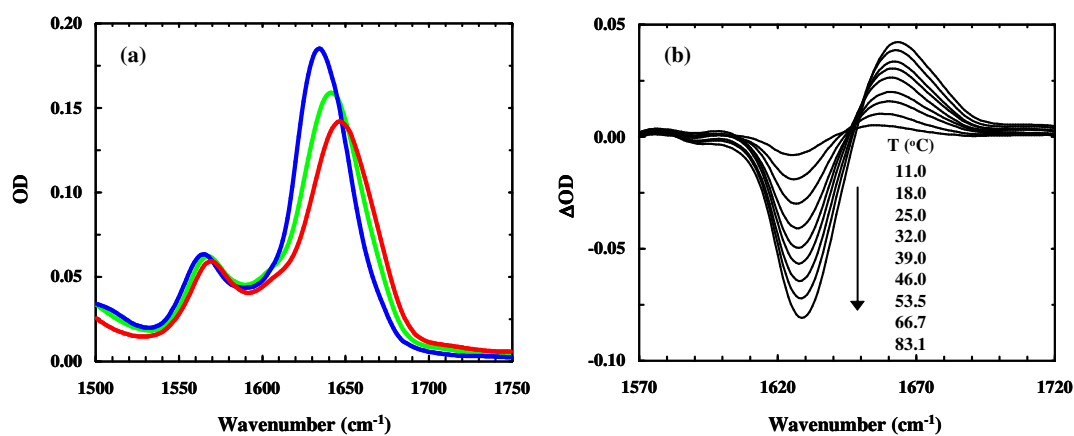


Figure 7.4 A representative T -jump relaxation trace (pink) of L9:41-74 measured with a CW IR laser of 1631 cm^{-1} . The corresponding T -jump is $10.6\text{ }^{\circ}\text{C}$, from 23.9 to $34.5\text{ }^{\circ}\text{C}$. The blue line is a convolution of the instrument response function with $\Delta\text{OD}(t) = A \cdot [1 - B \cdot \exp(-t/\tau)]$, with $A = -0.012$, $B = 0.48$, and $\tau = 0.53\text{ }\mu\text{s}$.

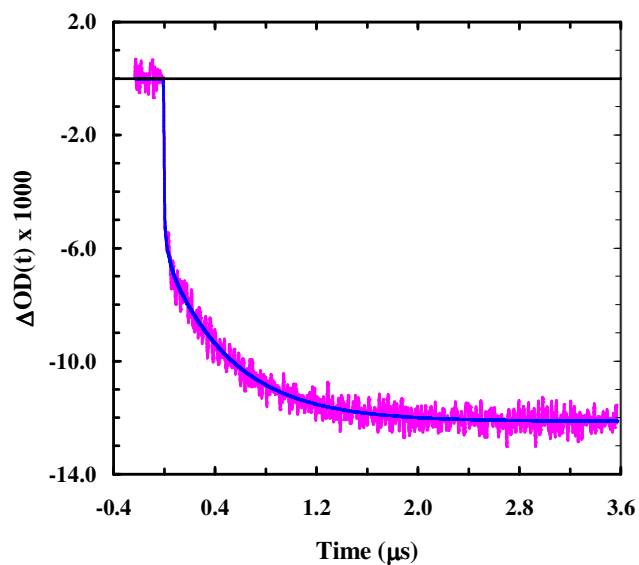
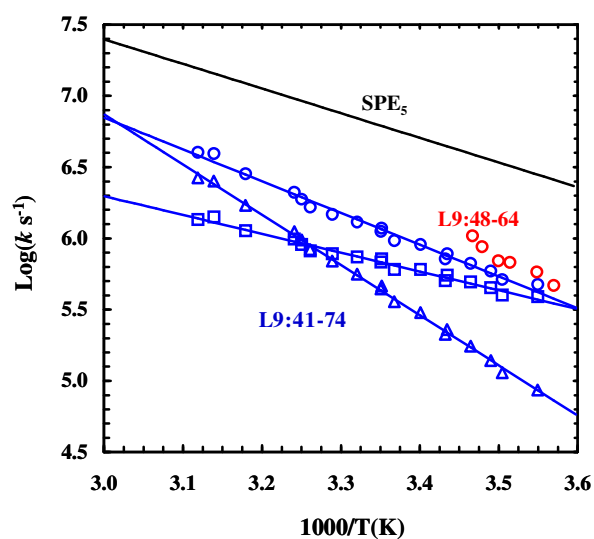


Figure 7.5 Arrhenius plot of the T -jump induced conformational relaxation rates of L9:41-74 (blue circles) and L9:48-64 (red circles). The blue squares and triangles correspond to the two-state folding and unfolding rates of L9:41-74, respectively. Also shown for comparison are the relaxation rates (Wang et al., 2004) of an alanine-based, 34-residue, α -helical peptide, SPE₅.



Chapter 8: Effect of Macromolecular Crowding on Protein Folding Dynamics at the Secondary Structure Level

This work has been published: Effect of macromolecular crowding on protein folding dynamics at the secondary structure level. S. Mukherjee, M. M. Waegelé, P. Chowdhury, L. Guo, and F. Gai. *Journal of Molecular Biology* 2009 **393**, 227-236.⁶

S. M. and M. M. W collected and analyzed the thermodynamic and kinetic data and contributed equally to the paper. Particularly, S. M. collected data on L9:41-74 and trpzip4-m1 and M. M. W. collected data on Z34C-m1. L. G. collected and analyzed the FCS data. S. M., M. M. W, P. C., L. G. and F. G. wrote the paper.

Macromolecular crowding is one of the key characteristics of the cellular environment and therefore, is intimately coupled to the process of protein folding *in vivo*. While previous studies have provided invaluable insight into the effect of crowding on the stability and folding rate of protein tertiary structures, very little is known about how crowding affects protein folding dynamics at the secondary structure level. Herein, we examine the thermal stability and folding-unfolding kinetics of three small folding motifs, i.e., a 34-residue α -helix, a 34-residue cross-linked helix-turn-helix, and a 16-residue β -hairpin, in the presence of two commonly used crowding agents, Dextran 70 (200 g/L) and Ficoll 70 (200 g/L). We find that these polymers do not induce any appreciable changes in the folding kinetics of the two helical peptides, which is somewhat surprising

⁶ Reproduced with permission from [S. Mukherjee, M. M. Waegelé, P. Chowdhury, L. Guo, and F. Gai. *Journal of Molecular Biology* 2009 **393**, 227-236.] Copyright (2009), Elsevier Ltd.

as the helix-coil transition kinetics have been shown to depend on viscosity. Also to our surprise and in contrast to what has been observed for larger proteins, we find that crowding leads to an appreciable decrease in the folding rate of the shortest β -hairpin peptide, indicating that besides the excluded volume effect, other factors also need to be considered when evaluating the net effect of crowding on protein folding kinetics. A model considering both the static and dynamic effects arising from the crowding agent is proposed to rationalize these results.

8.1 Introduction

Understanding how proteins fold *in vivo* poses a formidable challenge. Thus, a majority of protein folding studies have been carried out *in vitro* and under conditions wherein only dilute aqueous solutions were used. While such studies have provided invaluable insights into our understanding of the protein folding problem, these however did not take into account the possible effects arising from macromolecular crowding; an important but often neglected aspect of the intracellular environment (Ellis, 2001b; Minton, 2001; Zhou, 2008b; Zhou et al., 2008). For instance, the presence of macromolecules near a protein could alter its folding energy landscape simply through the excluded volume effect since folding results in a compaction of the polypeptide chain (Minton, 2005). Indeed, several recent experimental and computational studies have shown that such effects of volume exclusion can significantly alter the stability and folding rate of a protein (Van den Berg et al., 2000; Qu and Bolen, 2002; Friedel et al., 2003; Ping et al., 2004; Tokuriki et al., 2004; Cheung et al., 2005; Ai et al., 2006; Charlton et al., 2008; Yuan et al., 2008; Homouz et al., 2009; Rivera et al., 2009).

Besides such entropic effects, macromolecular crowding could also affect the dynamics of protein folding through other mechanisms (in the present case the effect of macromolecular crowding is referred to as the net effect of an inert macromolecule on the folding properties of the protein or peptide molecule in question, which includes both static effects, such as that arising from confinement, and dynamic effects, such as modulation of the frictional drag experienced by conformational motions along the reaction coordinate). For example, it is well known that a high mass macromolecular

crowding agent (i.e., inert polymers) not only changes the dynamic viscosity of the solution (i.e., macroviscosity), but could also modulate the microviscosity of the protein environment in which the folding reaction occurs (Lavalette et al., 1999; Kozer and Schreiber, 2004; Kozer et al., 2007; Goins et al., 2008), thus perturbing the underlying chain dynamics, as shown by Sauer and coworkers (Neuweiler et al., 2007). However, most of the experimental studies carried out thus far on the effects of macromolecular crowding on protein folding have dealt with proteins of fairly large size (Van den Berg et al., 2000; Qu and Bolen, 2002; Tokuriki et al., 2004; Minton, 2005; Ai et al., 2006; Charlton et al., 2008; Yuan et al., 2008; Zhou et al., 2008; Homouz et al., 2009), wherein the excluded volume effect appears to dominate, thus obscuring other subtle but important effects arising from the presence of crowding agents. Herein, we study the folding thermodynamics and kinetics of three relatively small protein motifs in the presence of two commonly used crowding agents, Dextran 70 and Ficoll 70, with the aim of providing new insights into the effect of macromolecular crowding on folding events taking place over a relatively short length scale. These peptides form different types of protein secondary and/or supersecondary structures in solution, specifically, a 34-residue monomeric α -helix (L9:41-74) (Mukherjee et al., 2008), a 34-residue, cross-linked helix-turn-helix (HTH) motif (Z34C-m1, which is the D20A mutant of Z34C) (Du and Gai, 2006), and a 16-residue β -hairpin (trpzip4-m1) (Du et al., 2006). Given the critical importance of protein secondary structure formation in several protein folding models, such as the framework model (Kim and Baldwin, 1982), this study is expected to also

have considerable implications for the applicability of those models in describing *in vivo* protein folding.

Dextran 70 is a flexible, linear (<5% branching) polymer of D-glucopyranose, which behaves as a quasi-random coil ($R_h \sim 63 \text{ \AA}$) (Lubyphelps et al., 1987; Wenner and Bloomfield, 1999; Ruhlmann et al., 2001; Venturoli and Rippe, 2005; Goins et al., 2008), whereas Ficoll 70 is a compact and highly cross-linked and branched co-polymer of sucrose and epichlorohydrin, which can be approximated as a semi-rigid sphere ($R_h \sim 55 \text{ \AA}$) (Lubyphelps et al., 1987; Wenner and Bloomfield, 1999; Venturoli and Rippe, 2005). Thus, comparative studies employing these two polymers allow one to examine how the nature and geometric shape of the respective crowding agent affects the folding dynamics of the protein system in question. Interestingly, only the thermodynamic stability of the shortest peptide studied here (i.e., trpzip4-m1) shows an appreciable change when its environment is crowded by Ficoll 70. Similar to that observed for large proteins, macromolecular crowding leads to an increase in the thermal stability of trpzip4-m1 in the presence of 200 g/L Ficoll 70, a concentration that falls within the concentration range that has been used in previous crowding studies (Van den Berg et al., 2000; Ellis, 2001b; Minton, 2001; Cheung et al., 2005). However, in contrast to the common notion that macromolecular crowding increases the rate of protein folding, our results show that the folding rate of trpzip4-m1 in fact decreases in the presence of either Ficoll 70 or Dextran 70. Taken together, these results indicate that besides the commonly encountered excluded volume effect, other factors need to be considered when assessing the effect of macromolecular crowding on protein folding.

8.2 Experimental Methods

Peptide synthesis and purification. All peptides used in this study were synthesized based on standard Fmoc-protocols on a PS3 automated peptide synthesizer (Protein Technologies, MA) and purified by reverse-phase chromatography. The peptide sequences are: ⁴¹PANLKALEAQ-⁵¹KQKEQRQAAE-⁶¹ELANAKKLKE-⁷¹QLEK (L9:41-74), ⁶FNMQCQRRFY-¹⁶EALHAPNLNE-²⁶EQRNAKIKSI-³⁶RDDC-NH₂ (Z34C-m1), and GEWTWADATKTWTWTE-NH₂ (trpzip4-m1). TMR-maleimide (Molecular Probes, CA), a thiol reactive dye, was used to label the cysteine variant of pHLIP peptide⁴⁹ (sequence: ACEQNPIYWA-RYADWLFTTP-LLLLDLALLV-DADEGTG) following the protocol available in the Molecular Probes Handbook. Oxidation of the Z34C mutant was done as previously described (Du and Gai, 2006). The identity of the peptide sample was further verified by matrix assisted laser desorption ionization mass spectroscopy. Multiple rounds of lyophilization against a 0.1 M DCI/D₂O solution were used to remove the exchangeable hydrogen atoms and also the residual trifluoroacetic acid from the peptide synthesis. Peptide solutions used in both CD and IR measurements were prepared by directly dissolving lyophilized peptide solids in 20 mM phosphate buffer (pH* = 7) with or without the presence of the crowding agent. The final peptide concentration for L9:41-74 was determined by comparing the published CD data (Kuhlman et al., 1997) and the concentrations for other peptides were determined as previously described (Du and Gai, 2006; Du et al., 2007) and were about 16-134 μ M and 0.8-1.5 mM for CD and IR samples, respectively.

Crowding agents. Dextran 70 and Ficoll 70 were purchased from Fisher Scientific, PA and GE Healthcare, NJ, respectively, and were used as received.

CD spectroscopy. All CD data were collected on an Aviv 62A DS circular dichroism spectrometer (Aviv Associate, NJ). The folding-unfolding thermodynamics of each peptide were obtained by fitting its CD thermal melting transition obtained at either 222 nm (for the helical peptides) or 229 nm (for the β -hairpin) to a two-state model described in detail in Chapter 2.

Infrared T-jump setup. The time-resolved T-jump infrared apparatus used in the current study has been described in Chapter 2. The relaxation kinetics of all peptides in response to a T-jump were probed at 1631 cm^{-1} . The observed relaxation rate constants (k_R) were further separated into folding (k_f) and unfolding (k_u) rate constants based on the thermodynamic results obtained from CD studies using the following equations:

$$k_R = k_f + k_u \quad (5)$$

$$K_{eq} = k_f / k_u \quad (6)$$

Fluorescence correlation spectroscopy. The detail of the FCS setup has been described elsewhere (Guo et al., 2007). For each measurement, either a 1 nM R6G or 1 nM TMR-labeled pHLIP peptide solution or a solution of 40 nM Nile Red and 20 μM HSA was loaded on a PEG-silane (Gelest Inc., Morrisville, PA) modified glass slip. Excitation of the dye was accomplished by the 514 nm line of an Ar⁺ ion laser (~100 μW before

entering the microscope), and the resultant fluorescence was equally split by a nonpolarizing beamsplitter (Newport, CA) and detected by two avalanche photodiodes (Perkin Elmer, NJ) using an integration time of 0.1 μ s. Correlating the fluorescence signals in the cross-correlation mode was accomplished by a Flex 03-LQ-01 correlator card (Correlator.com, NJ) for a duration of 120 s and the resulting autocorrelation traces were analyzed using the following equation (Haustein and Schwille, 2007),

$$G(\tau) = \left(\sum_{i=1}^n \frac{1}{N} \left(\frac{f_i}{1 + \frac{\tau}{\tau_D^i}} \right) \left(\frac{1}{1 + \frac{\tau}{\omega^2 \tau_D^i}} \right)^{1/2} \right) \times \left(1 - T + T \cdot e^{-\frac{\tau}{\tau_T}} \right) \quad (7)$$

where τ_D^i represents the characteristic diffusion time constant of species i , ω refers to the axial to lateral dimension ratio of the confocal volume element, N represents the number of fluorescent molecules in the confocal volume, f_i represents the fraction of species i , τ_T is the triplet lifetime of the fluorophore and T represents the corresponding triplet amplitude.

8.3 Results

All crowding experiments were carried out in 20 mM phosphate buffer in D₂O at pH* = 7 in the presence of either 200 g/L Dextran 70 or 200 g/L Ficoll 70, whereas all other experiments were carried out in 20 mM phosphate buffer in D₂O at pH* = 7.

L9:41-74. The far-UV CD spectra of *L9:41-74* in both Dextran 70 and Ficoll 70 solutions at 4 °C exhibit the characteristic double minima of α -helices at 208 and 222 nm, respectively, and also overlap with that of *L9:41-74* in D₂O buffer solution (Figure 8.1).

In addition, as shown (Figure 8.2 A and B), the presence of these crowding agents has little effect on the CD thermal denaturation profile of L9:41-74, indicating that the thermodynamics of the underlying helix-coil transition is not sensitive to the environmental changes induced by these crowding agents.

The relaxation kinetics of L9:41-74 in these polymer solutions were studied by the laser-induced temperature-jump (*T*-jump) infrared method, the details of which have been described elsewhere (Huang et al., 2002b). Similar to those observed in dilute solution (Mukherjee et al., 2008), the *T*-jump induced relaxation kinetics of L9:41-74 contain two distinct phases (Figure 8.3). The fast phase cannot be resolved by our setup and has been attributed to temperature-induced spectral shift of the amide-I' band (Mukherjee et al., 2007b). On the other hand, the slow phase, which arises from the conformational redistribution process of the peptide in response to the *T*-jump, is well resolved and can be described by a single-exponential function. As shown (Figure 8.2 B), within the temperature range studied, the *T*-jump induced conformational relaxation rates of L9:41-74 in both Dextran 70 and Ficoll 70 solutions are almost identical to that of the peptide in D₂O buffer solution. For example, at 20 °C the relaxation time constants of L9:41-74 in Dextran 70 and Ficoll 70 solutions are $1.4 \pm 0.2 \mu\text{s}$ and $1.5 \pm 0.2 \mu\text{s}$, respectively, whereas in D₂O buffer solution the relaxation time constant is $1.17 \pm 0.15 \mu\text{s}$ (Mukherjee et al., 2008). Taken together, these thermodynamic and kinetic results indicate that the folding-unfolding transition of this α -helical peptide is not sensitive to macromolecular crowding, at least not to that induced by 200 g/L Dextran 70 or Ficoll 70.

Z34C-m1. The far-UV CD spectra of Z34C-m1 obtained at 4 °C in both Dextran 70 and Ficoll 70 solutions are almost completely superimposable with that obtained in D₂O buffer solution (Figure 8.4), indicating that the helical nature of the folded conformation is not affected by the crowding agents. The thermal denaturation of Z34C-m1 in both Dextran 70 and Ficoll 70 solutions, measured by monitoring the change in its helical CD signal at 222 nm with increasing temperature (Figure 8.5A), also shows that these crowding agents do not change the thermal stability of the peptide to any appreciable extent. Indeed, globally fitting the CD data to a two-state model reveal that the thermal melting temperature (T_m) of Z34C-m1 in these crowded environments is only increased by less than 4 °C (Table 1), compared to that in D₂O buffer (Du and Gai, 2006). Consistent with these thermodynamic assessments, the *T*-jump induced relaxation rates of Z34C-m1 in these polymer solutions also show only a moderate decrease from those measured in dilute aqueous solution (Table 8.1 and Figure 8.5B).

Trpzip4-m1. Similar to that obtained in D₂O buffer solution (Du et al., 2006), the far-UV CD spectra of trpzip4-m1 in both Dextran 70 and Ficoll 70 solutions exhibit a positive band centered at ~229 nm (Figure 8.6), arising from excitonic coupling between the paired tryptophan side chains. As shown (Figure 8.7), the thermal unfolding transitions of trpzip4-m1 in these solutions, as monitored by the change in the CD signal at 229 nm, show characteristics of a cooperative thermal unfolding process. As indicated (Table 8.1), the thermal melting temperature (T_m) of trpzip4-m1 in Dextran 70 solution is increased only slightly compared to that (32 °C) in D₂O buffer, whereas in Ficoll 70 solution the T_m of this peptide shows a substantial increase to ~44 °C (Table 8.1).

The relaxation kinetics of trpzip4-m1 in response to a *T*-jump were also probed at 1631 cm⁻¹ where antiparallel β -sheets are known to absorb (Figure 8.8) (Du et al., 2006). As shown (Figure 8.9 A and B), unlike L9:41-74, the folding and unfolding rates of trpzip4-m1 are distinctly slower in the presence of the crowding agents. For example, at 35 °C the folding and unfolding time constants of trpzip4-m1 in Dextran 70 solution are 96 ± 14 and 92 ± 14 μ s, respectively, whereas in dilute aqueous solution (Du et al., 2006) this peptide folds in 47.5 ± 2.3 μ s and unfolds in 38.1 ± 2.0 μ s (Table 8.1).

8.4 Discussion

Since macromolecular crowding is an intrinsic feature of the cellular environment (Fulton, 1982; Zimmerman and Trach, 1991), there has been considerable interest in recent years in investigating its effect on protein folding, both experimentally (Van den Berg et al., 2000; Qu and Bolen, 2002; Tokuriki et al., 2004; Ai et al., 2006; Charlton et al., 2008; Yuan et al., 2008; Zhou, 2008b; Zhou et al., 2008; Homouz et al., 2009) and computationally (Friedel et al., 2003; Ping et al., 2004; Tokuriki et al., 2004; Yuan et al., 2008; Zhou, 2008b; Zhou et al., 2008; Rivera et al., 2009). However, almost all of the previous experimental efforts in this area have been focused on large proteins (Van den Berg et al., 2000; Qu and Bolen, 2002; Tokuriki et al., 2004; Charlton et al., 2008; Yuan et al., 2008; Zhou, 2008b; Zhou et al., 2008; Homouz et al., 2009), thus providing little, if any, information on the effect of macromolecular crowding on protein folding at the secondary structure level. While such a bias in focus is understandable because most protein secondary structural elements (e.g., monomeric α -helix and β -hairpin) are probably too small to be profoundly affected by the excluded volume effect (Minton,

2005; Zhou et al., 2008), however, understanding the influence of crowding on the folding dynamics of such small structural moieties could provide new insights into the otherwise complex interplay between different crowding effects. In addition, in view of the important role of secondary structure formation in existing protein folding models such as the framework model (Kim and Baldwin, 1982), there is a strong need for investigation of folding dynamics of secondary structural elements in crowded environment in order to understand protein folding *in vivo*. Herein, we study the folding thermodynamics and kinetics of three distinct secondary structural elements, i.e., a monomeric α -helix (L9:41-74), a β -hairpin (trpzip4-m1) and a HTH motif (Z34C-m1) in the presence of two commonly used crowding agents, namely, Dextran 70 and Ficoll 70.

L9:41-74. L9:41-74 is the central α -helix of ribosomal protein L9 from the bacterium *Bacillus stearothermophilus*. Owing to a series of favorable side chain-side chain interactions, mostly electrostatic in nature, this peptide remains folded even in isolation in aqueous solution (Kuhlman et al., 1997). Previously, we have shown that this peptide folds on a timescale that is significantly slower than that of alanine-based peptides and its folding time may be a more realistic representation of the time scale in which α -helices in proteins fold (Mukherjee et al., 2008). Thus, it would be quite interesting to further examine how crowding affects its folding-unfolding dynamics. Our CD measurements (Figure 8.2A) show that the thermal stability of L9:41-74 in either Dextran 70 or Ficoll 70 solution remains practically unchanged from that in dilute aqueous solution, suggesting that the helix-coil transition experiences little, if any, crowding effect. This observation is however unexpected because the chain length of this α -helix is estimated

to be ~ 50 Å (assuming a full helical structure), which is comparable to the hydrodynamic radii of Dextran 70 and Ficoll 70.

Besides the apparent excluded volume effect, addition of a polymer to aqueous solution is also known to affect the dynamic viscosity of the solution. For example, the dynamic viscosities of 200 g/L Dextran 70 and 200 g/L Ficoll 70 solutions are about 18 and 10 times greater than that of water at 20 °C (Phillies and Quinlan, 1992; Wenner and Bloomfield, 1999), respectively. Previously, Eaton and coworkers (Jas et al., 2001) have shown that the *T*-jump induced relaxation rate of an alanine-based helical peptide is inversely proportional to $\eta^{0.6}$ (where η represents the viscosity of the solution) when small viscogens, such as glucose and sucrose, were used to increase the viscosity of the solution. Thus, our observation that the *T*-jump induced relaxation kinetics of L9:41-74 in both Dextran 70 and Ficoll 70 solutions are almost the same as those obtained in dilute D₂O solution (Figure 8.2 B) is quite interesting and warrants further discussion.

The viscosity dependence of protein folding rates stems from the diffusive nature of the associated barrier-crossing events (Bhattacharyya and Sosnick, 1999; Jacob and Schmid, 1999; Hagen et al., 2005; Frauenfelder et al., 2006), namely, from the requirement of polypeptide chain motion to form the stabilizing native contacts via diffusion. Previous studies have shown that under the current crowding conditions the polymer molecules can form porous networks (Lavalette et al., 1999; Kozer et al., 2007; Neuweiler et al., 2007) wherein the viscosity determined via the diffusion of a probe molecule can be significantly lower than the dynamic viscosity of the bulk solution (Barshtein et al., 1995; Lavalette et al., 1999; Neuweiler et al., 2007). To differentiate

these viscosities, we referred to the one measured via molecular diffusion as the microviscosity of the solution. Since the sizes of the three peptides used in present study are relatively small, it is reasonable to assume that their folding rates would respond more to the microviscosity rather than the dynamic viscosity of the polymer solution. Thus, to further probe the microviscosity of the current crowding solutions, we have also measured the characteristic translational diffusion times (τ_D , a quantity that is inversely proportional to the diffusion constant D) of three molecular systems of varying sizes using Fluorescence Correlation Spectroscopy (FCS), namely, (i) a fluorescent dye: Rhodamine 6G (R6G), (ii) a 37-residue fluorescently labeled pH (low) insertion peptide (pHLIP), and (iii) the Human Serum Albumin (HSA) protein complexed with the dye Nile Red (HSA-NR). As shown (Table 8.2), the translational diffusion times of all three probes indicate that the microviscosities of Ficoll 70 and Dextran 70 solutions are about 4-6 times larger than that of water, depending on the size of the probe and also the crowding agent.

These FCS measurements indicate that not only the dynamic (or bulk) viscosity but even the microviscosity measurements fall short of providing a rationale behind the observation that the relaxation rate of L9:41-74 is insensitive to the presence of crowding agents, this being in stark contrast to the well-documented notion that the rate of α -helix formation is susceptible to viscosity (Jas et al., 2001). However, this apparent discrepancy may be reconciled by taking into account the notion that diffusion constant could also be distance-dependent (Masuda et al., 2001; Masuda et al., 2004). For

example, the diffusion constant (D) of a probe molecule in a polymer solution (Figure 8.10) consisting of porous networks is (Ogston et al., 1973):

$$D = D_0 \exp(-ac^{1/2}) \quad (1)$$

where c is the concentration of the polymer and D_0 is the diffusion constant of the probe at $c = 0$. The constant a has been shown to characterize the length scale (ξ) of the pores embedded in the porous networks, at least for a simple pore model (Masuda et al., 2004). Thus, for short diffusion modes or diffusion events during which the diffusing particles travels a distance smaller than the pore size ξ of the polymer solution, the particles rarely come into contact with the polymer chains and hence their diffusion constant is close to that found in bulk water. On the other hand, for long diffusion modes or diffusion events during which the particles travel a distance much larger than ξ , the resultant diffusion constant becomes smaller than that measured in bulk water, similar to those observed in our FCS measurements. In this context, it is clear that the viscosity effect exerted by a polymeric crowding agent on the folding rate of a peptide depends on the length scale that the polypeptide chain has to traverse from the unfolded to the transitions state along the folding coordinate.

The formation of an α -helix can be regarded as a series of local events wherein a hydrogen bond between the amino acids at 'i' and 'i+4' positions along the polypeptide chain is formed. Thus, the length-scale (a few \AA) over which the key α -helix folding events take place is far less than the pore size of the polymer solutions used in the current

study and therefore the corresponding folding rate does not show any significant deviation from that in dilute aqueous solution. In contrast, in studies where small viscosogens (e.g., glucose or sucrose) are used to increase the viscosity, the resulting solution viscosity is microscopically homogeneous and therefore the effect of increased solvent friction can be experienced down to a very short length-scale. Thus, in such cases, the viscosity dependence of the folding kinetics of protein secondary structural elements might become more pronounced, as has been shown in a previous study (Jas et al., 2001).

Z34C-m1. Z34C-m1 is a mutant of Z34C (i.e., D20A), which forms a crossed-linked HTH structure, a common structural motif found in DNA-binding proteins (Starovasnik et al., 1997). Previously we have shown that Z34C-m1 folds significantly slower than Z34C since the mutation deletes a hydrogen bond that is critical to the stability of the reverse turn (Du and Gai, 2006). Z34C-m1 constitutes a good model system to further examine the effect of microviscosity on the folding-unfolding kinetics of α -helices in a protein context, as the disulfide cross-linker prevents the protein to become extended upon unfolding and hence makes it less likely to experience the excluded volume effect. As expected, the folding thermodynamics and kinetics of Z34C-m1 are only moderately affected by the crowding agents employed herein (Figure 8.5 and Table 8.1). Thus, these results are consistent with those of L9:41-74 and further corroborate the notion that macromolecular crowding does not affect to any significant extent the folding dynamics of α -helices that can fold independently. However, in a protein context the frictional drag along the folding coordinate of an α -helix may be position-dependent and thus, could

exert a more complex effect on the folding dynamics. Apparently, for β -sheets whose folding requires relatively large-scale chain diffusions, the effect of microviscosity is expected to play a more important role as discussed below.

Trpzip4-m1. To further explore to what extent the nature of the folded topology determines the effect of macromolecular crowding, we have also studied the folding thermodynamics and kinetics of trpzip4-m1, the D46A mutant of the 16-residue β -hairpin trpzip4 (Du et al., 2006) in both Dextran 70 and Ficoll 70 solutions. While the thermal denaturation properties of trpzip4-m1 is almost unaffected by addition of Dextran 70, its thermal melting temperature in Ficoll 70 solution (Figure 8.7) however shows a substantial increase from that in D₂O buffer (Du et al., 2006). This difference manifests the disparity in terms of crowding efficiency of these crowding agents and can be rationalized based on the overall difference in the molecular structures of these polymers. Previous studies have shown that the persistence length of Dextran is about 0.4 nm (Rief et al., 1998), which renders it to be a relatively flexible polymer. On the other hand, Ficoll 70 is comparatively more rigid due to its cross-linked structure (Bohrer et al., 1984; Venturoli and Rippe, 2005). Thus, based on these considerations, it is conceivable that at the same concentration Dextran 70 can accommodate more interstitial spaces in comparison to Ficoll 70, therefore allowing the unfolded polypeptide chain of trpzip4-m1 more space to escape and hence leading to a weaker excluded volume effect.

In contrast to that observed in other studies (Van den Berg et al., 2000; Ping et al., 2004; Cheung et al., 2005), macromolecular crowding results in a decrease in the folding rate of trpzip4-m1. This result thus clearly indicates that a macromolecular crowding

agent can affect not only the protein stability via the excluded volume effect, but also the folding dynamics through modulation of the effective viscosity of the protein environment. In the case of Dextran 70, the thermal stability of the β -hairpin exhibits only a very modest change (Table 8.1), thus implying that the observed reduction in the folding and unfolding rates is unlikely to result from the excluded volume effect, but rather arises from a viscosity effect. This interpretation is consistent with the notion that the dynamics of peptide loop closure and β -hairpin folding require relatively large-scale and non-local motions, in contrast to the folding of an α -helix wherein the chain primarily undergoes a series of local structural reorganizations. Thus, during such a folding event the peptide chain has a higher chance of colliding with the polymer network formed by the crowding molecules, resulting in a slower folding/unfolding rate. This picture is consistent with a recent FCS study by Sauer and coworkers (Neuweiler et al., 2007), who showed that the intrachain diffusion rate of a series of fluorescently labeled short poly(GS)-peptides in Ficoll 70 depends on the net effect of two opposing forces, the excluded volume effect and the increased viscous drag of the polymer solution.

The effect of viscosity on protein folding or unfolding rate constant (k_{obs}) can often be described by the hydrodynamic approximation of the Kramers equation in the high friction limit, i.e.,

$$k_{\text{obs}} = \frac{A}{\eta(T)^\alpha} \exp\left(-\frac{\Delta G^\ddagger}{RT}\right) \quad (2)$$

where $\eta(T)$ is the effective viscosity of the medium at temperature T and has been assumed here to be independent of the spatial location of the peptide, α is equal to unity in many cases, A is a constant, and ΔG^\ddagger is the apparent free energy barrier at temperature T , and R is the gas constant. Thus, a crowding agent can modulate the folding and unfolding rate constants of a protein by changing either η or ΔG^\ddagger or both. Apparently, the effect related to η is a dynamic one, whereas that related to ΔG^\ddagger is static (or the excluded volume) in nature.

For a simple two-state scenario, assuming that A is the same for both folding and unfolding and also that it is independent of crowding, one can easily show that (assuming no change in the position of the transition state)

$$\ln\left(\frac{k_f^c}{k_f^0}\right) + \ln\left(\frac{k_u^c}{k_u^0}\right) = 2\alpha \ln\left(\frac{\eta_0(T)}{\eta_c(T)}\right) + \frac{1}{RT}(\Delta G_u^{c-0} + \Delta G_f^{c-0}) \quad (3)$$

where k_f and k_u are the folding and unfolding rate constants, $\Delta G_u^{c-0} = G_u^c - G_u^0$ and $\Delta G_f^{c-0} = G_f^c - G_f^0$ where G_u and G_f represent the free energies of the unfolded and folded states, respectively, and in all cases, the superscripts “0” and “c” represent the dilute and crowded solutions, respectively. In addition, $\eta_0(T)$ and $\eta_c(T)$ are the effective viscosities of the dilute and crowded solutions at temperature T , respectively. For Dextran 70, the increased stabilization of the β -hairpin conformation of trpzip4-m1 arising from crowding is considered to be negligible (i.e., $\Delta G_u^{c-0} + \Delta G_f^{c-0} \approx 0$). Thus, using the

measured folding and unfolding rate constants of trpzip4-m1 in the presence and absence of crowding agents, in conjunction with the assumption that α is approximately unity for β -hairpin folding (Jas et al., 2001), the value of η_c/η_0 is calculated to be 3.5 ± 0.5 at 20 °C, which is comparable to the ratio of diffusion times $\tau_c/\tau_0 = 3.8$ of the pHLIP peptide in 200 g/L Dextran 70 and water at room temperature (Table 8.2). Therefore, this agreement further corroborates the idea that Dextran 70 affects trpzip4-m1 folding via mostly the dynamic (or viscosity) effect.

In the case of Ficoll 70, the presence of the crowding agent leads to not only a decrease in the folding rate of trpzip4-m1, but also a significant increase in the stability of β -hairpin conformation (Figure 8.7 and 8.9 B and Table 8.1), indicating that the folding and unfolding dynamics of trpzip4-m1 experience both the excluded volume and viscosity effects. As a result, the unfolding rate is decreased to a larger extent than the folding rate, compared to their respective values in D₂O buffer solution (Table 8.1). This is because both the excluded volume and viscosity effects slow down the rate of unfolding, whereas they exhibit opposite effects on the folding rate.

Furthermore, it is easy to show that

$$\frac{k_f^c}{k_f^0} = \left(\frac{\eta_0}{\eta_c} \right)^\alpha \exp\left(\frac{\Delta\Delta G^\ddagger}{RT} \right) \quad (4)$$

where $\Delta\Delta G^\ddagger = \Delta G_0^\ddagger - \Delta G_c^\ddagger$ which is a quantitative measure of the excluded volume effect on the folding dynamics. Thus, it is possible to dissect the static and dynamic contributions to the total crowding effect if η_c/η_0 is known. While η_c/η_0 cannot be determined independently from the current study, the result obtained with Dextran 70 nevertheless suggests that it approaches the ratio τ_c/τ_0 measured by the FCS method. Thus, using the ratio $\tau_c/\tau_0 = 4.1$ (Table 2) we estimated the $\Delta\Delta G^\ddagger$ value to be $\sim 0.3 \pm 0.1$ kcal mol⁻¹ at 35 °C for the folding of trpzip4-m1 in 200 g/L Ficoll 70 solution. As expected, the decrease in the folding free energy barrier of trpzip4-m1 due to the excluded volume effect is very modest, as the additional stabilization (i.e., $\Delta\Delta G^0 = |\Delta G_c^0| - |\Delta G_0^0|$) of trpzip4-m1 due to the presence of 200g/L Ficoll 70 at 35 °C is only about 0.5 ± 0.1 kcal mol⁻¹, owing to the small size of the peptide relative to the size of the crowding agent, which is in agreement with the theoretical prediction by Minton (Minton, 2005). However, we expect that the approach outlined above will be very useful for dissecting the static and dynamic effects of a crowding agent for other protein systems.

8.5 Conclusions

Employing two commonly used crowding agents, Dextran 70 (200 g/L) and Ficoll 70 (200 g/L), we have studied how macromolecular crowding affects the folding-unfolding kinetics of three peptides, which fold into different conformations in solution, namely an α -helix (L9:41-74), a cross-linked helix-turn-helix (Z34C-m1), and a β -hairpin (trpzip4-m1). Interestingly, only the folding thermodynamics and kinetics of the

shortest peptide, trpzip4-m1, were found to show significant changes in the Ficoll 70 solution, thus indicating that the effect of macromolecular crowding is sensitive to the size and shape of both the peptide and the crowding agent. In addition, the observation that macromolecular crowding does not alter significantly the folding dynamics of the two helical peptides is consistent with the notion that α -helix formation involves mostly local interactions. Furthermore, and in contrast to that observed for large proteins, macromolecular crowding results in a decrease in the folding rate of trpzip4-m1, indicating that the motion of the peptide chain experiences a higher friction arising from the presence of the crowding agent, and that this viscosity effect in this case outplays the excluded volume effect on the folding kinetics of the β -hairpin.

Table 8.1 Summary of the thermodynamic and kinetic data for Z34C-m1 and trpzip4-m1 obtained under different conditions. *The folding and unfolding times were obtained at 55 °C for Z34C-m1 and 35 °C for trpzip4-m1.

	Z34C-m1			Trpzip4-m1		
	D ₂ O buffer	Dextran 70	Ficoll 70	D ₂ O buffer	Dextran 70	Ficoll 70
ΔH_m (kcal mol ⁻¹)	16.2 ± 0.7	17.1 ± 0.8	16.8 ± 0.7	13.8 ± 0.2	12.5 ± 0.3	15.6 ± 0.2
ΔS_m (cal K ⁻¹ mol ⁻¹)	49.4 ± 3.8	52.0 ± 2.6	50.9 ± 2.0	45.1 ± 2.5	40.6 ± 0.9	49.1 ± 0.7
ΔC_p (cal K ⁻¹ mol ⁻¹)	118 ± 34	245 ± 105	120 ± 54	343 ± 41	238 ± 19	223 ± 15
T_m (°C)	54.7 ± 1.0	55.3 ± 1.5	57.7 ± 0.5	32.1 ± 0.9	34.3 ± 0.5	44.0 ± 0.2
τ_f (μs)*	5.3 ± 0.8	8.6 ± 1.3	7.3 ± 1.1	47.5 ± 2.3	96 ± 14	122 ± 18
τ_u (μs)*	5.1 ± 0.8	8.8 ± 1.3	9.0 ± 1.4	38.1 ± 2.0	92 ± 14	240 ± 36

Table 8.2 Translational diffusion times determined by FCS at room temperature for R6G, the pHLIP peptide, and the HSA–NR complex.

	D ₂ O	Dextran 70 (200 g/L)	Ficoll 70 (200 g/L)
Rhodamine 6G (μs)	53 ± 2	216 ± 5	256 ± 5
pHLIP (μs)	75 ± 3	286 ± 5	305 ± 8
HSA-NR (μs)	419 ± 15	2000 ± 30	2460 ± 60

Figure 8.1 Far-UV CD spectra of L9:41-74 at 4.0 °C in D₂O, Dextran 70 (200 g/L), and Ficoll 70 (200 g/L) solutions, as indicated. All solutions contain 20 mM phosphate (pH* = 7).

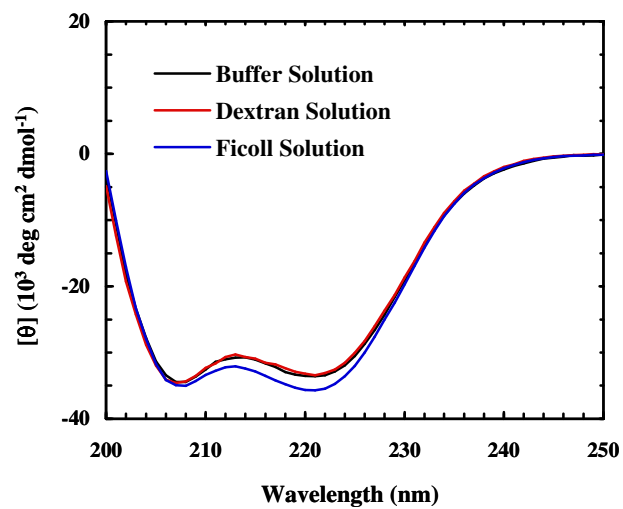


Figure 8.2 (A) CD thermal melting curves of L9:41-74 in 200 g/L Dextran 70 (red) and in 200 g/L Ficoll 70 (blue), respectively. (B) Arrhenius plot of the T -jump induced conformational relaxation rates of L9:41-74 in 200 g/L Dextran 70 (red) and in 200 g/L Ficoll 70 (blue), respectively. Also shown for comparison are the CD thermal melting curve [black crosses in A] and relaxation rates [black dashed line in B] of the same peptide in 20 mM phosphate D₂O buffer (derived from reference (Mukherjee et al., 2008)).

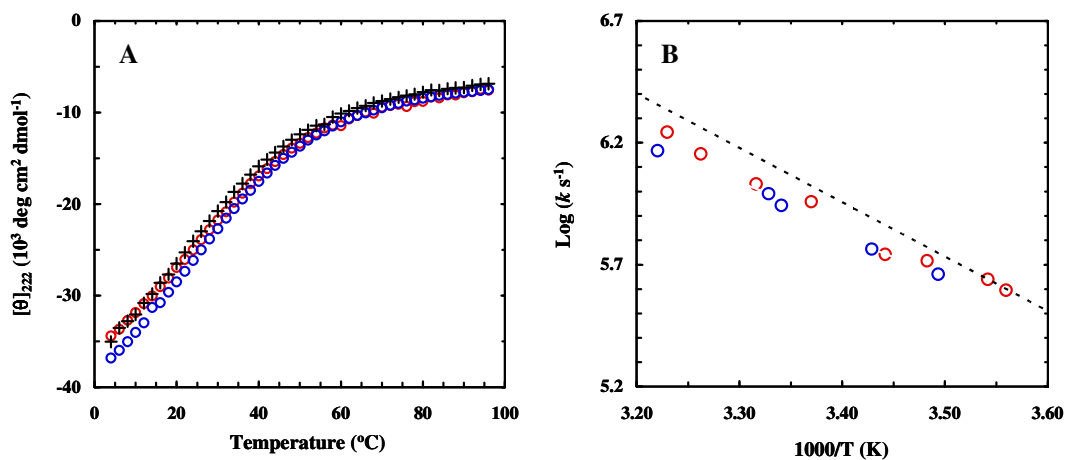


Figure 8.3 Representative T -jump relaxation traces (blue and red) of L9:41-74 in 200 g/L Dextran 70 (20 mM phosphate buffer, $\text{pH}^* = 7$) in response to a T -jump of 5.5 °C (blue), from 22.9 to 28.4 °C, and 5.9 °C (red), from 8.1 to 14.0 °C (scaled 1.5 times). The smooth lines are convolutions of the instrument response function with $\Delta\text{OD}(t) = A \cdot [1 - B \cdot \exp(-t/\tau)]$, with $A = -0.0033$, $B = 0.59$, and $\tau = 0.93 \mu\text{s}$ for the higher final temperature data and $A = -0.0019$, $B = 0.78$, and $\tau = 1.9 \mu\text{s}$ for the lower final temperature data.

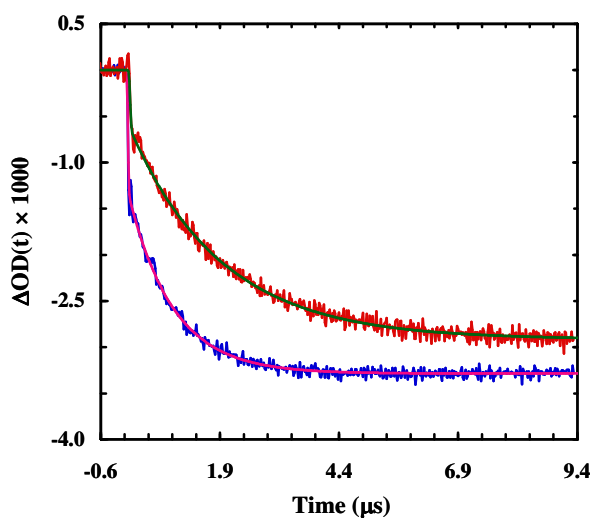


Figure 8.4 Far-UV CD spectra of Z34C-m1 at 4.0 °C in D₂O, Dextran 70 (200 g/L) and Ficoll 70 (200 g/L) solutions, as indicated. All solutions contain 20 mM phosphate (pH* = 7).

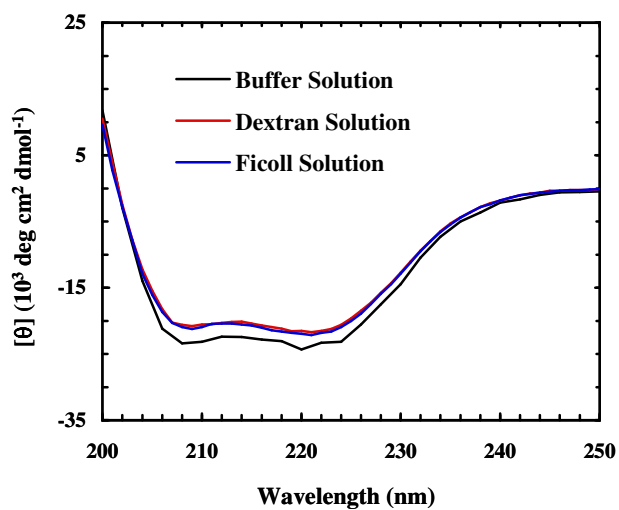


Figure 8.5 (A) CD thermal melting curves of Z34C-m1 in 200 g/L Dextran 70 (red) and in 200 g/L Ficoll 70 (blue), respectively. Lines are global fits of these data to the two-state model described in the text. (B) Arrhenius plot of the T -jump induced conformational relaxation rates (open circles) of Z34C-m1 in 200 g/L Dextran 70 (red) and in 200 g/L Ficoll 70 (blue), respectively. Open triangles and squares correspond to the two-state folding and unfolding rates of Z34C-m1 in 200 g/L Dextran 70. Also shown are the CD thermal melting curve [black crosses in A] and folding [black dashed line in B] and unfolding [black solid line in B] rate constants of Z34C-m1 in 20 mM phosphate D₂O buffer (derived from reference (Du and Gai, 2006)).

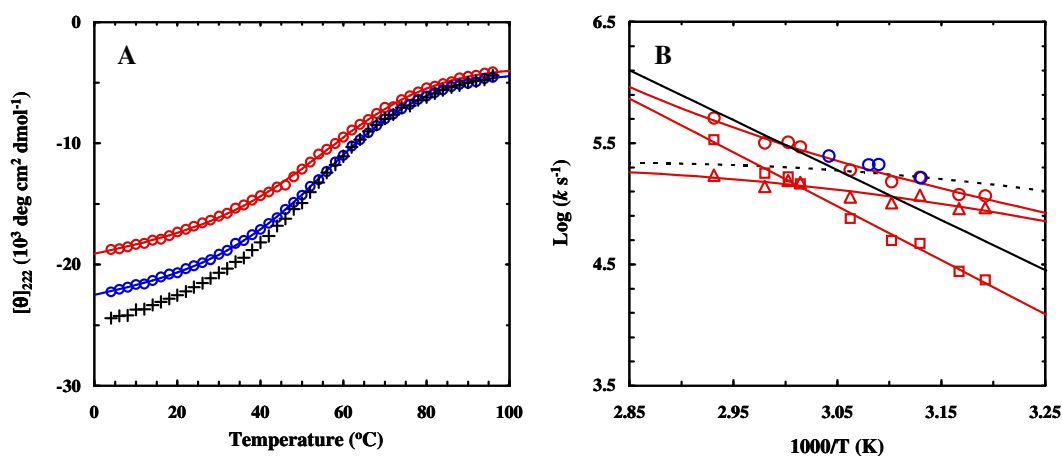


Figure 8.6 Far-UV CD spectrum of trpzip4-m1 at 4.0 °C in D₂O, Dextran 70 (200 g/L), and Ficoll 70 (200 g/L) solutions, as indicated. All solutions contain 20 mM phosphate (pH* = 7).

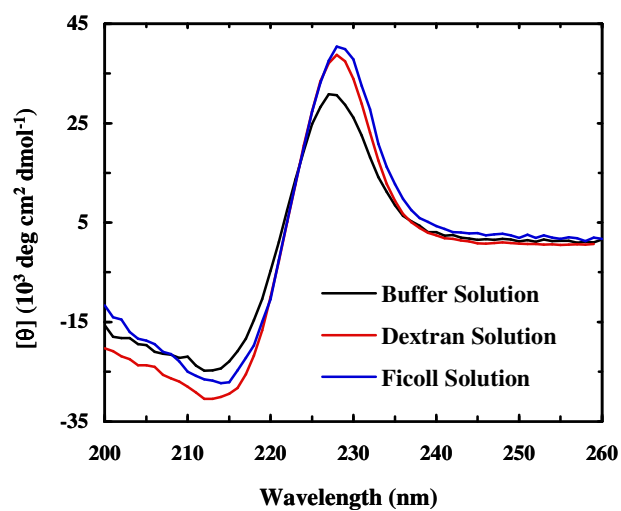


Figure 8.7 CD thermal melting curves of trpzip4-m1 in 200 g/L Dextran 70 (red) and in 200 g/L Ficoll 70 (blue), respectively. Lines are global fits of these data to the two-state model described in the text. Also shown is the CD thermal melting curve (black) of the same peptide in 20 mM phosphate D₂O buffer (derived from reference (Du et al., 2006)).

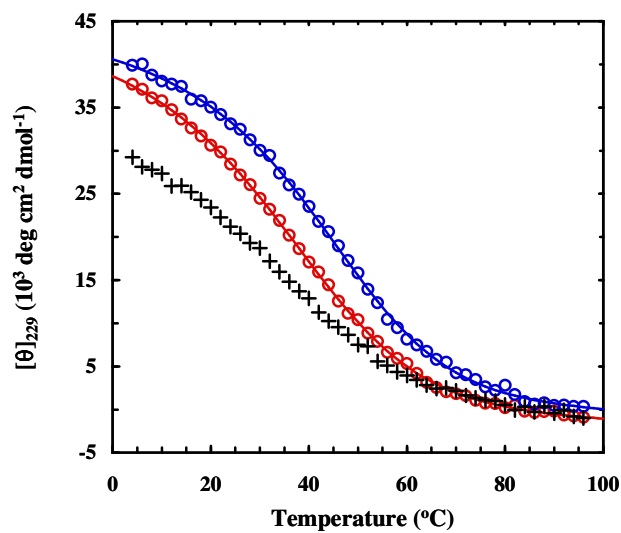


Figure 8.8 A representative relaxation trace (blue) of trpzip4-m1 in 200 g/L Dextran 70 (20 mM phosphate buffer, pH* = 7) in response to a T -jump of about 4.2 °C, from 22.2 to 26.4 °C. The smooth red line is a convolution of the instrument response function with $\Delta OD(t) = A \cdot [1 - B \cdot \exp(-t/\tau)]$, with $A = -0.0092$, $B = 0.89$, and $\tau = 106 \mu\text{s}$.

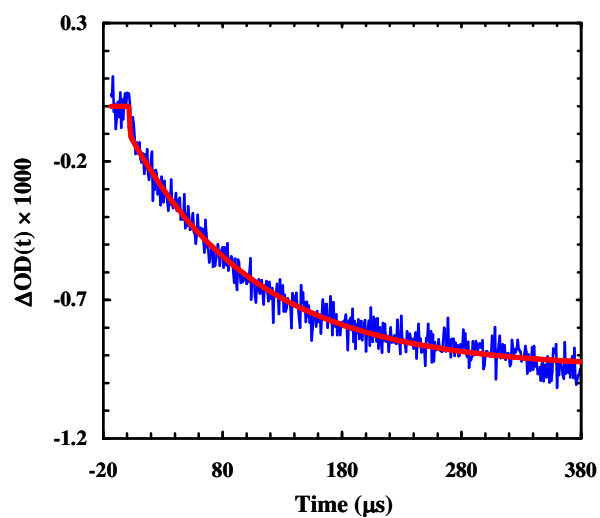


Figure 8.9 Arrhenius plots of the T -jump induced conformational relaxation rates (open circles) of trpzip4-m1 in 200 g/L Dextran 70 (A) and in 200 g/L Ficoll 70 (B), respectively. Open triangles and squares correspond to their respective two-state folding and unfolding rates. Also shown in each case are the folding (blue dashed line) and unfolding (red dashed line) rate constants of trpzip4-m1 in 20 mM phosphate D₂O buffer (derived from reference (Du et al., 2006)).

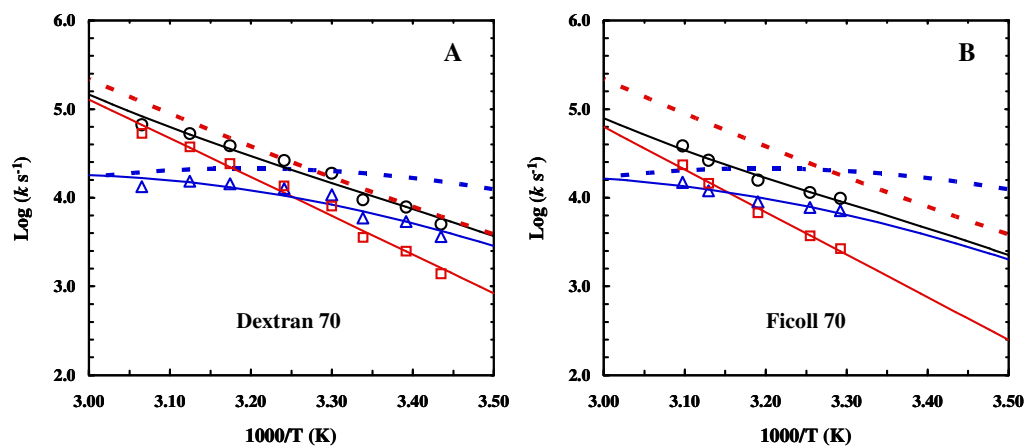
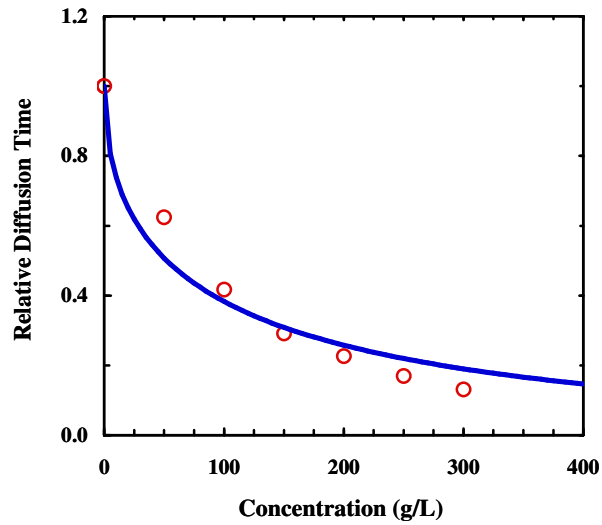


Figure 8.10 Relative diffusion time of R6G versus Ficoll 70 concentration, measured via FCS at room temperature. The solid line represents the best fit of these data to eq. (1) in the text with $a = 0.096$. The model given in (Masuda et al., 2004) suggests that the characteristic length scale (ξ) of the pores of a polymer solution is related to a via the following equation, $\xi = (b/a)c^{-1/2}$, where b is the diameter of the diffusing probe molecules and c is the concentration of the polymer. However, this simple pore model seems to fail in the present case as the length scale of Ficoll 70 at 200 g/L is predicted to be smaller than the hydrodynamic diameter of the Rhodamine 6G dye.



Chapter 9: Summary and Future Directions

Macromolecular crowding and confinement effects that are intrinsically associated with the cellular environment are often neglected in protein folding and aggregation studies conducted under *in vitro* conditions wherein typically dilute aqueous solutions are used. For example, the presence of high concentrations of macromolecules near a protein could alter its folding energy landscape through the excluded volume effect and also through changes in its solvation status. These differences in protein environment between *in vivo* and *in vitro* conditions have motivated the studies presented in this thesis wherein we investigate how degrees of hydration and macromolecular crowding affect the conformation, aggregation and folding kinetics of short peptides.

However, experimentally it is not trivial to control the amount of water molecules available to a peptide or protein molecule of interest. While using a cosolvent can allow one to probe the various effects of peptide backbone dehydration (Starzyk et al., 2005), such a method may encounter the added complexity of interactions between the cosolvent and the peptide which need to be considered. Here we propose the use of reverse micelles formed by sodium bis(2-ethylhexyl) sulfosuccinate (AOT) as a platform to directly test how the degree of hydration affects the conformation of peptides. The advantage of using AOT reverse micelles is that one can systematically vary the amount of water available to guest molecules solubilized inside the aqueous micellar core. In practice, this can be achieved by preparing reverse micelles with different w_0 values, a parameter defined as

the ratio of the molar concentration of water to that of the surfactant ($w_0 = [\text{water}]/[\text{AOT}]$).

Previous studies indicated (Vila et al., 2000; Vila et al., 2001; Garcia and Sanbonmatsu, 2002; Ghosh et al., 2003) that water molecules can act as denaturants toward the helical conformation by competing for hydrogen bonds with the amide CO and NH groups. This therefore suggests that one should be able to tune the stability of helical peptides by varying the degree of backbone hydration. Baldwin and coworkers demonstrated that alanine-based peptides with a typical sequence of XAAAA repeats, with X being a polar or charged amino acid (e.g., lysine and arginine) can form helices in water (Marqusee et al., 1989). To examine how degrees of hydration affect the conformation of peptides, we therefore solubilized the alanine-based peptides in the aqueous core of AOT reverse micelles at different water contents. Our results show that indeed the helicity of these alanine-rich peptides is significantly increased in AOT reverse micelles of low water content, as compared to the corresponding helical content in water at 4 °C. More importantly, our temperature-dependent infrared (IR) and circular dichroism (CD) studies show that these alanine-based peptides undergo a thermally induced conformational transition in reverse micelles of low w_0 values (e.g., $w_0 = 6$), resulting in soluble peptide aggregates rich in antiparallel beta-sheets. However, increasing the water content in reverse micelles, i.e., using higher w_0 values, leads to an increase in the onset temperature at which such beta-aggregates begin to form. In D₂O these peptides do not form any measurable aggregates, even at a molar concentration that is 25-50 times larger than that used in the reverse micellar studies. Thus, these results

strongly suggest that limited hydration facilitates aggregate formation in alanine-based peptides and that removal of water imposes a free energy barrier to peptide association and subsequent aggregation.

Motivated by these results, we sought to investigate whether the aggregation properties of biologically relevant peptides are also dependent on their solvation status. In this regard, we monitored the aggregation kinetics of amyloid forming segments derived from amyloid β peptides and yeast prion protein Sup35 in reverse micelles of different water contents and also in bulk water. Using infrared spectroscopy and transmission electron microscopy as a means to monitor aggregate formation, we show that the rate of the early steps of peptide aggregation is increased under conditions where limited hydration of the peptide molecule is expected to occur and that the actual effect of dehydration on aggregation kinetics depends on the peptide sequence. In addition, the morphology of the aggregates formed in reverse micelles is annular as opposed to the fibrillar aggregates seen for these peptides under bulk water conditions (Balbach et al., 2000; Balbirnie et al., 2001); indicating a role of the reverse micelles/environment in dictating the aggregate morphology. Taken together, our results obtained with peptides of varying sequence identities in reverse micelles at different w_0 values and in bulk water demonstrate how degrees of hydration control peptide conformation and aggregation properties. Furthermore, these results have implications for understanding aggregate formation *in vivo* where crowding is expected to affect the solvation status of the protein.

Our next effort was to investigate how macromolecular crowding affects protein folding dynamics at the secondary structure level. To make the study biologically

relevant, we studied the folding dynamics of monomeric helices derived from naturally occurring proteins rather than using designed alanine-based peptides as such alanine-rich sequences are rarely encountered in proteins. We first studied the relaxation kinetics of the central helix (L9:41-74) of the ribosomal protein L9 from the bacterium *Bacillus stearothermophilus*, in response to a temperature-jump (T -jump) using infrared spectroscopy, in dilute aqueous buffer. Our results show that the monomeric helical peptide L9:41-74 folds much slower than helical peptides rich in alanine residues. We rationalize that for L9:41-74, the multiple stabilizing side chain-side chain interactions that need to be spatially disposed/aligned in a proper manner increases the folding free energy barrier, thereby resulting in a decrease in the rate at which the peptide folds in comparison to alanine-based peptides which are devoid of such side chain-side chain interactions. These results further suggest that great caution must be taken when interpreting the folding kinetics of alanine-based peptides in the context of protein folding models. In order to examine how the thermal stability and folding-unfolding kinetics of L9:41-74 is affected by macromolecular crowding; we studied its folding dynamics in the presence of two different crowding agents (i.e., inert high mass polymers). We further extended this study to include two other secondary/supersecondary structural elements, i.e., a 34-residue cross-linked helix-turn-helix, and a 16-residue β -hairpin peptide with the aim of providing new insights into the effect of macromolecular crowding on folding events taking place over a relatively short length scale; a topic on which very little experimental and computational work has been performed. Our thermodynamic and kinetic results indicate that the folding-unfolding transition of alpha

helical peptides is insensitive to macromolecular crowding, at least to that induced by 200 g/L of crowding agents which is consistent with the notion that alpha-helix formation involves mostly local interactions. Furthermore, and in contrast to that observed for large proteins, macromolecular crowding results in a decrease in the folding rate of the shortest β -hairpin peptide, indicating that the motion of the peptide chain experiences a higher friction arising from the presence of the crowding agent. We propose that besides the excluded volume effect, other factors like the frictional drag experienced by conformational motions along the reaction coordinate also need to be considered when evaluating the net effect of crowding on protein folding kinetics. Our approach outlined in Chapter 8 will be very useful for dissecting the static and dynamic effects of a crowding agent for other protein systems.

The studies presented in this thesis provide new insight into our understanding of factors that may affect the process of protein folding and misfolding. However, there are many questions that remain unanswered and we list some future experiments that can be pursued based on the results presented above. (1) We wish to address two limitations regarding the studies involving peptides dissolved in reverse micelles. Firstly, the carbonyl groups present in the AOT molecule (Figure 1.4) has a strong IR absorbance band at 1736 cm^{-1} which interferes with the amide I' band of the polypeptide chains (Jain et al., 1989). Therefore, for all the spectra shown in Chapters 3-6 which were collected in AOT reverse micelles, a background arising from imperfect subtraction of AOT signals was estimated and subtracted which renders these spectra as semi-quantitative. Secondly, it is possible that there might be electrostatic interactions between the positively charged

lysine residues of the alanine-based peptides (Chapters 3 and 5) and the negatively charged head groups of AOT molecules. Therefore, to mitigate the two issues stated above, we propose to use reverse micelles formed by the surfactant molecule Brij 30 in cyclohexane. The advantage of using reverse micelles formed by Brij 30 is that the IR spectrum of Brij 30 does not contain any absorption bands that could possibly interfere with the amide I' band arising from the polypeptide backbone and is also non-ionic in nature which eliminates the possibility of electrostatic interactions between the peptide and the surfactant molecules. Using such a neutral reverse micellar system we can then quantitatively analyze the contribution of the solvated and desolvated helical amide groups for the IR spectra of alanine-based peptides in reverse micelles and also possibly observe differences in the conformation/aggregation behavior of the dissolved peptides.

(2) Protein folding in confined spaces is a ubiquitous theme in biology. Many computational studies have been done to study the effects of confinement on the kinetics of protein folding and unfolding (Klimov et al., 2002; Hayer-Hartl and Minton, 2006; Lucent et al., 2007; Mittal and Best, 2008; Zhou et al., 2008). However, no experimental studies have been done on the rates of folding-unfolding of small peptides under confinement. Therefore, it will be interesting to monitor the relaxation kinetics of helical and β -hairpin peptides in the confined environment of reverse micelles, in response to a laser-induced *T*-jump using infrared (IR) spectroscopy. This study will complement the results presented in Chapter 8 regarding the effects of macromolecular crowding on the folding dynamics of secondary structural elements. (3) As discussed in Chapter 8, the thermal stability and folding-unfolding kinetics of helical peptides remained unchanged

in the presence of 200 g/L crowding agents. It is possible that the dynamics of the helical peptides will change in the presence of higher concentrations of crowding agents. Therefore, it is worth investigating the effects of higher concentration of crowding agents on the folding dynamics of not only the helical peptides but also that of the β -hairpin peptide, especially given the fact the concentration of macromolecules in the cell can be as high as 400 mg/ml (Zimmerman and Trach, 1991). (4) Proteins in the cell exist in the presence of macromolecules with various sizes and shapes. Therefore, it is appealing to test the effects of different ratios of mixed macromolecular crowding agents (i.e. crowding agents with different chemical compositions, shapes and molecular weight) (Zhou, 2008a) on folding dynamics of peptides and proteins using the approach outlined in Chapter 8.

REFERENCES

- Abe, Y., and Krimm, S. 1972. Normal vibrations of crystalline polyglycine i. *Biopolymers* **11**: 1817-1839.
- Abel, S., Waks, M., Urbach, W., and Marchi, M. 2006. Structure, stability, and hydration of a polypeptide in aot reverse micelles. *J. Am. Chem. Soc.* **128**: 382-383.
- Adachi, M., Harada, M., Shioi, A., and Sato, Y. 1991. Extraction of amino acids to microemulsion. *J. Phys. Chem.* **95**: 7925-7931.
- Ai, X., Zhou, Z., Bai, Y., and Choy, W.-Y. 2006. ¹⁵N nmr spin relaxation dispersion study of the molecular crowding effects on protein folding under native conditions. *J. Am. Chem. Soc.* **128**: 3916-3917.
- Andersen, N.H., Dyer, R.B., Fesinmeyer, R.M., Gai, F., Liu, Z., Neidigh, J.W., and Tong, H. 1999. Effect of hexafluoroisopropanol on the thermodynamics of peptide secondary structure formation. *J. Am. Chem. Soc.* **121**: 9879-9880.
- Arrondo, J.L.R., and Goni, F.M. 1999. Structure and dynamics of membrane proteins as studied by infrared spectroscopy. *Prog. Biophys. Mol. Biol.* **72**: 367-405.
- Avidan-Shpalter, C., and Gazit, E. 2006. The early stages of amyloid formation: Biophysical and structural characterization of human calcitonin pre-fibrillar assemblies. *Amyloid* **13**: 216-225.
- Balakrishnan, G., Hu, Y., Bender, G.M., Getahun, Z., DeGrado, W.F., and Spiro, T.G. 2007. Enthalpic and entropic stages in alpha -helical peptide unfolding, from laser t-jump/uv raman spectroscopy. *J. Am. Chem. Soc.* **129**: 12801-12808.
- Balbach, J.J., Ishii, Y., Antzutkin, O.N., Leapman, R.D., Rizzo, N.W., Dyda, F., Reed, J., and Tycko, R. 2000. Amyloid fibril formation by abeta 16-22, a seven-residue fragment of the alzheimer's beta -amyloid peptide, and structural characterization by solid state nmr. *Biochemistry* **39**: 13748-13759.
- Balbirnie, M., Grothe, R., and Eisenberg, D.S. 2001. An amyloid-forming peptide from the yeast prion sup35 reveals a dehydrated beta -sheet structure for amyloid. *Proc. Natl. Acad. Sci. U. S. A.* **98**: 2375-2380.
- Ballew, R.M., Sabelko, J., Reiner, C., and Gruebele, M. 1996. A single-sweep, nanosecond time resolution laser temperature-jump apparatus. *Rev. Sci. Instrum.* **67**: 3694-3699.

- Barshtein, G., Almagor, A., Yedgar, S., and Gavish, B. 1995. Inhomogeneity of viscous aqueous-solutions. *Physical Review E* **52**: 555-557.
- Barth, A. 2001. The infrared absorption of amino acid side chains. *Prog. Biophys. Mol. Biol.* **74**: 141-173.
- Barth, A., and Zscherp, C. 2002. What vibrations tell us about proteins. *Q. Rev. Biophys.* **35**: 369-430.
- Baumketner, A., Jewett, A., and Shea, J.E. 2003. Effects of confinement in chaperonin assisted protein folding: Rate enhancement by decreasing the roughness of the folding energy landscape. *J. Mol. Biol.* **332**: 701-713.
- Baumketner, A., and Shea, J.E. 2003. Kinetics of the coil-to-helix transition on a rough energy landscape. *Physical Review E: Statistical, Nonlinear, and Soft Matter Physics* **68**: 051901/051901-051901/051910.
- Belletete, M., Lachapelle, M., and Durocher, G. 1990. Polarity of aot micellar interfaces: Use of the preferential solvation concepts in the evaluation of the effective dielectric constants. *J. Phys. Chem.* **94**: 5337-5341.
- Berne, B.J., and Pecora, R. (1976). Dynamic light scattering: With applications to chemistry, biology, and physics (New York: Wiley).
- Berova, N., Nakanishi, K., and Woody, R.W. (2000). Circular dichroism. Principles and applications, Second edn (New York, NY: Wiley-VCH, Inc.).
- Bhattacharyya, K. 2003. Solvation dynamics and proton transfer in supramolecular assemblies. *Acc. Chem. Res.* **36**: 95-101.
- Bhattacharyya, R.P., and Sosnick, T.R. 1999. Viscosity dependence of the folding kinetics of a dimeric and monomeric coiled coil. *Biochemistry* **38**: 2601-2609.
- Bieschke, J., Siegel, S.J., Fu, Y., and Kelly, J.W. 2008. Alzheimer's abeta peptides containing an isostructural backbone mutation afford distinct aggregate morphologies but analogous cytotoxicity. Evidence for a common low-abundance toxic structure(s)? *Biochemistry* **47**: 50-59.
- Bohidar, H.B., and Behboudnia, M. 2001. Characterization of reverse micelles by dynamic light scattering. *Colloids and Surfaces a-Physicochemical and Engineering Aspects* **178**: 313-323.
- Bohrer, M.P., Patterson, G.D., and Carroll, P.J. 1984. Hindered diffusion of dextran and ficoll in microporous membranes. *Macromolecules* **17**: 1170-1173.

- Bredenbeck, J., Helbing, J., Kumita, J.R., Woolley, G.A., and Hamm, P. 2005. Alpha - helix formation in a photoswitchable peptide tracked from picoseconds to microseconds by time-resolved ir spectroscopy. *Proc. Natl. Acad. Sci. U. S. A.* **102**: 2379-2384.
- Buchete, N.-V., and Straub, J.E. 2001. Mean first-passage time calculations for the coil-to-helix transition: The active helix ising model. *Journal of Physical Chemistry B* **105**: 6684-6697.
- Budker, V.G., Slattum, P.M., Monahan, S.D., and Wolff, J.A. 2002. Entrapment and condensation of DNA in neutral reverse micelles. *Biophys. J.* **82**: 1570-1579.
- Bunagan, M.R., Yang, X., Saven, J.G., and Gai, F. 2006. Ultrafast folding of a computationally designed trp-cage mutant: Trp2-cage. *Journal of Physical Chemistry B* **110**: 3759-3763.
- Byler, D.M., and Susi, H. 1986. Examination of the secondary structure of proteins by deconvolved ftir spectra. *Biopolymers* **25**: 469-487.
- Callender, R., and Dyer, R.B. 2006. Advances in time-resolved approaches to characterize the dynamical nature of enzymatic catalysis. *Chemical Reviews (Washington, DC, United States)* **106**: 3031-3042.
- Cammers-Goodwin, A., Allen, T.J., Oslick, S.L., McClure, K.F., Lee, J.H., and Kemp, D.S. 1996. Mechanism of stabilization of helical conformations of polypeptides by water containing trifluoroethanol. *J. Am. Chem. Soc.* **118**: 3082-3090.
- Chakrabartty, A., Doig, A.J., and Baldwin, R.L. 1993. Helix capping propensities in peptides parallel those in proteins. *Proc. Natl. Acad. Sci. U. S. A.* **90**: 11332-11336.
- Charlton, L.M., Barnes, C.O., Li, C.G., Orans, J., Young, G.B., and Pielak, G.J. 2008. Residue-level interrogation of macromolecular crowding effects on protein stability. *J. Am. Chem. Soc.* **130**: 6826-6830.
- Chen, M., Margittai, M., Chen, J., and Langen, R. 2007. Investigation of alpha -synuclein fibril structure by site-directed spin labeling. *J. Biol. Chem.* **282**: 24970-24979.
- Chen, R., and Spiro, T.G. 2002. Monitoring the allosteric transition and co rebinding in hemoglobin with time-resolved ftir spectroscopy. *Journal of Physical Chemistry A* **106**: 3413-3419.

- Cheng, H., Sukal, S., Deng, H., Leyh, T.S., and Callender, R. 2001. Vibrational structure of gdp and gtp bound to ras: An isotope-edited ftir study. *Biochemistry* **40**: 4035-4043.
- Cheung, M.S., Garcia, A.E., and Onuchic, J.N. 2002. Protein folding mediated by solvation: Water expulsion and formation of the hydrophobic core occur after the structural collapse. *Proc. Natl. Acad. Sci. U. S. A.* **99**: 685-690.
- Cheung, M.S., Klimov, D., and Thirumalai, D. 2005. Molecular crowding enhances native state stability and refolding rates of globular proteins. *Proc. Natl. Acad. Sci. U. S. A.* **102**: 4753-4758.
- Chin, D.-H., Woody, R.W., Rohl, C.A., and Baldwin, R.L. 2002. Circular dichroism spectra of short, fixed-nucleus alanine helices. *Proc. Natl. Acad. Sci. USA* **99**: 15416-15421.
- Chiti, F., and Dobson, C.M. 2006. Protein misfolding, functional amyloid, and human disease. *Annu. Rev. Biochem.* **75**: 333-366.
- Chowdhury, P.K., Ashby, K.D., Datta, A., and Petrich, J.W. 2000. Effect of ph on the fluorescence and absorption spectra of hypericin in reverse micelles. *Photochem. Photobiol.* **72**: 612-618.
- Chowdhury, S., Zhang, W., Wu, C., Xiong, G., and Duan, Y. 2003. Breaking non-native hydrophobic clusters is the rate-limiting step in the folding of an alanine-based peptide. *Biopolymers* **68**: 63-75.
- Christ, S., and Schurtenberger, P. 1994. Optical contrast variation experiments in water-in-oil microemulsions - size distribution and structure of protein-free and protein-containing microemulsions. *J. Phys. Chem.* **98**: 12708-12714.
- Chu, B. (1992). Laser light scattering: Basic principles and practice. : Academic Press).
- Clarke, D.T., Doig, A.J., Stapley, B.J., and Jones, G.R. 1999a. The alpha -helix folds on the millisecond time scale. *Proc. Natl. Acad. Sci. U. S. A.* **96**: 7232-7237.
- Clarke, D.T., Doig, A.J., Stapley, B.J., and Jones, G.R. 1999b. The α -helix folds on the millisecond time scale. *Proc. Natl. Acad. Sci. U. S. A.* **96**: 7232-7237.
- Couch, V.A., Cheng, N., Nambiar, K., and Fink, W. 2006. Structural characterization of alpha -helices of implicitly solvated poly-alanine. *Journal of Physical Chemistry B* **110**: 3410-3419.

- Cringus, D., Bakulin, A., Lindner, J., Voehringer, P., Pshenichnikov, M.S., and Wiersma, D.A. 2007. Ultrafast energy transfer in water-aot reverse micelles. *Journal of Physical Chemistry B* **111**: 14193-14207.
- Cringus, D., Lindner, J., Milder, M.T.W., Pshenichnikov, M.S., Voehringer, P., and Wiersma, D.A. 2005. Femtosecond water dynamics in reverse-micellar nanodroplets. *Chem. Phys. Lett.* **408**: 162-168.
- Daggett, V., and Fersht, A.R. 2003. Is there a unifying mechanism for protein folding? *Trends Biochem. Sci.* **28**: 18-25.
- Dante, S., Hauss, T., and Dencher, N.A. 2002. Beta -amyloid 25 to 35 is intercalated in anionic and zwitterionic lipid membranes to different extents. *Biophys. J.* **83**: 2610-2616.
- De Simone, A., Dodson, G.G., Verma, C.S., Zagari, A., and Fraternali, F. 2005. Prion and water: Tight and dynamical hydration sites have a key role in structural stability. *Proc. Natl. Acad. Sci. U. S. A.* **102**: 7535-7540.
- De, T.K., and Maitra, A. 1995. Solution behavior of aerosol ot in non-polar solvents. *Adv. Colloid Interface Sci.* **59**: 95-193.
- Decatur, S.M. 2006. Elucidation of residue-level structure and dynamics of polypeptides via isotope-edited infrared spectroscopy. *Acc. Chem. Res.* **39**: 169-175.
- Decatur, S.M., and Antonic, J. 1999. Isotope-edited infrared spectroscopy of helical peptides. *J. Am. Chem. Soc.* **121**: 11914-11915.
- Dobson, C.M. 1999. Protein misfolding, evolution and disease. *Trends Biochem. Sci.* **24**: 329-332.
- Dobson, C.M. 2003. Protein folding and misfolding. *Nature (London, United Kingdom)* **426**: 884-890.
- Dokter, A.M., Woutersen, S., and Bakker, H.J. 2006. Inhomogeneous dynamics in confined water nanodroplets. *Proc. Natl. Acad. Sci. U. S. A.* **103**: 15355-15358.
- Dong, A., Huang, P., and Caughey, W.S. 1990. Protein secondary structures in water from second-derivative amide i infrared spectra. *Biochemistry* **29**: 3303-3308.
- Dong, F., and Zhou, H.-X. 2006. Electrostatic contribution to the binding stability of protein-protein complexes. *Proteins: Structure, Function, and Bioinformatics* **65**: 87-102.

- Doshi, U.R., and Munoz, V. 2004. The principles of alpha-helix formation: Explaining complex kinetics with nucleation-elongation theory. *Journal of Physical Chemistry B* **108**: 8497-8506.
- Du, D., Bunagan, M.R., and Gai, F. 2007. The effect of charge-charge interactions on the kinetics of alpha -helix formation. *Biophys. J.* **93**: 4076-4082.
- Du, D., and Gai, F. 2006. Understanding the folding mechanism of an alpha -helical hairpin. *Biochemistry* **45**: 13131-13139.
- Du, D.G., Tucker, M.J., and Gai, F. 2006. Understanding the mechanism of beta-hairpin folding via phi-value analysis. *Biochemistry* **45**: 2668-2678.
- Dyer, R.B., Gai, F., Woodruff, W.H., Gilmanshin, R., and Callender, R.H. 1998a. Infrared studies of fast events in protein folding. *Acc. Chem. Res.* **31**: 709-716.
- Dyer, R.B., Gai, F., Woodruff, W.H., Gilmanshin, R., and Callender, R.H. 1998b. Infrared studies of fast events in protein folding. *Acc. Chem. Res.* **31**: 709-716.
- Dzwolak, W., Ravindra, R., Nicolini, C., Jansen, R., and Winter, R. 2004. The diastereomeric assembly of polylysine is the low-volume pathway for preferential formation of beta -sheet aggregates. *J. Am. Chem. Soc.* **126**: 3762-3768.
- Eggers, D.K., and Valentine, J.S. 2001a. Crowding and hydration effects on protein conformation: A study with sol-gel encapsulated proteins. *J. Mol. Biol.* **314**: 911-922.
- Eggers, D.K., and Valentine, J.S. 2001b. Molecular confinement influences protein structure and enhances thermal protein stability. *Protein Sci.* **10**: 250-261.
- Eigen, M., and deMaeyer, L. 1963. Relaxation methods. *Tech. Org. Chem. (S. L. Friess, E. S. Lewis, and A. Weissberger, editors. Interscience)* **8**: 895-1054.
- Ellis, R.J. 2001a. Macromolecular crowding: An important but neglected aspect of the intracellular environment. *Curr. Opin. Struct. Biol.* **11**: 114-119.
- Ellis, R.J. 2001b. Macromolecular crowding: Obvious but underappreciated. *Trends Biochem. Sci.* **26**: 597-604.
- Esposito, L., Pedone, C., and Vitagliano, L. 2006. Molecular dynamics analyses of cross-beta -spine steric zipper models: Beta -sheet twisting and aggregation. *Proc. Natl. Acad. Sci. U. S. A.* **103**: 11533-11538.

- Fabian, H., Chapman, D., and Mantsch, H.H. 1996. New trends in isotope-edited infrared spectroscopy. *Infrared Spectroscopy of Biomolecules*: 341-352.
- Faeder, J., and Ladanyi, B.M. 2000. Molecular dynamics simulations of the interior of aqueous reverse micelles. *Journal of Physical Chemistry B* **104**: 1033-1046.
- Favrin, G., Irbaeck, A., and Mohanty, S. 2004. Oligomerization of amyloid abeta 16-22 peptides using hydrogen bonds and hydrophobicity forces. *Biophys. J.* **87**: 3657-3664.
- Fernandez, A., and Scheraga, H.A. 2003. Insufficiently dehydrated hydrogen bonds as determinants of protein interactions. *Proc. Natl. Acad. Sci. U. S. A.* **100**: 113-118.
- Fersht, A.R. 1995. Optimization of rates of protein folding: The nucleation-condensation mechanism and its implications. *Proc. Natl. Acad. Sci. U. S. A.* **92**: 10869-10873.
- Fersht, A.R. (1999). Structure and mechanism in protein science: A guide to enzyme catalysis and protein folding (New York, NY: W. H. Freeman and Company).
- Fletcher, P.D.I. 1987. Characterization of aerosol ot-stabilized oil-in-water microemulsions using a time-resolved fluorescence method. *Journal of the Chemical Society-Faraday Transactions I* **83**: 1493-1506.
- Frauenfelder, H., Fenimore, P.W., Chen, G., and McMahon, B.H. 2006. Protein folding is slaved to solvent motions. *Proc. Natl. Acad. Sci. U. S. A.* **103**: 15469-15472.
- Freda, M., Onori, G., Paciaroni, A., and Santucci, A. 2002. Hydration and dynamics of aerosol ot reverse micelles. *Journal of Molecular Liquids* **101**: 55-68.
- Friedel, M., Sheeler, D.J., and Shea, J.-E. 2003. Effects of confinement and crowding on the thermodynamics and kinetics of folding of a minimalist β -barrel protein. *J. Chem. Phys.* **118**: 8106-8113.
- Fulton, A.B. 1982. How crowded is the cytoplasm? *Cell* **30**: 345-347.
- Gallay, J., Vincent, M., Nicot, C., and Waks, M. 1987. Conformational aspects and rotational dynamics of synthetic adrenocorticotropin-(1-24) and glucagon in reverse micelles. *Biochemistry* **26**: 5738-5747.
- Garcia, A.E., Hummer, G., and Soumpasis, D.M. 1997. Hydration of an alpha -helical peptide: Comparison of theory and molecular dynamics simulation. *Proteins: Struct., Funct., Genet.* **27**: 471-480.

- Garcia, A.E., and Sanbonmatsu, K.Y. 2002. Alpha-helical stabilization by side chain shielding of backbone hydrogen bonds. *Proc. Natl. Acad. Sci. U. S. A.* **99**: 2782-2787.
- Getahun, Z., Huang, C.-Y., Wang, T., De Leon, B., DeGrado, W.F., and Gai, F. 2003. Using nitrile-derivatized amino acids as infrared probes of local environment. *J. Am. Chem. Soc.* **125**: 405-411.
- Ghosh, T., Garde, S., and Garcia, A.E. 2003. Role of backbone hydration and salt-bridge formation in stability of alpha-helix in solution. *Biophys. J.* **85**: 3187-3193.
- Gilmanshin, R., Williams, S., Callender, R.H., Woodruff, W.H., and Dyer, R.B. 1997. Fast events in protein folding: Relaxation dynamics and structure of the i form of apomyoglobin. *Biochemistry* **36**: 15006-15012.
- Gnanakaran, S., and Garcia, A.E. 2005. Helix-coil transition of alanine peptides in water: Force field dependence on the folded and unfolded structures. *Proteins: Structure, Function, and Bioinformatics* **59**: 773-782.
- Gnanakaran, S., Hochstrasser, R.M., and Garcia, A.E. 2004. Nature of structural inhomogeneities on folding a helix and their influence on spectral measurements. *Proc. Natl. Acad. Sci. U. S. A.* **101**: 9229-9234.
- Goins, A.B., Sanabria, H., and Waxham, M.N. 2008. Macromolecular crowding and size effects on probe microviscosity. *Biophys. J.* **95**: 5362-5373.
- Goodsell, D.S. (1994). *The machinery of life*: New York: Springer-Verlag).
- Gorman, P.M., Yip, C.M., Fraser, P.E., and Chakrabarty, A. 2003. Alternate aggregation pathways of the alzheimer beta -amyloid peptide: Abeta association kinetics at endosomal pH. *J. Mol. Biol.* **325**: 743-757.
- Grishina, I.B., and Woody, R.W. 1994. Contributions of tryptophan side-chains to the circular-dichroism of globular-proteins - exciton couplets and coupled oscillators. *Faraday Discuss.* **99**: 245-262.
- Gulari, E., Bedwell, B., and Alkhafaji, S. 1980. Quasi-elastic light-scattering investigation of micro-emulsions. *J. Colloid Interface Sci.* **77**: 202-212.
- Guo, H., and Karplus, M. 1994. Solvent influence on the stability of the peptide hydrogen bond: A supramolecular cooperative effect. *J. Phys. Chem.* **98**: 7104-7105.
- Guo, L., Chowdhury, P., Fang, J., and Gai, F. 2007. Heterogeneous and anomalous diffusion inside lipid tubules. *Journal of Physical Chemistry B* **111**: 14244-14249.

- Guo, W., Lampoudi, S., and Shea, J.-E. 2003. Posttransition state desolvation of the hydrophobic core of the src-sh3 protein domain. *Biophys. J.* **85**: 61-69.
- Haass, C., and Selkoe, D.J. 2007. Soluble protein oligomers in neurodegeneration: Lessons from the alzheimer's amyloid beta -peptide. *Nature Reviews Molecular Cell Biology* **8**: 101-112.
- Hagen, S.J., Qiu, L.L., and Pabit, S.A. 2005. Diffusional limits to the speed of protein folding: Fact or friction? *Journal of Physics-Condensed Matter* **17**: S1503-S1514.
- Hamm, P., Lim, M., DeGrado, W.F., and Hochstrasser, R.M. 1999. The two-dimensional ir nonlinear spectroscopy of a cyclic penta-peptide in relation to its three-dimensional structure. *Proc. Natl. Acad. Sci. USA* **96**: 2036-2041.
- Hamm, P., Lim, M., and Hochstrasser, R.M. 1998. Structure of the amide i band of peptides measured by femtosecond nonlinear-infrared spectroscopy. *J. Phys. Chem. B* **102**: 6123-6138.
- Harano, Y., and Kinoshita, M. 2004. Large gain in translational entropy of water is a major driving force in protein folding. *Chem. Phys. Lett.* **399**: 342-348.
- Haris, P.I., and Chapman, D. 1994. Analysis of polypeptide and protein structures using fourier transform infrared spectroscopy. *Methods in Molecular Biology (Totowa, NJ, United States)* **22**: 183-202.
- Haris, P.I., and Chapman, D. 1995. The conformational analysis of peptides using fourier transform ir spectroscopy. *Biopolymers* **37**: 251-263.
- Harper, J.D., and Lansbury, P.T., Jr. 1997. Models of amyloid seeding in alzheimer's disease and scrapie: Mechanistic truths and physiological consequences of the time-dependent solubility of amyloid proteins. *Annu. Rev. Biochem.* **66**: 385-407.
- Haustein, E., and Schwille, P. 2007. Fluorescence correlation spectroscopy: Novel variations of an established technique. *Annu. Rev. Biophys. Biomol. Struct.* **36**: 151-169.
- Havel, H.A. (1996). Spectroscopic methods for determining protein structure in solution (New York, NY: VCH Publishers, Inc.).
- Hayer-Hartl, M., and Minton, A.P. 2006. A simple semiempirical model for the effect of molecular confinement upon the rate of protein folding. *Biochemistry* **45**: 13356-13360.

- Heimburg, T., Schuenemann, J., Weber, K., and Geisler, N. 1996. Specific recognition of coiled coils by infrared spectroscopy: Analysis of the three structural domains of type iii intermediate filament proteins. *Biochemistry* **35**: 1375-1382.
- Higashijima, T., Burnier, J., and Ross, E.M. 1990. Regulation of gi and go by mastoparan, related amphiphilic peptides, and hydrophobic amines. Mechanism and structural determinants of activity. *J. Biol. Chem.* **265**: 14176-14186.
- Higashijima, T., Wakamatsu, K., Takemitsu, M., Fujino, M., Nakajima, T., and Miyazawa, T. 1983. Conformational change of mastoparan from wasp venom on binding with phospholipid membrane. *FEBS Lett.* **152**: 227-230.
- Hirai, Y., Kuwada, M., Yasuhara, T., Yoshida, H., and Nakajima, T. 1979. A new mast cell degranulating peptide homologous to mastoparan in the venom of japanese hornet (*vespa xanthoptera*). *Chem. Pharm. Bull.* **27**: 1945-1946.
- Homouz, D., Stagg, L., Wittung-Stafshede, P., and Cheung, M.S. 2009. Macromolecular crowding modulates folding mechanism of alpha/beta protein apoflavodoxin. *Biophys. J.* **96**: 671-680.
- Hong, D.-P., Hoshino, M., Kuboi, R., and Goto, Y. 1999. Clustering of fluorine-substituted alcohols as a factor responsible for their marked effects on proteins and peptides. *J. Am. Chem. Soc.* **121**: 8427-8433.
- Hori, Y., Demura, M., Iwadate, M., Ulrich, A.S., Niidome, T., Aoyagi, H., and Asakura, T. 2001. Interaction of mastoparan with membranes studied by 1h-nmr spectroscopy in detergent micelles and by solid-state 2h-nmr and 15n-nmr spectroscopy in oriented lipid bilayers. *Eur. J. Biochem.* **268**: 302-309.
- Hua, L., Huang, X.H., Liu, P., Zhou, R.H., and Berne, B.J. 2007. Nanoscale dewetting transition in protein complex folding. *Journal of Physical Chemistry B* **111**: 9069-9077.
- Huang, C.-Y., Getahun, Z., Wang, T., DeGrado, W.F., and Gai, F. 2001a. Time-resolved infrared study of the helix-coil transition using ¹³c-labeled helical peptides. *J. Am. Chem. Soc.* **123**: 12111-12112.
- Huang, C.-Y., Getahun, Z., Wang, T., DeGrado, W.F., and Gai, F. 2001b. Time-resolved infrared study of the helix-coil transition using ¹³c-labeled helical peptides. *J. Am. Chem. Soc.* **123**: 12111-12112.
- Huang, C.-y., Getahun, Z., Zhu, Y., Klemke, J.W., DeGrado, W.F., and Gai, F. 2002a. Helix formation via conformation diffusion search. *Proc. Natl. Acad. Sci. USA* **99**: 2788-2793.

- Huang, C.-Y., Getahun, Z., Zhu, Y., Klemke, J.W., DeGrado, W.F., and Gai, F. 2002b. Helix formation via conformation diffusion search. *Proc. Natl. Acad. Sci. U. S. A.* **99**: 2788-2793.
- Huang, C.-Y., Klemke, J.W., Getahun, Z., DeGrado, W.F., and Gai, F. 2001c. Temperature-dependent helix-coil transition of an alanine based peptide. *J. Am. Chem. Soc.* **123**: 9235-9238.
- Huang, C.-Y., Wang, T., and Gai, F. 2003a. Temperature dependence of the cn stretching vibration of a nitrile-derivatized phenylalanine in water. *Chem. Phys. Lett.* **371**: 731-738.
- Huang, X., Margulis, C.J., and Berne, B.J. 2003b. Dewetting-induced collapse of hydrophobic particles. *Proc. Natl. Acad. Sci. U. S. A.* **100**: 11953-11958.
- Hudgins, R.R., and Jarrold, M.F. 1999. Helix formation in unsolvated alanine-based peptides: Helical monomers and helical dimers. *J. Am. Chem. Soc.* **121**: 3494-3501.
- Hummer, G., Garcia, A.E., and Garde, S. 2001. Helix nucleation kinetics from molecular simulations in explicit solvent. *Proteins: Struct., Funct., Genet.* **42**: 77-84.
- Hummer, G., and Garde, S. 1998. Cavity expulsion and weak dewetting of hydrophobic solutes in water. *Phys. Rev. Lett.* **80**: 4193-4196.
- Im, W., and Brooks, C.L., III 2005. Interfacial folding and membrane insertion of designed peptides studied by molecular dynamics simulations. *Proc. Natl. Acad. Sci. U. S. A.* **102**: 6771-6776.
- Jacob, M., and Schmid, F.X. 1999. Protein folding as a diffusional process. *Biochemistry* **38**: 13773-13779.
- Jain, T.K., Varshney, M., and Maitra, A. 1989. Structural studies of aerosol of reverse micellar aggregates by ft-ir spectroscopy. *J. Phys. Chem.* **93**: 7409-7416.
- Jarrett, J.T., Berger, E.P., and Lansbury, P.T., Jr. 1993. The carboxy terminus of the beta amyloid protein is critical for the seeding of amyloid formation: Implications for the pathogenesis of alzheimer's disease. *Biochemistry* **32**: 4693-4697.
- Jarrold, M.F. 2000. Peptides and proteins in the vapor phase. *Annu. Rev. Phys. Chem.* **51**: 179-207.

- Jas, G.S., Eaton, W.A., and Hofrichter, J. 2001. Effect of viscosity on the kinetics of alpha -helix and beta -hairpin formation. *Journal of Physical Chemistry B* **105**: 261-272.
- Kauzmann, W. 1959. Some factors in the interpretation of protein denaturation. *Advances in Protein Chem.* (C. B. Anfinsen, M. L. Anson, Kenneth Bailey, and John T. Edsall, editors, Academic Press Inc.) **14**: 1-63.
- Kelly, J.W. 1998. The alternative conformations of amyloidogenic proteins and their multi-step assembly pathways. *Curr. Opin. Struct. Biol.* **8**: 101-106.
- Kentsis, A., and Sosnick, T.R. 1998. Trifluoroethanol promotes helix formation by destabilizing backbone exposure: Desolvation rather than native hydrogen bonding defines the kinetic pathway of dimeric coiled coil folding. *Biochemistry* **37**: 14613-14622.
- Kim, P.S., and Baldwin, R.L. 1982. Specific intermediates in the folding reactions of small proteins and the mechanism of protein folding. *Annu. Rev. Biochem.* **51**: 459-489.
- Kim, Y.S., Liu, L., Axelsen, P.H., and Hochstrasser, R.M. 2008. Two-dimensional infrared spectra of isotopically diluted amyloid fibrils from abeta 40. *Proc. Natl. Acad. Sci. U. S. A.* **105**: 7720-7725.
- Klimov, D.K., Newfield, D., and Thirumalai, D. 2002. Simulations of beta-hairpin folding confined to spherical pores using distributed computing. *Proc. Natl. Acad. Sci. U. S. A.* **99**: 8019-8024.
- Klimov, D.K., and Thirumalai, D. 2003. Dissecting the assembly of abeta 16-22 amyloid peptides into antiparallel beta sheets. *Structure (Cambridge, MA, United States)* **11**: 295-307.
- Kotlarchyk, M., Chen, S.H., Huang, J.S., and Kim, M.W. 1984. Structure of 3-component microemulsions in the critical region determined by small-angle neutron-scattering. *Phys. Rev. A* **29**: 2054-2069.
- Kozer, N., Kuttner, Y.Y., Haran, G., and Schreiber, G. 2007. Protein-protein association in polymer solutions: From dilute to semidilute to concentrated. *Biophys. J.* **92**: 2139-2149.
- Kozer, N., and Schreiber, G. 2004. Effect of crowding on protein-protein association rates: Fundamental differences between low and high mass crowding agents. *J. Mol. Biol.* **336**: 763-774.

- Krimm, S., and Bandekar, J. 1986. Vibrational spectroscopy and conformation of peptides, polypeptides, and proteins. *Adv. Protein Chem.* **38**: 181-364.
- Krone, M.G., Hua, L., Soto, P., Zhou, R.H., Berne, B.J., and Shea, J.E. 2008. Role of water in mediating the assembly of alzheimer amyloid-beta a beta 16-22 protofilaments. *J. Am. Chem. Soc.* **130**: 11066-11072.
- Kubelka, J., Hofrichter, J., and Eaton, W.A. 2004. The protein folding 'speed limit'. *Curr. Opin. Struct. Biol.* **14**: 76-88.
- Kuhlman, B., Yang, H.Y., Boice, J.A., Fairman, R., and Raleigh, D.P. 1997. An exceptionally stable helix from the ribosomal protein 19: Implications for protein folding and stability. *J. Mol. Biol.* **270**: 640-647.
- Kumar, S., and Nussinov, R. 1999. Salt bridge stability in monomeric proteins. *J. Mol. Biol.* **293**: 1241-1255.
- Lashuel, H.A., Hartley, D., Petre, B.M., Walz, T., and Lansbury, P.T. 2002. Neurodegenerative disease: Amyloid pores from pathogenic mutations. *Nature (London, United Kingdom)* **418**: 291.
- Lavalette, D., Tetreau, C., Tourbez, M., and Blouquit, Y. 1999. Microscopic viscosity and rotational diffusion of proteins in a macromolecular environment. *Biophys. J.* **76**: 2744-2751.
- Lednev, I.K., Karnoup, A.S., Sparrow, M.C., and Asher, S.A. 1999a. Alpha -helix peptide folding and unfolding activation barriers: A nanosecond uv resonance raman study. *J. Am. Chem. Soc.* **121**: 8074-8086.
- Lednev, I.K., Karnoup, A.S., Sparrow, M.C., and Asher, S.A. 1999b. Nanosecond uv resonance raman examination of initial steps in α -helix secondary structure evolution. *J. Am. Chem. Soc.* **121**: 4076-4077.
- Leodidis, E.B., and Hatton, T.A. 1990. Amino acids in aot reversed micelles. 2. The hydrophobic effect and hydrogen bonding as driving forces for interfacial solubilization. *J. Phys. Chem.* **94**: 6411-6420.
- Leser, M.E., and Luisi, P.L. 1990. Application of reverse micelles for the extraction of amino-acids and proteins. *Chimia* **44**: 270-282.
- Lesser, G.J., and Rose, G.D. 1990. Hydrophobicity of amino acid subgroups in proteins. *Proteins: Struct., Funct., Genet.* **8**: 6-13.
- Levinger, N.E. 2002. Chemistry. Water in confinement. *Science* **298**: 1722-1723.

- Levinger, N.E., and Swafford, L.A. 2009. Ultrafast dynamics in reverse micelles. *Annu. Rev. Phys. Chem.* **60**: 385-406.
- Levy, Y., Jortner, J., and Becker, O.M. 2001. Solvent effects on the energy landscapes and folding kinetics of polyalanine. *Proc. Natl. Acad. Sci. U. S. A.* **98**: 2188-2193.
- Levy, Y., and Onuchic, J.N. 2006. Water mediation in protein folding and molecular recognition. *Annu. Rev. Biophys. Biomol. Struct.* **35**: 389-415.
- Lipfert, J., Franklin, J., Wu, F., and Doniach, S. 2005. Protein misfolding and amyloid formation for the peptide gnnqqny from yeast prion protein sup35: Simulation by reaction path annealing. *J. Mol. Biol.* **349**: 648-658.
- Liu, P., Huang, X., Zhou, R., and Berne, B.J. 2005. Observation of a dewetting transition in the collapse of the melittin tetramer. *Nature (London, United Kingdom)* **437**: 159-162.
- Liu, Z., and Chan, H.S. 2005. Desolvation is a likely origin of robust enthalpic barriers to protein folding. *J. Mol. Biol.* **349**: 872-889.
- Luby-Phelps, K. 2000. Cytoarchitecture and physical properties of cytoplasm: Volume, viscosity, diffusion, intracellular surface area. *Int. Rev. Cytol.* **192**: 189-221.
- Lubyphelps, K., Castle, P.E., Taylor, D.L., and Lanni, F. 1987. Hindered diffusion of inert tracer particles in the cytoplasm of mouse 3t3 cells. *Proc. Natl. Acad. Sci. U. S. A.* **84**: 4910-4913.
- Lucent, D., Vishal, V., and Pande, V.S. 2007. Protein folding under confinement: A role for solvent. *Proc. Natl. Acad. Sci. U. S. A.* **104**: 10430-10434.
- Ludlam, C.F.C., Arkin, I.T., Liu, X.-M., Rothman, M.S., Rath, p., Aimoto, S., Smith, S.O., Engelman, D.M., and Rothschild, K.J. 1996. Fourier transform infrared spectroscopy and site-directed isotope labeling as a probe of local secondary structure in the transmembrane domain of phospholamban. *Biophys. J.* **70**: 1728-1736.
- Luisi, P.L. 1985. Enzymes hosted in reverse micelles in hydrocarbon solution. *Angewandte Chemie-International Edition in English* **24**: 439-450.
- Luisi, P.L., Giomini, M., Pileni, M.P., and Robinson, B.H. 1988. Reverse micelles as hosts for proteins and small molecules. *Biochimica et Biophysica Acta, Reviews on Biomembranes* **947**: 209-246.

- Lum, K., Chandler, D., and Weeks, J.D. 1999. Hydrophobicity at small and large length scales. *Journal of Physical Chemistry B* **103**: 4570-4577.
- Luo, P., and Baldwin, R.L. 1997. Mechanism of helix induction by trifluoroethanol: A framework for extrapolating the helix-forming properties of peptides from trifluoroethanol/water mixtures back to water. *Biochemistry* **36**: 8413-8421.
- Ma, B., and Nussinov, R. 2002. Stabilities and conformations of alzheimer's beta - amyloid peptide oligomers (abeta 16-22, abeta 16-35, and abeta 10-35): Sequence effects. *Proc. Natl. Acad. Sci. U. S. A.* **99**: 14126-14131.
- MacCallum, J.L., Moghaddam, M.S., Chan, H.S., and Tieleman, D.P. 2007. Hydrophobic association of alpha -helices, steric dewetting, and enthalpic barriers to protein folding. *Proc. Natl. Acad. Sci. U. S. A.* **104**: 6206-6210.
- Maeda, A. 1995. Application of ftir spectroscopy to the structural study on the function of bacteriorhodopsin. *Isr. J. Chem.* **35**: 387-400.
- Maitra, A. 1984. Determination of size parameters of water-aerosol ot-oil reverse micelles from their nuclear magnetic resonance data. *J. Phys. Chem.* **88**: 5122-5125.
- Manas, E.S., Getahun, Z., Wright, W.W., DeGrado, W.F., and Vanderkooi, J.M. 2000. Infrared spectra of amide groups in alpha -helical proteins: Evidence for hydrogen bonding between helices and water. *J. Am. Chem. Soc.* **122**: 9883-9890.
- Marek, P., Abedini, A., Song, B., Kanungo, M., Johnson, M.E., Gupta, R., Zaman, W., Wong, S.S., and Raleigh, D.P. 2007. Aromatic interactions are not required for amyloid fibril formation by islet amyloid polypeptide but do influence the rate of fibril formation and fibril morphology. *Biochemistry* **46**: 3255-3261.
- Marqusee, S., and Baldwin, R.L. 1987. Helix stabilization by glu-...Lys+ salt bridges in short peptides of de novo design. *Proc. Natl. Acad. Sci. U. S. A.* **84**: 8898-8902.
- Marqusee, S., Robbins, V.H., and Baldwin, R.L. 1989. Unusually stable helix formation in short alanine-based peptides. *Proc. Natl. Acad. Sci. U. S. A.* **86**: 5286-5290.
- Martinez, G., and Millhauser, G. 1995. Ftir spectroscopy of alanine-based peptides: Assignment of the amide i' modes for random coil and helix. *J. Struct. Biol.* **114**: 23-27.
- Massi, F., and Straub, J.E. 2003. Structural and dynamical analysis of the hydration of the alzheimer's beta -amyloid peptide. *J. Comput. Chem.* **24**: 143-153.

- Masuda, A., Ushida, K., Koshino, H., Yamashita, K., and Kluge, T. 2001. Novel distance dependence of diffusion constants in hyaluronan aqueous solution resulting from its characteristic nano-microstructure. *J. Am. Chem. Soc.* **123**: 11468-11471.
- Masuda, A., Ushida, K., Nishimura, G., Kinjo, M., Tamura, M., Koshino, H., Yamashita, K., and Kluge, T. 2004. Experimental evidence of distance-dependent diffusion coefficients of a globular protein observed in polymer aqueous solution forming a network structure on nanometer scale. *J. Chem. Phys.* **121**: 10787-10793.
- Matsuzaki, K., Yoneyama, S., Murase, O., and Miyajima, K. 1996. Transbilayer transport of ions and lipids coupled with mastoparan x translocation. *Biochemistry* **35**: 8450-8456.
- Mattos, C., and Clark, A.C. 2008. Minimizing frustration by folding in an aqueous environment. *Arch. Biochem. Biophys.* **469**: 118-131.
- Matzke, S.F., Creagh, A.L., Haynes, C.A., Prausnitz, J.M., and Blanch, H.W. 1992. Mechanisms of protein solubilization in reverse micelles. *Biotechnol. Bioeng.* **40**: 91-102.
- Mayor, U., Johnson, C.M., Daggett, V., and Fersht, A.R. 2000. Protein folding and unfolding in microseconds to nanoseconds by experiment and simulation. *Proc. Natl. Acad. Sci. U. S. A.* **97**: 13518-13522.
- McPhie, P., Ni, Y.-s., and Minton, A.P. 2006. Macromolecular crowding stabilizes the molten globule form of apomyoglobin with respect to both cold and heat unfolding. *J. Mol. Biol.* **361**: 7-10.
- Medalia, O., Weber, I., Frangakis, A.S., Nicastro, D., Gerisch, G., and Baumeister, W. 2002. Macromolecular architecture in eukaryotic cells visualized by cryoelectron tomography. *Science (Washington, DC, United States)* **298**: 1209-1213.
- Minton, A.P. 1983. The effect of volume occupancy upon the thermodynamic activity of proteins: Some biochemical consequences. *Mol. Cell. Biochem.* **55**: 119-140.
- Minton, A.P. 2001. The influence of macromolecular crowding and macromolecular confinement on biochemical reactions in physiological media. *J. Biol. Chem.* **276**: 10577-10580.
- Minton, A.P. 2005. Models for excluded volume interaction between an unfolded protein and rigid macromolecular cosolutes: Macromolecular crowding and protein stability revisited. *Biophys. J.* **88**: 971-985.

- Minton, A.P. 2006. How can biochemical reactions within cells differ from those in test tubes? *J. Cell Sci.* **119**: 2863-2869.
- Mitsutake, A., and Okamoto, Y. 2000. Helix-coil transitions of amino-acid homo-oligomers in aqueous solution studied by multicanonical simulations. *J. Chem. Phys.* **112**: 10638-10647.
- Mittal, J., and Best, R.B. 2008. Thermodynamics and kinetics of protein folding under confinement. *Proc. Natl. Acad. Sci. U. S. A.* **105**: 20233-20238.
- Morozov, A.N., and Lin, S.H. 2006. Modeling of folding and unfolding mechanisms in alanine-based alpha -helical polypeptides. *Journal of Physical Chemistry B* **110**: 20555-20561.
- Mukherjee, P., Kass, I., Arkin, I., and Zanni, M.T. 2006a. Picosecond dynamics of a membrane protein revealed by 2d ir. *Proc. Natl. Acad. Sci. U. S. A.* **103**: 3528-3533.
- Mukherjee, S., Chowdhury, P., Bunagan, M.R., and Gai, F. 2008. Folding kinetics of a naturally occurring helical peptide: Implication of the folding speed limit of helical proteins. *Journal of Physical Chemistry B* **112**: 9146-9150.
- Mukherjee, S., Chowdhury, P., DeGrado, W.F., and Gai, F. 2007a. Site-specific hydration status of an amphipathic peptide in aot reverse micelles. *Langmuir* **23**: 11174-11179.
- Mukherjee, S., Chowdhury, P., and Gai, F. 2006b. Tuning the cooperativity of the helix-coil transition by aqueous reverse micelles. *Journal of Physical Chemistry B* **110**: 11615-11619.
- Mukherjee, S., Chowdhury, P., and Gai, F. 2007b. Infrared study of the effect of hydration on the amide i band and aggregation properties of helical peptides. *Journal of Physical Chemistry B* **111**: 4596-4602.
- Mukherjee, S., Chowdhury, P., and Gai, F. 2009. Effect of dehydration on the aggregation kinetics of two amyloid peptides. *Journal of Physical Chemistry B* **113**: 531-535.
- Murphy, R.M. 2007. Kinetics of amyloid formation and membrane interaction with amyloidogenic proteins. *Biochimica et Biophysica Acta, Biomembranes* **1768**: 1923-1934.

- Nelson, R., Sawaya, M.R., Balbirnie, M., Madsen, A.O., Riekel, C., Grothe, R., and Eisenberg, D. 2005. Structure of the cross-beta spine of amyloid-like fibrils. *Nature (London, United Kingdom)* **435**: 773-778.
- Neuweiler, H., Loellmann, M., Doose, S., and Sauer, M. 2007. Dynamics of unfolded polypeptide chains in crowded environment studied by fluorescence correlation spectroscopy. *J. Mol. Biol.* **365**: 856-869.
- Nguyen, H.D., Marchut, A.J., and Hall, C.K. 2004. Solvent effects on the conformational transition of a model polyalanine peptide. *Protein Sci.* **13**: 2909-2924.
- Nicot, C., Vacher, M., Vincent, M., Gallay, J., and Waks, M. 1985. Membrane proteins as reverse micelles: Myelin basic protein in a membrane-mimetic environment. *Biochemistry* **24**: 7024-7032.
- Nielsen, L., Khurana, R., Coats, A., Frokjaer, S., Brange, J., Vyas, S., Uversky, V.N., and Fink, A.L. 2001. Effect of environmental factors on the kinetics of insulin fibril formation: Elucidation of the molecular mechanism. *Biochemistry* **40**: 6036-6046.
- Nucci, N.V., and Vanderkooi, J.M. 2005. Temperature dependence of hydrogen bonding and freezing behavior of water in reverse micelles. *Journal of Physical Chemistry B* **109**: 18301-18309.
- Nymeyer, H., Woolf, T.B., and Garcia, A.E. 2005. Folding is not required for bilayer insertion: Replica exchange simulations of an alpha -helical peptide with an explicit lipid bilayer. *Proteins: Structure, Function, and Bioinformatics* **59**: 783-790.
- Ogston, A.G., Preston, B.N., Wells, J.D., Ogston, A.G., Preston, B.N., Snowden, J.M., and Wells, J.D. 1973. Transport of compact particles through solutions of chain-polymers. *Proceedings of the Royal Society of London Series a-Mathematical Physical and Engineering Sciences* **333**: 297-316.
- Onori, G., and Santucci, A. 1993. Ir investigations of water structure in aerosol ot reverse micellar aggregates. *J. Phys. Chem.* **97**: 5430-5434.
- Parrish, J.R., Jr., and Blout, E.R. 1972. Conformation of poly-l-alanine in hexafluoroisopropanol. *Biopolymers* **11**: 1001-1020.
- Peng, Y., Hansmann, U.H.E., and Alves, N.A. 2003. Solution effects and the order of the helix-coil transition in polyalanine. *J. Chem. Phys.* **118**: 2374-2380.
- Perham, M., Stagg, L., and Wittung-Stafshede, P. 2007. Macromolecular crowding increases structural content of folded proteins. *FEBS Lett.* **581**: 5065-5069.

- Peterson, R.W., Anbalagan, K., Tommos, C., and Wand, A.J. 2004. Forced folding and structural analysis of metastable proteins. *J. Am. Chem. Soc.* **126**: 9498-9499.
- Petty, S.A., and Decatur, S.M. 2005. Experimental evidence for the reorganization of beta-strands within aggregates of the abeta (16-22) peptide. *J. Am. Chem. Soc.* **127**: 13488-13489.
- Petty, S.A., and Volk, M. 2004. Fast folding dynamics of an alpha-helical peptide with bulky side chains. *Physical Chemistry Chemical Physics* **6**: 1022-1030.
- Phillies, G.D.J., and Quinlan, C.A. 1992. Glass temperature effects on probe diffusion in dextran solutions. *Macromolecules* **25**: 3110-3116.
- Pileni, M.P. 1993. Reverse micelles as microreactors. *J. Phys. Chem.* **97**: 6961-6973.
- Piletic, I.R., Moilanen, D.E., Spry, D.B., Levinger, N.E., and Fayer, M.D. 2006. Testing the core/shell model of nanoconfined water in reverse micelles using linear and nonlinear ir spectroscopy. *Journal of Physical Chemistry A* **110**: 4985-4999.
- Ping, G., Yuan, J.M., Sun, Z.F., and Wei, Y. 2004. Studies of effects of macromolecular crowding and confinement on protein folding and protein stability. *J. Mol. Recognit.* **17**: 433-440.
- Prestrelski, S., Tedeschi, N., Arakawa, T., and Carpenter, J.F. 1993. Dehydration-induced conformational transitions in proteins and their inhibition by stabilizers. *Biophys. J.* **65**: 661-671.
- Qu, Y., and Bolen, D.W. 2002. Efficacy of macromolecular crowding in forcing proteins to fold. *Biophys. Chem.* **101-102**: 155-165.
- Raghuraman, H., and Chattopadhyay, A. 2003. Organization and dynamics of melittin in environments of graded hydration: A fluorescence approach. *Langmuir* **19**: 10332-10341.
- Rajan, R., and Balaram, P. 1996. A model for the interaction of trifluoroethanol with peptides and proteins. *Int. J. Pept. Protein Res.* **48**: 328-336.
- Rathore, N., Knotts, T.A.I.V., and de Pablo, J.J. 2006. Confinement effects on the thermodynamics of protein folding: Monte carlo simulations. *Biophys. J.* **90**: 1767-1773.
- Reisdorf, W.C., Jr., and Krimm, S. 1996. Infrared amide i' band of the coiled coil. *Biochemistry* **35**: 1383-1386.

- Rief, M., Fernandez, J.M., and Gaub, H.E. 1998. Elastically coupled two-level systems as a model for biopolymer extensibility. *Phys. Rev. Lett.* **81**: 4764-4767.
- Riter, R.E., Undiks, E.P., and Levinger, N.E. 1998a. Impact of counterion on water motion in aerosol ot reverse micelles. *J. Am. Chem. Soc.* **120**: 6062-6067.
- Riter, R.E., Willard, D.M., and Levinger, N.E. 1998b. Water immobilization at surfactant interfaces in reverse micelles. *Journal of Physical Chemistry B* **102**: 2705-2714.
- Rivera, E., Straub, J., and Thirumalai, D. 2009. Sequence and crowding effects in the aggregation of a 10-residue fragment derived from islet amyloid polypeptide. *Biophys. J.* **96**: 4552-4560.
- Roccatano, D., Colombo, G., Fioroni, M., and Mark, A.E. 2002. Mechanism by which 2,2,2-trifluoroethanol/water mixtures stabilize secondary-structure formation in peptides: A molecular dynamics study. *Proc. Natl. Acad. Sci. U. S. A.* **99**: 12179-12184.
- Roccatano, D., Fioroni, M., Zacharias, M., and Colombo, G. 2005. Effect of hexafluoroisopropanol alcohol on the structure of melittin: A molecular dynamics simulation study. *Protein Sci.* **14**: 2582-2589.
- Rothschild, K.J. 1992. Ftir difference spectroscopy of bacteriorhodopsin: Toward a molecular model. *J. Bioenerg. Biomembr.* **24**: 147-167.
- Ruhlmann, C., Thieme, M., and Helmstedt, M. 2001. Interaction between dextran and human low density lipoproteins (ldl) observed using laser light scattering. *Chem. Phys. Lipids* **110**: 173-181.
- Sasahara, K., McPhie, P., and Minton, A.P. 2003. Effect of dextran on protein stability and conformation attributed to macromolecular crowding. *J. Mol. Biol.* **326**: 1227-1237.
- Schurr, J.M. 1977. Dynamic light-scattering of biopolymers and biocolloids. *CRC Crit. Rev. Biochem.* **4**: 371-431.
- Scott, K.A., Alonso, D.O.V., Pan, Y., and Daggett, V. 2006. Importance of context in protein folding: Secondary structural propensities versus tertiary contact-assisted secondary structure formation. *Biochemistry* **45**: 4153-4163.
- Senapati, S., and Chandra, A. 2001. Dielectric constant of water confined in a nanocavity. *Journal of Physical Chemistry B* **105**: 5106-5109.

- Sessions, R.B., Thomas, G.L., and Parker, M.J. 2004. Water as a conformational editor in protein folding. *J. Mol. Biol.* **343**: 1125-1133.
- Shashilov, V.A., and Lednev, I.K. 2008. 2d correlation deep uv resonance raman spectroscopy of early events of lysozyme fibrillation: Kinetic mechanism and potential interpretation pitfalls. *J. Am. Chem. Soc.* **130**: 309-317.
- Shastry, M.C.R., and Eftink, M.R. 1996. Reversible thermal unfolding of ribonuclease t-1 in reverse micelles. *Biochemistry* **35**: 4094-4101.
- Shea, J.-E., Onuchic, J.N., and Brooks, C.L., III 2002. Probing the folding free energy landscape of the src-sh3 protein domain. *Proc. Natl. Acad. Sci. U. S. A.* **99**: 16064-16068.
- Sheinerman, F.B., and Brooks, C.L., III 1998. Calculations on folding of segment b1 of streptococcal protein g. *J. Mol. Biol.* **278**: 439-456.
- Shen, C.-L., and Murphy, R.M. 1995. Solvent effects on self-assembly of beta -amyloid peptide. *Biophys. J.* **69**: 640-651.
- Sigle, W. 2005. Analytical transmission electron microscopy. *Annual Review of Materials Research* **35**: 239-314.
- Sorin, E.J., and Pande, V.S. 2005. Exploring the helix-coil transition via all-atom equilibrium ensemble simulations. *Biophys. J.* **88**: 2472-2493.
- Soto, C. 2001. Protein misfolding and disease; protein refolding and therapy. *FEBS Lett.* **498**: 204-207.
- Sreerama, N., and Woody, R.W. (2004). Computation and analysis of protein circular dichroism spectra, In *Methods in enzymology, numerical computer methods*, part d (Elsevier), pp. 318-351.
- Srinivasan, R., Marchant, R.E., and Zagorski, M.G. 2004. Abri peptide associated with familial british dementia forms annular and ring-like protofibrillar structures. *Amyloid* **11**: 10-13.
- Stagg, L., Zhang, S.-Q., Cheung, M.S., and Wittung-Stafshede, P. 2007. Molecular crowding enhances native structure and stability of alpha/beta protein flavodoxin. *Proc. Natl. Acad. Sci. U. S. A.* **104**: 18976-18981.

- Starovasnik, M.A., Braisted, A.C., and Wells, J.A. 1997. Structural mimicry of a native protein by a minimized binding domain. *Proc. Natl. Acad. Sci. U. S. A.* **94**: 10080-10085.
- Starzyk, A., Barber-Armstrong, W., Sridharan, M., and Decatur, S.M. 2005. Spectroscopic evidence for backbone desolvation of helical peptides by 2,2,2-trifluoroethanol: An isotope-edited ftir study. *Biochemistry* **44**: 369-376.
- Strasfeld, D.B., Ling, Y.L., Shim, S.H., and Zanni, M.T. 2008. Tracking fiber formation in human islet amyloid polypeptide with automated 2d-ir spectroscopy. *J. Am. Chem. Soc.* **130**: 6698-6699.
- Strodel, B., Whittleston, C.S., and Wales, D.J. 2007. Thermodynamics and kinetics of aggregation for the gnnqqny peptide. *J. Am. Chem. Soc.* **129**: 16005-16014.
- Sul, S., Karaiskaj, D., Jiang, Y., and Ge, N.-H. 2006. Conformations of n-acetyl-l-prolinamide by two-dimensional infrared spectroscopy. *Journal of Physical Chemistry B* **110**: 19891-19905.
- Surewicz, W.K., Mantsch, H.H., and Chapman, D. 1993. Determination of protein secondary structure by fourier transform infrared spectroscopy: A critical assessment. *Biochemistry* **32**: 389-394.
- Susi, H., and Byler, D.M. 1987. Fourier transform infrared study of proteins with parallel beta-chains. *Arch. Biochem. Biophys.* **258**: 465-469.
- Suydam, I.T., and Boxer, S.G. 2003. Vibrational stark effects calibrate the sensitivity of vibrational probes for electric fields in proteins. *Biochemistry* **42**: 12050-12055.
- Takagi, F., Koga, N., and Takada, S. 2003. How protein thermodynamics and folding mechanisms are altered by the chaperonin cage: Molecular simulations. *Proc. Natl. Acad. Sci. U. S. A.* **100**: 11367-11372.
- Takano, M., Nakamura, H.K., Nagayama, K., and Suyama, A. 2003. Investigating a link between all-atom model simulation and the ising-based theory on the helix-coil transition. II. Nonstationary properties. *J. Chem. Phys.* **118**: 10312-10322.
- Tang, J., and Gai, F. 2006. A millisecond infrared stopped-flow apparatus. *Appl. Spectrosc.* **60**: 1477-1481.
- Tarus, B., Straub, J.E., and Thirumalai, D. 2005. Probing the initial stage of aggregation of the abeta 10-35-protein: Assessing the propensity for peptide dimerization. *J. Mol. Biol.* **345**: 1141-1156.

- Tarus, B., Straub, J.E., and Thirumalai, D. 2006. Dynamics of asp23-lys28 salt-bridge formation in abeta 10-35 monomers. *J. Am. Chem. Soc.* **128**: 16159-16168.
- Teplow, D.B., Lazo, N.D., Bitan, G., Bernstein, S., Wyttenbach, T., Bowers, M.T., Baumketner, A., Shea, J.-E., Urbanc, B., Cruz, L., *et al.* 2006. Elucidating amyloid beta -protein folding and assembly: A multidisciplinary approach. *Acc. Chem. Res.* **39**: 635-645.
- Thirumalai, D., Klimov, D., and Dima, R. 2003. Emerging ideas on the molecular basis of protein and peptide aggregation. *Curr. Opin. Struct. Biol.* **13**: 146-159.
- Thompson, P.A., Eaton, W.A., and Hofrichter, J. 1997. Laser temperature jump study of the helix-coil kinetics of an alanine peptide interpreted with a 'kinetic zipper' model. *Biochemistry* **36**: 9200-9210.
- Todokoro, Y., Yumen, I., Fukushima, K., Kang, S.-W., Park, J.-S., Kohno, T., Wakamatsu, K., Akutsu, H., and Fujiwara, T. 2006. Structure of tightly membrane-bound mastoparan-x, a g-protein-activating peptide, determined by solid-state nmr. *Biophys. J.* **91**: 1368-1379.
- Tokuriki, N., Kinjo, M., Negi, S., Hoshino, M., Goto, Y., Urabe, I., and Yomo, T. 2004. Protein folding by the effects of macromolecular crowding. *Protein Sci.* **13**: 125-133.
- Tucker, M.J., Getahun, Z., Nanda, V., DeGrado, W.F., and Gai, F. 2004a. A new method for determining the local environment and orientation of individual side chains of membrane-binding peptides. *J. Am. Chem. Soc.* **126**: 5078-5079.
- Tucker, M.J., Getahun, Z., Nanda, V., DeGrado, W.F., and Gai, F. 2004b. A new method for determining the local environment and orientation of individual side chains of membrane-binding peptides. *J. Am. Chem. Soc.* **126**: 5078-5079.
- Tucker, M.J., Oyola, R., and Gai, F. 2005. Conformational distribution of a 14-residue peptide in solution: A fluorescence resonance energy transfer study. *Journal of Physical Chemistry B* **109**: 4788-4795.
- Tycko, R. 2003. Insights into the amyloid folding problem from solid-state nmr. *Biochemistry* **42**: 3151-3159.
- Van den Berg, B., Ellis, R.J., and Dobson, C.M. 1999. Effects of macromolecular crowding on protein folding and aggregation. *EMBO J.* **18**: 6927-6933.

- Van den Berg, B., Wain, R., Dobson, C.M., and Ellis, R.J. 2000. Macromolecular crowding perturbs protein refolding kinetics: Implications for folding inside the cell. *EMBO J.* **19**: 3870-3875.
- Van Giessen, A.E., and Straub, J.E. 2006. Coarse-grained model of coil-to-helix kinetics demonstrates the importance of multiple nucleation sites in helix folding. *Journal of Chemical Theory and Computation* **2**: 674-684.
- Venables, D.S., Huang, K., and Schmuttenmaer, C.A. 2001. Effect of reverse micelle size on the librational band of confined water and methanol. *Journal of Physical Chemistry B* **105**: 9132-9138.
- Venturoli, D., and Rippe, B. 2005. Ficoll and dextran vs. Globular proteins as probes for testing glomerular permselectivity: Effects of molecular size, shape, charge, and deformability. *American Journal of Physiology-Renal Physiology* **288**: F605-F613.
- Venyaminov, S.Y., and Prendergast, F.G. 1997. Water (H₂O and D₂O) molar absorptivity in the 1000-4000 cm⁻¹ range and quantitative infrared spectroscopy of aqueous solutions. *Anal. Biochemistry* **248**: 234-245.
- Viguera, A.R., and Serrano, L. 1999. Stable proline box motif at the n-terminal end of alpha-helices. *Protein Sci.* **8**: 1733-1742.
- Vila, J.A., Ripoll, D.R., and Scheraga, H.A. 2000. Physical reasons for the unusual alpha-helix stabilization afforded by charged or neutral polar residues in alanine-rich peptides. *Proc. Natl. Acad. Sci. U. S. A.* **97**: 13075-13079.
- Vila, J.A., Ripoll, D.R., and Scheraga, H.A. 2001. Influence of lysine content and pH on the stability of alanine-based copolypeptides. *Biopolymers* **58**: 235-246.
- Volk, M., Kholodenko, Y., Lu, H.S.M., Gooding, E.A., DeGrado, W.F., and Hochstrasser, R.M. 1997. Peptide conformational dynamics and vibrational Stark effects following photoinitiated disulfide cleavage. *Journal of Physical Chemistry B* **101**: 8607-8616.
- Vu, D.M., Myers, J.K., Oas, T.G., and Dyer, R.B. 2004. Probing the folding and unfolding dynamics of secondary and tertiary structures in a three-helix bundle protein. *Biochemistry* **43**: 3582-3589.
- Wakamatsu, K., Okada, A., Miyazawa, T., Ohya, M., and Higashijima, T. 1992. Membrane-bound conformation of mastoparan-x, a G-protein-activating peptide. *Biochemistry* **31**: 5654-5660.

- Walsh, S.T.R., Cheng, R.P., Wright, W.W., Alonso, D.O.V., Daggett, V., Vanderkooi, J.M., and DeGrado, W.F. 2003. The hydration of amides in helices; a comprehensive picture from molecular dynamics, ir, and nmr. *Protein Sci.* **12**: 520-531.
- Wand, A.J., Ehrhardt, M.R., and Flynn, P.F. 1998. High-resolution nmr of encapsulated proteins dissolved in low-viscosity fluids. *Proc. Natl. Acad. Sci. U. S. A.* **95**: 15299-15302.
- Wang, J., Chen, J., and Hochstrasser, R.M. 2006. Local structure of beta -hairpin isotopomers by ftir, 2d ir, and ab initio theory. *Journal of Physical Chemistry B* **110**: 7545-7555.
- Wang, T., Du, D., and Gai, F. 2003. Helix-coil kinetics of two 14-residue peptides. *Chem. Phys. Lett.* **370**: 842-848.
- Wang, T., Zhu, Y., Getahun, Z., Du, D., Huang, C.-Y., DeGrado, W.F., and Gai, F. 2004. Length dependent helix-coil transition kinetics of nine alanine-based peptides. *Journal of Physical Chemistry B* **108**: 15301-15310.
- Wenner, J.R., and Bloomfield, V.A. 1999. Crowding effects on ecorv kinetics and binding. *Biophys. J.* **77**: 3234-3241.
- Werner, J.H., Dyer, R.B., Fesinmeyer, R.M., and Andersen, N.H. 2002. Dynamics of the primary processes of protein folding: Helix nucleation. *Journal of Physical Chemistry B* **106**: 487-494.
- Whiles, J.A., Brasseur, R., Glover, K.J., Melacini, G., Komives, E.A., and Vold, R.R. 2001. Orientation and effects of mastoparan x on phospholipid bicelles. *Biophys. J.* **80**: 280-293.
- Williams, D.B., and Carter, C.B. (1996). Transmission electron microscopy (New York: Plenum Press).
- Williams, S., Causgrove, T.P., Gilmanishin, R., Fang, K.S., Callender, R.H., Woodruff, W.H., and Dyer, R.B. 1996. Fast events in protein folding: Helix melting and formation in a small peptide. *Biochemistry* **35**: 691-697.
- Wolf, M.G., Jongejan, J.A., Laman, J.D., and de Leeuw, S.W. 2008. Quantitative prediction of amyloid fibril growth of short peptides from simulations: Calculating association constants to dissect side chain importance. *J. Am. Chem. Soc.* **130**: 15772-15773.

- Wood, S.J., Maleeff, B., Hart, T., and Wetzel, R. 1996. Physical, morphological and functional differences between pH 5.8 and 7.4 aggregates of the Alzheimer's amyloid peptide A β . *J. Mol. Biol.* **256**: 870-877.
- Woody, R.W. 2005. The exciton model and the circular dichroism of polypeptides. *Monatshefte für Chemie* **136**: 347-366.
- Wu, X., and Wang, S. 2001. Helix folding of an alanine-based peptide in explicit water. *Journal of Physical Chemistry B* **105**: 2227-2235.
- Wu, Y., Vadrevu, R., Kathuria, S., Yang, X., and Matthews, C.R. 2007. A tightly packed hydrophobic cluster directs the formation of an off-pathway sub-millisecond folding intermediate in the α subunit of tryptophan synthase, a TIM barrel protein. *J. Mol. Biol.* **366**: 1624-1638.
- Wytenbach, T., Liu, D., and Bowers, M.T. 2005. Hydration of small peptides. *International Journal of Mass Spectrometry* **240**: 221-232.
- Xu, Y., Wang, T., and Gai, F. 2006. Strange temperature dependence of the folding rate of a 16-residue β -hairpin. *Chem. Phys.* **323**: 21-27.
- Xue, W.-F., Homans, S.W., and Radford, S.E. 2008. Systematic analysis of nucleation-dependent polymerization reveals new insights into the mechanism of amyloid self-assembly. *Proc. Natl. Acad. Sci. U. S. A.* **105**: 8926-8931.
- Yang, D.-S., Yip, C.M., Huang, T.H.J., Chakrabarty, A., and Fraser, P.E. 1999. Manipulating the amyloid- β aggregation pathway with chemical chaperones. *J. Biol. Chem.* **274**: 32970-32974.
- Yang, S., and Cho, M. 2007. Thermal denaturation of polyalanine peptide in water by molecular dynamics simulations and theoretical prediction of infrared spectra: Helix-coil transition kinetics. *Journal of Physical Chemistry B* **111**: 605-617.
- Yip, C.M., and McLaurin, J. 2001. Amyloid- β peptide assembly: A critical step in fibrillogenesis and membrane disruption. *Biophys. J.* **80**: 1359-1371.
- Yoder, G., Pancoska, P., and Keiderling, T.A. 1997. Characterization of alanine-rich peptides, ac-(aakaa) $_n$ -gy-nh $_2$ ($n = 1-4$), using vibrational circular dichroism and Fourier transform infrared. Conformational determination and thermal unfolding. *Biochemistry* **36**: 15123-15133.
- Yuan, J.M., Chyan, C.L., Zhou, H.X., Chung, T.Y., Peng, H.B., Ping, G.H., and Yang, G.L. 2008. The effects of macromolecular crowding on the mechanical stability of protein molecules. *Protein Sci.* **17**: 2156-2166.

- Zanni, M.T., Gnanakaran, S., Stenger, J., and Hochstrasser, R.M. 2001. Heterodyned two-dimensional infrared spectroscopy of solvent-dependent conformations of acetylproline-nh2. *Journal of Physical Chemistry B* **105**: 6520-6535.
- Zheng, J., Jang, H., Ma, B., and Nussinov, R. 2008. Annular structures as intermediates in fibril formation of alzheimer abeta 17-42. *Journal of Physical Chemistry B* **112**: 6856-6865.
- Zheng, J., Ma, B., Tsai, C.-J., and Nussinov, R. 2006. Structural stability and dynamics of an amyloid-forming peptide gnnqqny from the yeast prion sup-35. *Biophys. J.* **91**: 824-833.
- Zhou, H.-X. 2004. Protein folding and binding in confined spaces and in crowded solutions. *J. Mol. Recognit.* **17**: 368-375.
- Zhou, H.-X. 2008a. Effect of mixed macromolecular crowding agents on protein folding. *Proteins: Structure, Function, and Bioinformatics* **72**: 1109-1113.
- Zhou, H.-X. 2008b. Protein folding in confined and crowded environments. *Arch. Biochem. Biophys.* **469**: 76-82.
- Zhou, H.-X., and Dill, K.A. 2001. Stabilization of proteins in confined spaces. *Biochemistry* **40**: 11289-11293.
- Zhou, H.X. 2007. Helix formation inside a nanotube: Possible influence of backbone-water hydrogen bonding by the confining surface through modulation of water activity. *J. Chem. Phys.* **127**.
- Zhou, H.X., Rivas, G.N., and Minton, A.P. 2008. Macromolecular crowding and confinement: Biochemical, biophysical, and potential physiological consequences. *Annual Review of Biophysics* **37**: 375-397.
- Zhu, M., Han, S., Zhou, F., Carter, S.A., and Fink, A.L. 2004a. Annular oligomeric amyloid intermediates observed by in situ atomic force microscopy. *J. Biol. Chem.* **279**: 24452-24459.
- Zhu, Y., Alonso, D.O.V., Maki, K., Huang, C.-y., Lahr, S.J., Daggett, V., Roder, H., DeGrado, W.F., and Gai, F. 2003. Ultrafast folding of alpha 3d: A de novo designed three-helix bundle protein. *Proc. Natl. Acad. Sci. U. S. A.* **100**: 15486-15491.

- Zhu, Y., Fu, X., Wang, T., Tamura, A., Takada, S., Saven, J.G., and Gai, F. 2004b. Guiding the search for a protein's maximum rate of folding. *Chem. Phys.* **307**: 99-109.
- Zhuang, W., Abramavicius, D., and Mukamel, S. 2006. Two-dimensional vibrational optical probes for peptide fast folding investigation. *Proc. Natl. Acad. Sci. U. S. A.* **103**: 18934-18938.
- Zimmerman, S.B., and Minton, A.P. 1993. Macromolecular crowding: Biochemical, biophysical, and physiological consequences. *Annu. Rev. Biophys. Biomol. Struct.* **22**: 27-65.
- Zimmerman, S.B., and Trach, S.O. 1991. Estimation of macromolecule concentrations and excluded volume effects for the cytoplasm of escherichia coli. *J. Mol. Biol.* **222**: 599-620.
- Ziv, G., Haran, G., and Thirumalai, D. 2005. Ribosome exit tunnel can entropically stabilize α -helices. *Proc. Natl. Acad. Sci. U. S. A.* **102**: 18956-18961.
- Zulauf, M., and Eicke, H.F. 1979. Inverted micelles and microemulsions in the ternary system water/aerosol-ot/isooctane as studied by photon correlation spectroscopy. *J. Phys. Chem.* **83**: 480-486.